

ON TRANSITION BOILING
HEAT TRANSFER FROM A
HORIZONTAL SURFACE

by

PAUL JEROME BERENSON

S.B. Massachusetts Institute of Technology
(1956)

M.S. Massachusetts Institute of Technology
(1957)

Mech. E. Massachusetts Institute of Technology
(1958)

SUBMITTED IN PARTIAL FULFILLMENT OF THE
REQUIREMENTS FOR THE DEGREE OF
DOCTOR OF PHILOSOPHY

at the

MASSACHUSETTS INSTITUTE OF TECHNOLOGY

February 1960

Signature of Author . . . *Paul J. Berenson*
Department of Mechanical Engineering

Certified by *Peter Criffith*
Thesis Supervisor

Accepted by
Chairman, Departmental Committee on Graduate Students

ABSTRACT

ON TRANSITION BOILING HEAT TRANSFER FROM
A HORIZONTAL SURFACE

by

Paul Jerome Berenson

Submitted to the Department of Mechanical Engineering on
January 11, 1960, in partial fulfillment of
the requirements for the degree of
Doctor of Philosophy

An experiment, utilizing a condensing fluid as the heat source, was performed to determine the heat flux vs. temperature difference curve for transition pool boiling from a horizontal surface. The boiling curve was determined as a function of surface roughness, material, and cleanliness for n-pentane at atmospheric pressure. The results of the experiment show that the liquid contacts the solid heating surface in transition boiling. The burnout heat flux and the film boiling curve are independent of surface properties. For commercial heating surfaces, and probably provided that the combination of surface energies which exist do not result in spreading of the liquid on the solid heating surface, the location of the minimum point is independent of surface properties. It is concluded that transition boiling is a combination of unstable nucleate and unstable film boiling alternating at a given location on the heating surface. The heat transfer data in the transition region was found to be correlated by a straight line on log-log graph paper which connects the burnout point and the minimum point.

The bubble spacing and growth rates in film pool boiling from a horizontal surface are shown to be determined by Taylor Hydrodynamic Instability for temperature differences near the minimum. An analytical expression for the heat transfer coefficient in film pool boiling from a horizontal surface is derived. Combining this equation with the equation for the minimum heat flux yields an analytical expression for the temperature difference at the minimum, which defines the location of the minimum point. The above equations agree with the experimental measurements made on n-pentane and carbon tetrachloride within $\pm 10\%$.

Thesis Supervisor: Peter Griffith

Title: Assistant Professor of Mechanical Engineering

Massachusetts Institute of Technology
Cambridge 39, Massachusetts
January 11, 1960

Professor Philip Franklin
Secretary of the Faculty
Massachusetts Institute of Technology
Cambridge 39, Massachusetts

Dear Sir:

In accordance with the regulations of the faculty, I hereby submit a thesis entitled "On Transition Boiling Heat Transfer from a Horizontal Surface," in partial fulfillment of the requirements for the degree of Doctor of Philosophy in Mechanical Engineering.

Respectfully submitted,


Paul J. Berenson

Dedicated to my Wife

Grace

ACKNOWLEDGEMENTS

It is a pleasure to acknowledge the help and encouragement I have received in my studies.

To my parents, my sincerest thanks for giving me the chance to avail myself of the unlimited opportunities offered in the United States.

Professor Peter Griffith's stimulation, encouragement, guidance, and assistance during all phases of the thesis program was the major cause of its successful and prompt completion.

I want to thank Professor Warren Rohsenow for first encouraging me to undertake the doctoral program, and for his initial guidance.

My wife's presence, confidence, patience, and encouragement made the pursuance of the Doctor's Degree much more pleasant than it would have been otherwise.

The thesis was supported by a grant from the National Science Foundation.

TABLE OF CONTENTS

	Page
CHAPTER I INTRODUCTION	
A. General	1
B. Transition Boiling.	8
C. Object of Present Investigation	11
CHAPTER II EXPERIMENTAL PROGRAM	
A. Introduction.	13
B. Experiment Design	14
C. Variation of Surface Characteristics.	23
D. Test Procedure.	26
E. Test Program.	29
F. Results and Conclusions of Experimental Program	40
CHAPTER III THEORETICAL PROGRAM	
A. Introduction.	42
B. Taylor-Helmholtz Hydrodynamic Instability	43
C. Application of Taylor-Helmholtz Instability to Film Boiling from a Horizontal Surface	46
D. Analysis of Film Boiling from a Horizontal Surface.	54
E. Analysis of the Temperature Difference at the minimum Heat Flux.	62
CHAPTER IV CONCLUSION	
A. Discussion.	65
B. Summary of Results and Conclusions.	67

	Page
NOMENCLATURE	70
BIBLIOGRAPHY	73
APPENDICES	
A. Heater Design	76
B. Thermocouple Calibration.	79
C. Surface Temperature Calculation Equation.	81
D. Surface Tension, Contact Angle, and Spreading	83
E. Sample Calculation.	90
F. Vapor Velocity Parallel to Surface in Film Boiling.	93
G. Application of Helmholtz Instability to the Analysis of the Burnout Heat Flux.	94
H. Application of Taylor Instability to the Analysis of the Minimum Heat Flux.	99
TABLES	103
FIGURES.	121
BIOGRAPHICAL NOTES	142

LIST OF FIGURES

	Page
FIGURE 1	Nukiyama's Experimental Results. 121
FIGURE 2	Characteristic Boiling Curve 121
FIGURE 3	Photograph of Transition Boiling (25): $(q/A)_{\max} = 170,000 \text{ BTU/hr ft}^2$ 122
FIGURE 4	Photograph of Transition Boiling (25): $q/A = 69,000 \text{ BTU/hr ft}^2$ 122
FIGURE 5	Photograph of Transition Boiling (25): $q/A = 27,000 \text{ BTU/hr ft}^2$ 123
FIGURE 6	Photograph of Transition Boiling (25): $q/A = 13,000 \text{ BTU/hr ft}^2$ 123
FIGURE 7	Photograph of Transition Boiling (25): $q/A = 5,500 \text{ BTU/hr ft}^2$ 124
FIGURE 8	Heater Assembly. 124
FIGURE 9	Test Set Up Assembly 125
FIGURE 10	Electrical Power Lead Assembly 126
FIGURE 11	Typical Copper Heating Block Design. 126
FIGURE 12	Wiring Diagram for Power Supply. 127
FIGURE 13	Thermocouple Wiring Diagram. 128
FIGURE 14	Deviation Curve for Iron-Constantan Thermocouples. . 129
FIGURE 15	Heat Loss Calibration. 129
FIGURE 16	Copper Pentane Test Results. 130
FIGURE 17	Copper Pentane Test Results: Effect of Surface Cleanliness 130

	Page
FIGURE 18 Copper Pentane Test Results:	
Effect of Roughness.	131
FIGURE 19 Copper Pentane Test Results:	
Effect of Surface Cleanliness.	131
FIGURE 20 Copper Pentane Test Results:	
Effect of Wetting Agent.	132
FIGURE 21 Copper Pentane Test Results:	
Effect of Roughness.	132
FIGURE 22 Inconel-Pentane Test Results:	
Effect of Roughness.	133
FIGURE 23 Nickel Pentane Test Results:	
Effect of Roughness.	133
FIGURE 24 Pentane Lap E Circular Results:	
Effect of Material	134
FIGURE 25 Effect of Material Thermal Diffusivity on	
Nucleate Boiling Temperature Difference.	134
FIGURE 26 Copper Carbon Tetrachloride Test Results.	135
FIGURE 27 Plot of b as a Function of m for n-Pentane	
Neglecting the Effect of Velocity and fluid	
Depth.	135
FIGURE 28 Vapor Thermal Conductivity as a	
function of Temperature.	136
FIGURE 29 Vapor Specific Heat as a Function of Temperature.	136
FIGURE 30 Vapor Prandtl Number as a function of Temperature	137
FIGURE 31 Vapor Film Density as a Function of	
Temperature Difference	137

	Page
FIGURE 32 Plot of $k_f \Delta T$ as a Function of Temperature Difference	138
FIGURE 33 Saturated Vapor Enthalpy Change as a function of Temperature Difference	139
FIGURE 34 Vapor film Viscosity as a Function of Temperature Difference	139
FIGURE 35 Plot of b as a function of m from Eq. (III-17) for n-Pentane	140
FIGURE 36 Physical Model of Film Boiling from a Horizontal Surface	141

CHAPTER I
INTRODUCTION

A. GENERAL

1. Characteristic Boiling Curve

Boiling, the phenomenon of vaporization by bubble formation within a liquid due to the presence of a hot surface, has received significant attention only during the past few decades. The first great advance in the science of boiling, the simple experiment of Nukiyama (1)* in 1934, hinted that the phenomenon is considerably more complicated than might have been anticipated. It was found that at least two, and possibly three, distinct regimes of boiling existed.

Nukiyama submerged an electrically heated wire in a pool of saturated liquid water and measured the temperature of the wire as a function of the heat flux. The results of this experiment, summarized in Figure 1 and described below, have great practical importance.

When first heating the wire, bubbles did not appear until the temperature of the wire became a few degrees greater than the saturation temperature. As the heat flux was gradually increased beyond the point at which bubbles appeared, the wire temperature also gradually increased, following curve AB, to a value near 100 °F at point B.

An infinitesimal increase in the heat flux, beyond that at point B, resulted in a jump of the wire temperature to approximately 2000 °F at point C. At point C increasing the heat flux once again caused a

* The numbers in parentheses refer to the bibliography.

gradual increase in the wire temperature, but along curve CD.

If the heat flux was then slowly decreased to less than that at point C, the temperature also gradually decreased, no jump in temperature occurring from C back to B. Upon further lowering of the heat flux, the wire temperature continued to gradually decrease until point D was reached. Here the wire temperature suddenly jumped from D to point E, lying on curve AB.

Repeating the experiment many times led to similar results. It was possible to both increase and decrease the heat flux and follow curves AB and CD. However, to jump from B to C and from D to E it was necessary to increase and decrease the heat flux respectively. When using wires whose melting point was less than the temperature at C, the wire melted when the heat flux was raised above that at B. This has led to terming the heat flux associated with point B the "burnout" heat flux.

Nukiyama suggested that, in addition to the two boiling regimes represented by curves AB and CD, the boiling curve may be continuous between point B and D. If this is true, the curve connecting B and D would have the surprising characteristic that increasing the temperature difference would cause a decrease in the heat flux.

Farber and Scoriah (2) verified the above suggestion when they obtained the complete characteristic boiling curve shown in Figure 2. By carefully controlling their experiment they found it possible to obtain data in region III, in spite of the fact that, due to the negative slope, operation is inherently unstable in experiments where the heat flux is the controlled parameter.

The general shape of the boiling curve is the same for all fluids

at all pressures. The coordinates change as the preceding are varied, but the qualitative description of the curve remains the same.

As indicated in Figure 2, the characteristic boiling curve consists of four regions, in each of which the mechanism of heat transfer is distinct. In region I the wall superheat is not great enough to cause a significant number of bubbles to form. Heat is transferred by natural convection at the wall, evaporation occurring only at the liquid free surface.

As the surface temperature is increased to more than a few degrees above the saturation temperature, vapor bubbles begin to nucleate and grow at preferred locations on the surface in region II. The bubble motion affectively stirs the liquid in the vicinity of the wall, increasing the heat transfer rate around the bubbles due to the forced convection affect. As the temperature difference is increased, the bubble population also increases, causing a large increase in the heat transfer rate until point B is reached.

Increasing the temperature difference beyond point B results in a decrease in the heat transfer rate in region III. This effect is probably the result of the formation of a partial vapor blanket of low thermal conductivity, which effectively insulates a part of the surface. The heat flux continues to decrease as the temperature difference is increased until point D is reached, where the slope once again becomes positive. In region III, a dramatic change in the visual appearance of the boiling process takes place. From B, where the bubbles are relatively small and the fluid motion is extremely confused, one gradually changes to D, where the bubbles are relatively large and the fluid motion appears unhurried and regular.

The surface is completely covered by a thin vapor film beyond point D; heat transfer taking place due to conduction through the film. As the temperature of the surface is increased radiative heat transfer becomes increasingly important; the total heat transfer rate being the sum of that due to radiation and conduction.

2. Summary of the Knowledge of Each Boiling Heat Transfer Regime

It is impossible to derive one equation which will correlate all the boiling heat transfer data obtained, over the entire range of temperature differences. The fluid mechanics and the heat transfer mechanism are different in each regime, requiring a separate analytical formulation for each. Since the fluid flow pattern is also affected by the orientation of the heating surface in a gravitational field, it is in general also necessary to separately analyze each boiling regime according to the geometry; i.e., horizontal surface, vertical surface, and horizontal cylinder.

a. Natural Convection

Conventional natural convection analysis are independent of superheat, depending only on the total temperature difference, provided the fluid motion driving force is due only to the temperature coefficient of expansion. In the natural convection region of the boiling curve, the bubble motion has a negligible affect on the fluid mechanics and heat transfer. Therefore, the conventional correlation equations (3) correctly predict this portion of the curve.

b. Nucleate Boiling

The nucleate boiling regime has the greatest practical importance since it provides the opportunity to transfer very large quantities of

heat with small temperature differences. Most industrial equipment utilizing boiling heat transfer are designed to operate in this region. Due to the practical importance of nucleate boiling, most of the investigations of boiling heat transfer are concerned with this regime.

The high heat transfer rates obtained in nucleate boiling are a result of the agitation of the liquid in the vicinity of the wall by the bubbles which rapidly grow and depart. Since the bubble nucleation and growth cause the fluid motion at the surface, it is necessary to be able to predict both of these before analytically deriving a nucleate boiling correlation equation. The nucleation phenomenon, which is a function of the heating surface roughness, as well as the fluid properties, has been investigated by a number of workers (4, 5, 6). Although the results are very promising, it is not at present possible to predict bubble population and nucleation for a given commercial surface as a function of the superheat. The problem of bubble growth has been analyzed with considerable success by a few investigators (7, 8, 9). While the progress indicates a useful result will be forthcoming in the near future, the solution of the problem of bubble nucleation and growth has not yet progressed to the point where the results may be applied to commercial equipment.

In the absence of enough information to take a direct analytical approach to nucleate boiling, it was suggested by Rohsenow (10) that applying the conventional results of dimensional analysis for forced convection to the nucleate boiling process might yield useful results. Forming the appropriate dimensionless groups, scaled by the bubble dimensions, yielded an expression which successfully correlated the effect of fluid properties. The result contains an empirical constant,

which must be evaluated for each fluid surface combination, and requires the slope of the nucleate boiling curve to remain constant. A number of other semi-empirical nucleate boiling correlation equations have been proposed in the past few years. They offer no improvement in the accuracy of correlation and also do not analytically include the affect of surface roughness.

c. Maximum Nucleate Boiling Heat Flux

Since most industrial equipment will successfully operate only so long as it is in the nucleate boiling regime, it is extremely important to be able to predict the maximum nucleate boiling heat flux, the burnout heat flux. While a number of empirical correlations have been proposed, the first significant theoretical progress was a result of the suggestion of Kutateladze (11) that the burnout heat flux is due to hydrodynamic instability. Zuber (12) successfully applied the results of stability analysis to the problem of the maximum heat flux and obtained an analytical expression which adequately correlates all the available pool boiling data. The analysis is based on the assumption that the maximum heat flux is due to a hydrodynamically limited flow condition. Once the heat transfer rate is great enough to generate the maximum allowable vapor flow no further increase can be tolerated. In the derivation of the above equation it was assumed that the surface was vapor blanketed, which led to the conclusion that the fluid flow area normal to the heating surface was equally distributed between vapor and liquid.

d. Transition Boiling

Very little is known about transition boiling beyond the fact that such a regime actually exists. The decrease in heat transfer rate

must be due to a vapor blanketing affect, but the question of whether the surface is entirely covered with a very thin vapor film, or partially covered with both vapor and liquid has not been unequivocally resolved. Due to the uncertainty about the mechanism of heat transfer in the transition region, it has not been possible to derive any semi-empirical or analytical correlation equations to predict the heat flux at a given temperature difference.

e. Minimum Heat Flux

The minimum heat flux of transition boiling, which is also the minimum heat flux of film boiling, was investigated by Borishansky (13). He suggested that the minimum heat flux is a result of a hydrodynamic instability of the liquid-vapor boundary. Zuber (12) analytically derived an equation for the minimum heat flux based on the above assumption which satisfactorily predicts the experimental pool boiling results.

f. Film Boiling

The well defined fluid flow configuration which exists in film boiling from horizontal cylinders and vertical surfaces has made it possible to analyze this phenomenon in detail. Bromley (14) obtained the analytical result for the viscous vapor flow around a horizontal tube and successfully correlated the available data. A similar analysis was also applied to vertical surfaces. The flow pattern which exists in film boiling from a horizontal surface is not understood well enough to formulate the problem analytically.

The preceding description of the knowledge of boiling heat transfer is necessarily brief, omitting many interesting and important

details with which the curious reader may desire to become familiar. A thorough discussion of all the boiling regimes is contained in the writings of Westwater (15) and Rohsenow (16).

B. TRANSITION BOILING

1. Introduction

While a number of unsolved problems remain in the field of boiling heat transfer, one of the biggest voids is the almost complete lack of knowledge of transition boiling. Westwater (15) in a 150 page discussion of boiling devotes only three pages to a discussion of transition boiling, concluding with the remark that, "At present it is impossible to design commercial equipment to operate in the transition region."

The practical applications of transition boiling are limited to specialized equipment. Nuclear reactor overload and pump failure transients, quenching of metals, evaporator performance, and electronic cooling are typical areas where a knowledge of transition boiling is essential.

In addition to the practical significance of transition boiling, this phenomenon is particularly appealing from the academic point of view. It is the only case known where increasing the temperature difference decreases the heat transfer rate.

2. Historical Development

In addition to the experiments of Nukiyama (1), and Farber and Scorah (2), a few other investigators have also performed experiments in the transition region. Most of these exploratory experiments have

utilized horizontal tubes as the heating surface. This is unfortunate since, while it is one of the simplest geometries to test, it is possible that at different peripheral locations around the tube the boiling regime would be different. If this was the case, the measured average heat flux would correspond to the average of the different boiling regimes existing and would not in fact locate a particular point on the characteristic boiling curve of the fluid tested. In particular, the maximum heat flux measured would be less, by a significant per cent, than the actual burnout heat flux attained at specific positions on the tube.

Drew and Mueller (17) obtained data in the transition region for six organic compounds boiling from a horizontal, steam heated, copper tube. Their investigation was exploratory in nature, establishing, for the first time, the existence and general shape of the characteristic curve in the transition region, but not accurately determining the values of the heat flux and the temperature difference.

Braunlich (18), and Kaulakis and Sherman (19) obtained data for one fluid as a function of the fluid pressure. Their results are summarized by McAdams (20). Plotting the data on log-log graph paper yielded an approximately straight line in the transition region. They observed that the effect of pressure on the heat flux in the transition region is qualitatively the same as in the nucleate boiling regime.

Theses supervised by Westwater at the University of Illinois (21 - 24) have shown that surface roughness, surface material, fluid additives, and forced convection all qualitatively effect the transition region in the same manner in which they modify the nucleate boiling curve.

In addition to the quantitative data obtained in the transition region, two sets of high speed photographs are available. Westwater and Santangelo (25) photographed the entire nucleate and transition regimes while boiling methanol from a horizontal tube. Their excellent results in the transition region are reproduced in Figures 3 - 7. As a result of examining these photographs it was concluded that no liquid solid contact exists. Ellion (26) photographed transition boiling of a fluid pumped axially along a vertical tube and concluded, as a result of his photographs, that liquid-solid contact did exist.

The only theoretical considerations of transition boiling, those of Zuber (12), assume that the heating surface is always completely covered by a vapor film. The results of the analysis lead to equations for the maximum and minimum heat flux in transition boiling, but contain no information about the shape of the curve and its location along the temperature difference coordinate. The analysis implies that transition boiling is a change from one type of hydrodynamic wave pattern to another.

3. Present Status of Transition Boiling

The phenomenon of transition boiling was experimentally observed for all fluids tested, establishing without doubt the existence of the negative slope portion of the boiling curve. In general, transition boiling is effected by the same variables which effect nucleate boiling, and in the same qualitative manner.

The visual picture of transition boiling ranges from the chaos existing near the maximum heat flux, Figure 3, to the calm, regular

mode observed at the minimum, Figure 7. It is not surprising that the photographs of Santangelo and Ellion lead to contradictory conclusions. The vapor film thickness at the minimum is of the order of 10^{-3} inches. At the minimum the photograph, Figure 7, is uncluttered and clear, however it is still difficult to distinguish the vapor-liquid boundary from a solid-liquid boundary. At moderate heat flux in the transition region, Figure 4, the vapor film, if it exists, must be a factor of ten thinner than at the minimum. At the same time the visual picture is very confused, making it impossible to conclude, as a result of photographs alone, whether or not the liquid touches the surface.

The quantitative effect of the important variables has not been thoroughly investigated. Insufficient accurate data exists to provide adequate verification of analytical results. However, before attempting to derive theoretical results, it is first necessary to determine the mechanism of heat transfer. In particular, the question of liquid-solid contact must be resolved. Photographs cannot yield the answer, therefore some indirect method must be utilized.

C. OBJECT OF PRESENT INVESTIGATION

The object of the present work was to determine the characteristics of transition boiling, and develop a correlation technique for use in the prediction of the relationship between heat transfer rate and temperature difference.

1. Experimental Program

The objectives of the experimental program were as follows:

- a. Determine the mechanism of heat transfer in transition boiling.

- b. Determine the effect of surface material and finish, and fluid properties on the location and shape of the transition boiling curve.
- c. Make any measurements required by the theory.

2. Theoretical Program

The goal of the theoretical efforts was to develop a technique and any analytical results required to predict the transition boiling curve.

CHAPTER II

EXPERIMENTAL PROGRAM

A. INTRODUCTION

Most of the previous experiments designed to investigate boiling heat transfer were regulated by controlling the heat flux. Due to the shape of the characteristic boiling curve, operation within the transition region is inherently unstable in experiments in which only the heat flux is controlled. Referring to Figure 2, it is seen that at a given value of the heat flux, operation at three values of the temperature difference is possible; the lowest in the nucleate region, the next in the transition region, and the highest in the film region. Depending upon whether the heat flux is being increased or decreased, the temperature difference observed in general corresponds to the nucleate regime or the film regime, respectively.

It is observed, referring to Figure 2, that at each value of the temperature difference, operation within only one region is possible; i.e. there is a single value of heat flux associated with each value of temperature difference. Therefore, an experiment designed to control the temperature difference allows operation within the transition region, as well as the other two regions.

The most convenient technique for controlling the temperature difference utilizes a condensing fluid as the heat source. The temperature and pressure of a condensing fluid are dependent, therefore the temperature can be established by controlling the pressure at which condensation occurs; thereby imposing an overall temperature difference.

Before designing the experiment, it is prudent to consider some of the desirable characteristics of a heat transfer experiment. In general, the quantitative data consists of temperatures and heat transfer rates. In particular, the primary temperature of interest, the temperature of the surface from which boiling takes place, must be determined accurately, without disturbing the boiling process. Temperature measurements are also used to indicate the magnitude of edge effects.

The heat transfer rate can be determined by applying Ohms Law, the heat conduction equation, or the First Law of Thermodynamics. It is desirable in heat transfer experiments to determine the heat transfer rate by at least two independent methods, to establish the accuracy of the data. The experiment is also designed to allow easy modification to examine the effect of the important variables; eg., surface roughness and material.

B. EXPERIMENT DESIGN

1. Conceptual Design

The first design variable established, the geometry of the boiling surface was chosen from the three possibilities of a horizontal tube, a vertical tube or flat plate, and a horizontal flat surface. As mentioned above, a horizontal tube allows the possibility for different boiling regimes to exist at different peripheral locations around the tube, therefore this geometry was eliminated from consideration. There was little to choose between the vertical and the horizontal surfaces. They are both a unique, well defined geometry, although the fluid motion is distinct for each. The horizontal flat surface, chosen for

these experiments, allows relatively simple fluid containment, and an uncomplicated experiment. It was also a relatively unexplored geometry experimentally, while most theoretical treatments visualize the horizontal flat surface configuration.

The conceptual design of the experiment consisted of two cylindrical chambers, A and B, separated from one another by a block of high thermal conductivity metal. Chamber A was a constant volume chamber containing the condensing fluid. From the first Law of Thermodynamics, the pressure, and therefore the temperature, remains constant in chamber A provided the heat in equals the heat out. The heat out from the chamber was a result of condensation on fins on the bottom of the conducting block, and radial heat loss through the insulation placed around chamber A. The heat into chamber A was a result of an electric ohmic heater submerged in the liquid at the bottom of the chamber. The mechanism of heat transfer from the heating coil to the condensate was nucleate boiling. To increase the temperature in chamber B a net amount of heat was added, and to decrease the temperature a net amount of heat was removed. The electric power input was controlled to allow the above changes. The vapor in chamber A condenses on vertical fins extending down from the metal block, thereby minimizing the temperature drop between the two chambers.

The heat conducted through the metal block resulted in boiling of the test fluid in chamber B from the top surface of the block. The temperature, measured at various axial and radial locations in the metal, provided information for calculating the heat transfer rate, and also checked the uniformity of temperature at each axial location.

The fluid in chamber B boiled from the top of the metal block in whatever regime was characteristic of the surface temperature of the block. The evaporated fluid was recovered by use of a reflux condenser. Chamber B may be left open to the atmosphere or pressurized if desired. To enable visual observations of the boiling process to be made, the walls of chamber B were transparent.

During any one test run, the pressure in chamber B was maintained constant, while the pressure, and therefore the temperature, in chamber A was varied over a large enough range to include the entire transition region.

2. Working Fluids

The fluids utilized in chambers A and B had to satisfy a number of requirements. For handling ease, it was desirable for them to be liquid at atmospheric conditions. To provide the necessary temperature difference, without requiring extremely high pressures in chamber A, the saturation temperature at atmospheric pressure of the fluid in B had to be as close to atmospheric temperature as practical. The saturation temperature of the fluid in A had to be relatively high at atmospheric pressure, but not so high that it was necessary to operate at high vacuum to obtain the nucleate boiling portion of the curve. The critical pressure of the fluid in B had to be low so that the data was representative of a reasonable reduced pressure, without testing at high pressure.

At equilibrium the heat transferred to fluid A by the electrical heater is approximately equal to the heat transferred from the metal block to fluid B. Therefore, the heater had to be capable of taking fluid B through its maximum heat flux without itself burning out in

fluid A. It was therefore desirable that the burnout heat flux of fluid A be much greater than the burnout heat flux of fluid B.

The fluid used in chamber B had to be common enough for all the important thermodynamic and mechanical properties to be available. Both fluids should be easily obtainable, easy to store, safe to handle, and inexpensive. Fluid B had to be transparent.

The fluids which best satisfied the above requirements were water for chamber A and n-pentane for chamber B. Pentane has the additional advantage of having been tested and correlated in the nucleate regime. The saturation temperature of pentane at atmospheric pressure is 97 °F, and the critical pressure of 485 psia is very low.

To provide an overall temperature difference from 10 - 300 °F, the pressure of the water in chamber A had to be varied from approximately 1 to 200 psia, requiring neither extremely high vacuum on one end, nor extremely high pressure on the other.

Predicting the burnout heat flux utilizing the pool boiling correlation of Rohsenow and Griffith (27) resulted in values of approximately 100,000 BTU/hr ft² for n-pentane, and 500,000 BTU/hr ft² for water at atmospheric pressure. To allow the pressure in chamber A to be varied reasonably fast, the heater was designed to have twice the capacity required by the maximum heat flux of the test fluid. This also allowed other fluids, whose burnout heat fluxes are greater than that of n-pentane to be tested if necessary. To insure the heating coil against burnout, it was designed so that the heat flux it provided at maximum power was less than 300,000 BTU/hr ft².

3. Size of Heating Surface

The test fluid heating surface had to be large enough so that edge effects were negligible. Therefore, the diameter of the heating surface should probably be greater than 10 bubble diameters. The bubbles at the minimum are much larger than the bubbles at the maximum heat flux. The bubble diameter of approximately one quarter of an inch at the minimum (12) therefore specified a heating surface diameter of approximately 2 1/2" D.

The power supply available in the Heat Transfer Laboratory, without resorting to expensive supplementary equipment, was established by the 115V voltage supply. Combining this with the maximum current allowed by the variac, 9 amps, and assuming the entire voltage drop occurs in the heater, resulted in a maximum power of $115 \times 9 = 1035$ watts.

As a result of the design ground rules established above, this power must be equivalent to twice the maximum steady heat flux required by the pentane. Therefore,

$$2 \times (q/A)_{\max} \times \frac{\pi D^2}{4} \leq W \quad (\text{II-1})$$

Combining Eq. (II-1) with previously established values of W and $(q/A)_{\max}$, and solving for the maximum heating surface diameter results in D equal to 1.8".

The maximum diameter allowed by power limitations was somewhat less than the minimum diameter allowed by edge effect considerations. However, a small compromise of each of these figures was not prohibited, therefore a two inch diameter heater surface was chosen.

4. Heater Design

As a result of the above calculations, the heater had to be capable of a power output of approximately one kilowatt without exceeding a heat transfer rate of 300,000 BTU/hr ft², and fit within a cylindrical volume whose diameter was approximately 2 inches, and whose height was presumably also only a few inches. No commercial heater presently available satisfied these requirements, necessitating a special heater design and development.

The heater was visualized as a resistance wire which was coiled to obtain the high density heat generation required. The resistance of the wire had to be great enough so that at full voltage, the current did not exceed 9 amps, therefore

$$R \geq \frac{V_{\max}}{I_{\max}} = \frac{115}{9} = 12.8 \Omega \quad (\text{II-2})$$

Since the power output of the coil at maximum voltage is inversely proportional to the resistance, it was desirable to have the resistance as low as possible. Therefore, the heating coil was designed so that the resistance was 12.8 Ω .

For a given gauge resistance wire, the resistance per unit length and the diameter are fixed. At the maximum current of 9 amps the power generated must correspond to a heat flux from the surface of the wire equal to less than 300,000 BTU/hr ft², therefore

$$I^2 \frac{R}{L} \leq \pi D_w (q/A)_{\max}$$

or

$$\left(\frac{R}{L}\right) \frac{1}{D_w} \leq \frac{\pi (q/A)_{\max}}{I^2} \quad (\text{II-3})$$

In addition to satisfying Eq. (II-3), the wire had to be short enough to be coiled to fit in the specified volume and it had to be capable of supporting itself structurally.

The detailed design of the heater is contained in Appendix A. The resulting design consists of two 30" lengths of #26 Chromel-A wire coiled, connected in series, and attached to a teflon base. This heater, shown in Figure 8, easily meets all specifications and performs very well, even with a 10 amp current.

5. Test Vessel Design

An assembly drawing of the complete test set up is given in Figure 9. Note that chamber B may be assembled or disassembled without disturbing chamber A. A brief description of each of the components follows.

a. Vessel A

Vessel A consisted of a 5 1/4" length of 2 1/2" O.D., 0.109" wall thickness, hard drawn, round, seamless, brass tubing. A sight glass for observing the liquid level was located 3 1/4" from the bottom of the vessel. Opposite the sight glass, near the top of the chamber, a bleed line was connected, which also served as the loading line and the connection for the pressure gauge. The bleed line valve was closed except during start up and shut down.

b. Plate A

A 1/2" thick, half hard, brass strip cut into a 4" square was used as the bottom plate. Six holes, equally spaced on a 3" diameter, were drilled to receive Bolts A. The two electrical leads and seal, located 1 1/2" apart in the center of the plate, are shown in detail in Figure 10.

c. Block A

The entire block, including fins and flange, was machined from a 2 1/2" diameter pure copper rod. The flat plate fins were the result of milling 9 equally spaced slots in the bottom of the rod. Three separate, similar blocks were used; dimensions of a typical block are contained in Figure 11. Two sets of two holes each were drilled as indicated to receive thermocouples. At each axial location a hole was drilled to the center of the block and another located near the edge. The axial distribution provided a means for calculating the heat flux, while the radial distribution checked the assumed one dimensional heat flow.

d. Plate B

Plate B was identical in size and material to plate A. In addition to six holes matching those of plate A, three threaded holes, equally spaced on a 3 1/4" diameter, were formed to receive the bolts from plate C. A 2" D hole bored in the center of the plate allowed it to slip over the top of block A.

e. Seal A

A 3/8" thick teflon ring of 2 3/4" O.D. was used to seal the test fluid in the upper chamber. The inside diameter of the ring was bored at a 30° angle, until the minimum value of the I.D. was equal to 1 3/4".

f. Vessel B

A seven inch length of 60 m.m. O.D. pyrex tubing served as the transparent chamber for the fluid tested.

g. Plate C

A 4" square, 1/4" thick aluminum plate with a 2" D hole in the center served to apply sufficient force to vessel B and the teflon seal

to prevent leakage. Three holes, matching those in plate B, were drilled to pass bolts B.

h. Reflux Condenser

One quarter inch copper tubing formed into a 1" I.D. coil 5" long, where the spacing between the coils was 1/4", provided adequate condensation capacity to recover the pentane vapor generated at the burn-out point in this apparatus.

6. Instrumentation

The power supplied to the test chamber was measured as shown in Figure 12.

The pressure in chamber A, which was used only to determine the saturation temperature, was measured with a United States Gauge #12113-1. The accuracy of the pressure measurement is ± 1 psia below 100 psia, and $\pm 1\%$ above 100 psia.

Iron-constantan wire thermocouples, used for temperature measurements, were connected as shown in Figure 13. For highly accurate measurements of temperature, A Rubicon potentiometer, serial number 51194, combined with a Rubicon external galvanometer, was used. Calibration of the thermocouple is described in Appendix B and the results shown in Figure 14.

The heat transfer rate was calculated from the electric power supplied and from the axial temperature gradient.

C. VARIATION OF SURFACE CHARACTERISTICS

1. Surface Roughness

One of the most important variables in nucleate boiling (4) and, as a result of Miller's (21) work, probably a very important variable in transition boiling, is the surface roughness. The term roughness as used in reference to boiling surfaces is misleading since it implies mechanical roughness finish, i.e., the greater the rms roughness height, the greater the roughness. It was visually determined by Westwater et al. (5) that in general bubbles nucleate from cavities on the hot surface, and therefore the "rougher" surface with regard to boiling is that which has the greatest number of cavities of a given size, regardless of the rms roughness finish. Griffith (6) analytically verified the conclusion that the surface cavity size and density adequately describes the effect of surface roughness.

As a result of the above observations, the important surface mechanical characteristic to vary is the cavity size and density on the surface. The fewer the cavities and the smaller the effective cavity radius, the smaller is the heat flux at a given temperature difference.

In the present experiment, it was possible to refinish the surface before each run, since even with chamber A (Figure 9) assembled, chamber B can be disassembled. This exposed the heating surface of Block A, which was then mechanically finished by hand.

The spectrum of surface finishes utilized in these tests range from very fine emery paper at the smooth end, to a lapping compound at the rough extreme. Lapping is generally thought of as producing a smooth finish, and this is true in the conventional mechanical sense. However, a lapping compound contains small pieces of grit suspended in

oil which, when rubbed on a metallic surface, effectively saturate the surface with cavities. This condition, while corresponding to a small rms roughness, is ideal for bubble nucleation.

When specifying the surface finish, it is necessary to include the motion with which the surface is finished; i.e., whether the surface was rubbed in one direction, in two perpendicular directions, or with a circular motion, since this causes a change in the number of cavities. It is of course, also necessary to specify the particle size, both for the emery paper and the lapping compound.

The surface which is described as a "mirror finish" had to be prepared with great care as follows. The emery paper used to prepare the mirror surface was Tufbak 600A. It was rubbed in one direction on the dry metal surface, and alternately cleaned with another piece of the same emery until no scratches were visible on the surface to the naked eye. The finished surface when looked into produced as clear a reflection as a good quality mirror. Great care had to be taken not to scratch the surface, but while it was difficult, the experimental results demonstrate that it was possible to reproduce this surface.

2. Surface Material

In industrial apparatus which utilize boiling heat transfer, the heating surface is probably made from a relatively low thermal conductivity (diffusivity) material such as stainless steel or inconel. It was therefore important to determine the effect, if any, of surface material on the boiling process.

Copper was always used as the base material of the conducting block since its high thermal conductivity minimizes the temperature

drop from the condensing fluid to the test fluid. For most of the test runs, the surface of the copper block was directly used as the boiling surface, after the desired preparation with regard to roughness.

To vary the heating surface material, it was only necessary to solder a 2" D disk of the desired material to the top surface of the copper block. This introduced a slight inaccuracy in the determination of the surface temperature (Appendix C), but otherwise had no effect on the test procedure. The necessity for soldering the materials somewhat limited the choice of materials, but was not prohibitive. It was necessary to check the continuity of the solder to insure excellent thermal contact which would not result in radial temperature gradients. This was done by soldering with great care and examining the joint visually before and after testing. If the solder was not continuous, it was possible to detect this when removing the disk from the copper. The radial temperature measurements also provide a check of the solder integrity.

3. Surface Cleanliness

In addition to specifying the surface roughness and material, it is necessary to specify the method of cleaning the surface prior to a test run. The cleanliness of the surface was important due to its affect on the triple interface configuration by changing the values of the surface free energies. The physical meaning of surface tension and contact angle are discussed in Appendix D. Clean, as used here, refers to the cleanliness, or dirtiness, obtained in practice, and is not meant to imply the surface is perfectly pure. Wiping the surface with a dry rag, a towel saturated with a solvent, or letting the surface

become exposed to condensation of hydrocarbon particles in city air without subsequent wiping, all produce different states of surface "cleanliness," with respect to the values of the various surface free energies.

D. TEST PROCEDURE

1. Preliminary Preparation

The following assembling was normally completed prior to a given series of test runs. The wiring for the thermocouples and the power supply was connected and checked out. Chamber A, assembled and sealed, was insulated with 0.55 lb/ft³ density glass wool, whose thermal conductivity is approximately 0.025 BTU/hr ft °F, by winding a sheet around the vessel to an outside diameter of 7". A hole cut in the insulation made it possible to view the sight glass port. Chamber B was assembled immediately before a specific run so that the boiling surface could be prepared in detail as desired.

Prior to any test runs, a heat loss calibration was performed. The entire experiment was assembled as it would be for a regular test run, with the exception that instead of filling chamber B with the test fluid, it was packed with glass wool insulation. Since the heat transfer through the top surface was negligible under these circumstances, the power required to keep the pressure in chamber B constant must equal the heat loss to the atmosphere. Measurements of the power required as a function of the temperature difference between the fluid in Chamber A and the room were made at various times during the test program. The results of the heat loss calibrations are presented in Figure 15. They show that the data was reproducible within $\pm 5\%$ after reassembling the

experiment, even though copper blocks of slightly different geometry were used.

The entire experiment was supported by a wooden base which provided space for 4" of insulation for the bottom plate.

2. Start Up Procedure

With both the loading port and the valve (Figure 9) open, distilled water is slowly poured into the port until chamber A is completely filled, i.e., until any further addition of water results in a flow out past the valve. The loading port plug is then inserted and sealed.

The boiling test surface, the top of block A, is next prepared as desired with regard to roughness and cleanliness. The choice of material was made prior to assembling chamber A. Immediately after cleaning the boiling surface, chamber B is assembled, sealed, and filled to a depth of 1 - 2" with the test fluid. The reflux condenser is immediately inserted into the top of chamber B recovering all of the test fluid which evaporates.

At this point, the copper block, which is exposed to the atmosphere, is also wrapped with glass wool insulation to a diameter of 7". The upper surface of the insulation is level with the top of seal A.

With the valve wide open, so that atmospheric pressure exists in chamber A, power is supplied to the heating coil. Once the temperature of the water in A attains the boiling point, vapor is emitted from the open valve. The valve is kept open until the liquid level in chamber A, which is observed through the sight glass, divides the sight glass. At this point, there is sufficient liquid in chamber A to always cover the heating coil, and at the same time, the condensing fins are entirely exposed to saturated vapor. The valve is now closed tightly to seal

the saturated mixture of liquid and vapor water in chamber A. Evacuating the chamber in this way insured that essentially no air was present in the completely sealed chamber. After the valve was closed, insulation is wrapped around the valve and pipe.

3. Data Taking Procedure

Enough data points were taken in each run to define the complete boiling curve. In particular, great care was taken to define the location of the burnout point and the minimum. Before recording the instrument readings steady state had to be reached, otherwise the power supplied minus the heat lost to the atmosphere does not equal the heat transferred to the fluid in chamber A. The power input was varied to maintain the output of the thermocouples in the copper block constant, while a thermocouple placed in the side insulation was monitored. Steady state is reached when the variation of the temperature in the insulation with time was negligible. It normally took between 15 to 30 minutes to reach steady state operation when moving from one point to another. In general, data was taken both when increasing and decreasing the temperature difference to check the accuracy of the measurements and search for any hysteresis in the boiling curve. The accuracy of the data depended in part upon the location of the point being recorded on the boiling curve; data taken in the transition region having a greater uncertainty than that taken in the other regions.

4. Shut Down Procedure

When sufficient data had been obtained, the apparatus was shut down in the following order.

- a. Shut off power supply.

- b. Remove insulation from valve, pipe, and copper block.
- c. Slowly open valve, allowing chamber A to depressurize.
- d. Remove the reflux condenser from chamber B, allowing the test fluid to boil away.
- e. Disassemble chamber B.

E. TEST PROGRAM

1. Introduction

The test program had a number of objectives. It obtained information which made it possible to decide whether or not the liquid touches the solid surface in transition boiling. Once the mechanism of heat transfer was established, sufficient data was obtained with which to check the validity of any proposed correlation technique. In the development of analytical results, it was desirable to make specific measurements, evaluating proportionality constants, and substantiating assumptions utilized in the theory. The sum of the information obtained in all the tests provided a consistent, complete picture of transition boiling.

The boiling heat transfer data obtained during the test program are presented in Tables 2 - 16. Each table includes a description of the test fluid, the surface material, the surface roughness, and the surface cleanliness, as well as the estimated accuracy of each data point. The data is also presented in a series of figures, described in the following sections, showing the characteristic boiling curve. A sample calculation indicating the procedure for obtaining the final heat transfer data presented, from the actual measurements, is given in Appendix E.

2. First Series of Tests

a. Effect of Surface Roughness and Cleanliness

Due to the lack of experimental information regarding transition boiling, the initial group of tests were necessarily exploratory in nature. Investigating the effect of the potentially significant variables provided some insight into the phenomenon and as a result suggested what further specific tests should be performed. Each test was in general reproduced at least once.

Runs 2 and 3, summarized in Figure 16, for a mirror finished surface, are characterized by a nucleate boiling regime of relatively small slope located at relatively high temperature difference. The slope of the transition boiling curve is so great that it was impossible to operate here, even with the present experiment. It was, however, possible to locate the minimum with careful operation. The scatter of data in the nucleate region was due to the difficulty of reproducing the exact surface finish. The scatter in the film boiling region was a result of the inaccuracy of the measurements, which become a significant per cent at these low heat inputs.

Runs 4 to 6 in Figure 17, first showed the dramatic change possible in the transition region, even while maintaining the surface material and roughness constant. Before discussing this effect, it is interesting to compare runs 2, 3, and 4, in Figure 18, which show the effect of roughness alone. The important facts to observe are the large shift in the nucleate boiling curve, leading to a large shift in the transition curve, near the burnout point. Also, there is no apparent change in the film boiling curve; the location of the minimum remaining essentially the same. The fact that surface roughness is unimportant

in the film boiling regime, but quite important over most of the transition boiling regime implies that a continuous vapor film does not always cover the surface in the transition regime. This bears more investigation. It is also interesting to note that a good approximation of the transition boiling data is a straight line connecting the burnout point with the minimum point. The burnout heat flux remains approximately constant.

Returning to Figure 17, it was difficult to conceive of the cause of the large change observed. The only difference between run 4 and the other two was the fact that, while in the former the surface was lapped and cleaned with carbon tetrachloride immediately before running, in the latter the surface was tested after oxidation of the copper had occurred and the surface was not cleaned immediately before running.

Figure 19 shows the same effect appearing when utilizing a coarser lapping compound. A slight shift of the nucleate curve occurs due to a change in size and density of surface cavities. Focusing ones attention on the nucleate region of figures 17 and 19, it is observed that whatever is causing the change in the transition region also causes a similar change in the nucleate region. This effect is difficult to see in the nucleate region due to the high slope and could be erroneously interpreted as scatter in the data, which it is not. Drawing the best straight line through the data for the clean surface and comparing it with the best straight line through the data for the oxidized, not cleaned surface, shows a large change in the nucleate region. At a given temperature difference the heat flux for the clean surface is approximately one half that for the other.

In figure 19, the data in the transition region is excellently correlated by a straight line connecting the burnout point with the minimum point. Also, the location of the minimum has remained the same. The value of the burnout heat flux in runs 2 to 10 remained essentially constant, in spite of the large effects in the other sections of the boiling curve, at a value equal to $90,000 \pm 10\%$ BTU/hr ft².

At this point it was not at all clear what caused the change in the transition curve. Presumably it was due to either the effect of the oxide layer, or to the fact that the surface was not cleaned immediately before running. It was possible to isolate which of these effects caused the change by running a test with an oxidized surface, cleaned immediately before running. This was done in run 22, which is shown in Figure 20. The surface was lapped with a circular motion using lapping compound E (grit #120), producing another slight shift in the nucleate boiling curve, due to increasing the density of the surface cavities. Comparing runs 16, 17, 22, and 23 as is done in Figure 20, shows that the oxide has no effect on the boiling curve. This conclusion is valid as long as the oxide thickness is small enough so that the thermal characteristics of the metal surface are those of the pure base metal, as was the case in the above experiments. Use of a block of oxide as the heating surface could still change the boiling curve.

At this point it is well to review the observations and conclusions. Film boiling is not affected by surface roughness. The location of the minimum can be changed by allowing the surface to become contaminated, but provided the surface is clean, the minimum also does not vary. Both

nucleate boiling and transition boiling are affected by surface roughness and surface cleanliness. The burnout heat flux is approximately constant, independent of all surface variables.

b. Effect of Wetting Agent

Returning to the problem of surface cleanliness, it is possible that the copper surface, which was left exposed to the atmosphere, becomes contaminated with dirt particles from the air. The dirty surface would have a different affinity for the boiling fluid, thereby changing the contact angle. This conclusion is supported by the observations of Dunskus (24). It was, however, difficult to believe that changing the contact angle could produce the large effect shown in Figures 17 and 19. To verify the validity of this conclusion a test, run 25, was made in which the surface was prepared as regards material, roughness, and cleanliness exactly as in runs 17 and 23. Once the complete boiling curve had been defined, a couple drops of a known surface active agent (oleic acid) were added to the boiling fluid. The result was a complete change in the boiling process from the quiet mode of low film boiling to the chaos characteristic of the burnout point. In particular, the heat flux increased by a factor of ten. It was not possible to obtain the complete boiling curve under these conditions since the oleic acid apparently gradually disappears from the surface, resulting in the heat flux at a given temperature difference gradually decreasing with time towards the "clean" value. However, two points were measured immediately after adding the oleic acid, which define the general location of the boiling curve in the transition region. The data obtained in run 25 defining the boiling curve, are shown in Figure 20. The effect in the transition region is

the same as observed in the preceding runs. Therefore, surface contaminants are the cause of the change of the minimum.

Due to the method of applying the oleic acid, the question arose whether the change was in the liquid-vapor surface tension or in the contact angle alone. To resolve this question, both of these quantities were measured before and after the addition of a few drops of oleic acid to a pint of n-pentane. The liquid vapor surface tension was measured utilizing the capillary height method described by Harkins (31). The absolute value of the surface tension measured was equal to the value given in the literature (32) within the 5% accuracy of the measurement. As one drop at a time of oleic acid was added to the n-pentane, no observable change of the surface tension occurred. Harkins (33) states that this should be the case.

The contact angle was measured by photographing a drop of liquid n-pentane sitting on a horizontal surface. The estimated accuracy of the measurement and the reproducibility was $\pm 1^\circ$. For pure n-pentane on copper cleaned with CCl_4 , the measured contact angle was 10° . For n-pentane with a slight amount of oleic acid, no contact angle existed; a condition of spreading, discussed in Appendix D, existing. The spreading also occurred for copper left exposed to the atmosphere, confirming the conclusion that the large change in the transition boiling curve was due to a change in surface energy conditions.

c. Discussion

The results of the preceding section are extremely illuminating. The various aspects are therefore discussed in detail below. These results first make it possible to answer the question of whether the

liquid touches the surface. Previous work by other people mentioned in the introduction, and the initial runs in this work, showed that, in general, anything which changed the nucleate boiling curve also changed the transition boiling curve in a similar manner. Since the heat transfer in nucleate boiling is through the solid-liquid boundary, this implied that the liquid must also touch the surface in transition boiling. However, this was not an unequivocal way of proving this conclusion.

The wetting agent data provides a conclusive answer. Contact angle and spreading are phenomenon which can only occur when a triple interface is present (Appendix D). If changing the value of these quantities effects the data, then a triple interface must exist. This could only occur if liquid-solid contact existed, as well as vapor-solid contact. Therefore, since varying the contact angle, caused a change in the transition boiling curve, liquid-solid contact must occur in the transition region.

The value of the minimum heat flux for a clean surface might be called the minimum-minimum, since with a wetting agent added the minimum occurs at higher heat flux, but along the same film boiling curve. The minimum-minimum is independent of surface material and is therefore potentially much more promising analytically. The question of what is the dividing line between a clean surface and a dirty surface in regard to the location of the minimum, is therefore of practical interest. If surfaces are in general clean in this respect, then the minimum-minimum in general occurs.

As a result of the contact angle measurements, it is known that the minimum-minimum exists for contact angles as low as 10° , at least

for n-pentane. In general, engineering surfaces have a contact angle in the neighborhood of 50° (4, 5). Therefore, it appears that the minimum-minimum generally occurs in practice.

It is plausible to suggest that the minimum-minimum will occur as long as any finite value of the contact angle exists, i.e., as long as spreading does not occur. It is difficult to conceive of how a difference of a few degrees of contact angle could cause the large effect observed. However, the change from a condition where a drop statically sits on a surface, to where it rapidly spreads over the surface, is another matter. Assuming the liquid knows what surface condition exists at all times, even in the film boiling region, it is conceivable that a liquid which spreads sufficiently fast on the heating surface might not be entirely driven away. If this was the case, the location of the minimum would depend on the rate of spreading, about which nothing is known, and probably also on the transient thermal characteristics of the heating surface.

In general, it is expected that the minimum-minimum heat flux occurs in practice. This is true for moderate values of the contact angle and is probably true provided spreading does not occur. It is therefore of practical, as well as theoretical, interest to be able to predict the location of the minimum-minimum.

In the above discussion it was assumed that the liquid is always aware of the surface energy conditions, even in the film boiling regime. It is necessary to make this assumption since no hysteresis was observed in the transition boiling curve for any of the tests. Since the location of the minimum for the contaminated surfaces is dependent on the liquid-solid surface energy, the value of this quantity

must be known by the liquid, when decreasing the temperature difference in the film boiling regime, in order for the transition region to be entered. The solid-liquid surface energy could only be established if the liquid touched the surface in film boiling, if only for an instant, so as to not effect the average heat transfer rate.

Borishansky (34) passed an electric current through the liquid and the metal in series. He observed that the circuit was closed at the instant a vapor bubble departed. Physically this says that when the bubble breaks off and the boundary snaps back towards the surface due to the force of surface tension, the boundary actually contacts the surface for an instant. Therefore, the liquid is able to learn what surface condition exists and as the temperature difference is decreased below the critical value at the minimum the liquid begins to remain in contact with the surface, resulting in transition boiling.

3. Final Series of Test Runs

A number of tentative conclusions reached as a result of the first series of test runs require further verification. The independence of the burnout heat flux and the location of the minimum-minimum on the surface material and roughness require more thorough results.

a. Effect of Surface Roughness

Runs 2, 3, 17, and 22 for the two extremes of roughness, mirror finish and circular lapping, verify the above conclusions. However, two additional sets of data, runs 31 and 32, were obtained which provided roughness intermediate between the two extremes. Figure 21 presents the data for n-pentane boiling from a copper surface with the four different roughness finishes. All of the above conclusions are

adequately verified. The gradual minimum shown by the lapped surface is probably due to the fact that in cleaning the surface in the early tests, not enough care was taken to completely remove all the oil which is the base of the lapping compound. This oil acts like a wetting agent leading to the minor effect observed.

In the following tests on different materials, the roughness was varied between the two extremes to further substantiate the above conclusions.

b. Effect of Surface Material

Most boiling experiments are performed using copper heating surfaces, while a large fraction of industrial equipment utilizes materials like stainless steel and inconel. If the thermal properties of the surface material effect the process this is an unfortunate choice, since copper and inconel are at opposite extremes in this respect. A series of tests, runs 34 to 37, were performed with an inconel heating surface for the two extremes of roughness. The results of these tests are shown in figure 22. It is seen that varying the thermal properties by a factor of 25, changes position of the nucleate boiling curve, at least for the lapped surface, a significant amount. There is a slight decrease in the burnout heat flux and a slight increase in the minimum temperature difference, but these changes are not large enough to be of any practical significance. The change in the position of the boiling curve is much greater for the rough surface than for the mirror finished surface.

Nickel, whose thermal properties are between those of copper and inconel, was tested in runs 38 and 39. The results, summarized in

Figure 23, lie much closer to those of copper. Figure 24 compares the boiling curve for the three materials, with all other variables held constant. The conclusions regarding the maximum and minimum are adequately substantiated. The change in the location of the nucleate region is quite significant, the temperature difference necessary to sustain a given heat flux for this finish varying by a factor of two as shown in Figure 25. It must be mentioned again that this change is a function of the particular roughness, e.g., very little difference is observed for the mirror finish surfaces.

c. Effect of Fluid Properties

Since the location of the minimum is essentially only dependent on the fluid properties, it is necessary to have this information available for more than one fluid in order to check any analytical results. Within the limits on power and temperature fixed by the experiment, carbon tetrachloride was satisfactory and provided properties furthest from those of pentane. Runs 19 and 20 determined the location of the boiling curve for lapped copper-carbon tetrachloride as shown in Figure 26.

4. Bubble Diameter Measurements

One of the most critical assumptions it is necessary to make in any analysis of boiling heat transfer concerns the value or equation yielding the bubble diameter. Considering film boiling from a horizontal surface, a plausible assumption for the bubble diameter was made by Zuber (12) which resulted in the following equation

$$D_b = 5.5 \sqrt{\frac{g \cdot \sigma}{g(\rho_L - \rho_V)}} \quad (\text{II-4})$$

Assuming that the bubble departs from the interface due to static forces allows one to utilize the results of Bashforth and Adams (35) yielding the following relation for the bubble diameter.

$$D_b = 3.2 \sqrt{\frac{g \cdot \sigma}{g(\rho_L - \rho_V)}} \quad (\text{II-5})$$

While the constant is different, the fluid property dependency of each of the equations is the same. To determine the exact value of the constant a series of high speed still photographs were taken of both n-pentane and carbon tetrachloride in film boiling. The diameters of bubbles which had just or were just about to depart were measured at various heat fluxes. The results of these measurements are contained in Table 17 and yield the following expression for the bubble diameter in film boiling.

$$D_b = 4.7 \sqrt{\frac{g \cdot \sigma}{g(\rho_L - \rho_V)}} \pm 10\% \quad (\text{II-6})$$

F. RESULTS AND CONCLUSIONS OF EXPERIMENTAL PROGRAM

Due to the fact that the solid liquid surface energy is a very important variable in transition boiling, the liquid must be at least partially in contact with the heating surface. For contact angles generally found in practice, and probably providing any finite value of the contact angle exists, the location of the minimum point of transition boiling is independent of all surface parameters. The

value of the burnout heat flux varies slightly with roughness and material, but the change is not large enough to be of practical significance. It is satisfactory to consider the burnout heat flux independent of the surface conditions. The temperature difference at burnout varies significantly due to the effect of material and roughness on the location of the nucleate boiling curve.

A satisfactory correlation of the data in the transition regime is provided by connecting the burnout point and the minimum point with a straight line on log log graph paper.

The film boiling curve is completely independent of surface conditions, within the accuracy of the experiment. After a bubble breaks off from the liquid vapor interface, the interface snaps back and instantaneously contacts the solid surface. This informs the liquid of the surface conditions, eliminating hysteresis in the transition boiling curve, but does not effect the heat transfer rate in the film boiling regime.

The size of the bubbles which leave the interface in film boiling, measured for the two fluids tested at various heat fluxes, is predicted by Equation (II-6) within $\pm 10\%$.

A summary of the surface independent quantitative results are given below.

Fluid	$(q/A)_{\max}$	$(q/A)_{\min}$	$(\Delta T)_{\min}$
n-pentane	90,000 $\pm 10\%$	3,500 $\pm 10\%$	105° $\pm 10\%$
carbon tetrachloride	100,000 $\pm 10\%$	3,500 $\pm 10\%$	145° $\pm 5\%$

CHAPTER III
THEORETICAL PROGRAM

A. INTRODUCTION

The results of the experimental program show that the transition region is satisfactorily correlated by a straight line on log-log graph paper which joins the burnout point and the minimum point. An analytical expression for the burnout heat flux was derived by Zuber (36) considering a model which assumed the existence of a continuous vapor film in the transition region. While the present work invalidates this assumption, the controlling mechanism proposed by Zuber (36) and the analytical tools utilized can still be applied to the problem. A model of the burnout mechanism, which treats the burnout point as the limit of nucleate boiling, is analyzed in Appendix G, after discussing Taylor-Helmholtz Instability in the following section, which yields a result very similar to the one obtained by Zuber. Combining the semi-empirical correlation of the nucleate boiling regime (10) with the analytical expression for the burnout heat flux, Eq. (A-71), locates the burnout point.

An equation for the minimum heat flux was also derived by Zuber (36) based on a number of assumptions, some of which are verified in the following sections. The detailed analysis of the minimum heat flux is contained in Appendix H, incorporating slightly different assumptions. The resulting equation is identical to Zuber's equation.

The location of the minimum point can be established by combining the expression for the minimum heat flux, Eq. (A-83), with a relation

between the heat flux and the temperature difference in the film boiling regime. A relation of this type was derived by Bromley (14) for both horizontal tubes and vertical surfaces, but none exists for horizontal plates. Therefore, the theoretical program was directed towards an understanding of film boiling from a horizontal surface, and the application of this knowledge to an analysis of the problem. Once a valid expression describing film boiling from a horizontal surface was obtained, the location of the minimum point was defined. Therefore, all the necessary analytical tools are available which define the location of the heat flux versus temperature difference curve in transition pool boiling.

B. TAYLOR-HELMHOLTZ HYDRODYNAMIC INSTABILITY

1. Introduction

The difficulty which arose when attempting to analyze film boiling from a horizontal surface was the fact that the vapor flow geometry was not clear. In particular, the bubble spacing, and orientation with respect to one another had not been defined.

In analyzing film boiling from a horizontal tube one knows that the vapor flows up around the tube, departing as bubbles from the top of the tube. The vapor flow pattern on a horizontal plate was not so obvious. Visual observations by the author of the bubble pattern which exists on a horizontal surface give the impression that the bubbles are located in some type of regular lattice, perhaps hexagonal or square. The photograph shown by Borishansky (34) also exhibits an approximately regular bubble pattern.

Presumably the vapor generated in the vicinity of a given growing

bubble, flows in toward the bubble location, combines, and departs. This process repeats itself continuously, leading to a steady stream of individual bubbles departing from the liquid-vapor interface. If one knew the bubble spacing; i.e., the effective length of the vapor flow path, it would be possible to analyze this process utilizing the conventional approach of Bromley (14). It is demonstrated in the following section that the bubble spacing, and the rate of growth of the bubble are determined, independent of heat transfer effects, by hydrodynamic considerations.

2. Stability of the Interface Between Two Fluids of Different Density

The behavior of an interface separating two fluids of different density when subjected to disturbances, such as the liquid-vapor interface in film boiling, has received considerable attention in the past decade. At the present time it is possible to determine the effect of acceleration, surface tension, viscosity, relative velocity, and finite fluid depth on the interface dynamics.

Taylor (37) first clearly formulated the problem considering only the effect of acceleration and fluid depth. He showed that the interface is unstable; that is, a disturbance will grow with time, if the acceleration is directed from the lighter to the heavier fluid. An example of this is vapor beneath liquid in a gravitational field.

Taylor's analysis of the problem assumes potential flow. The form of the interface disturbance introduced into the first order perturbation analysis is given by the following equation.

$$\begin{aligned} \eta &= \eta_0 e^{-int} \cos mx \\ &= \eta_0 e^{bt} \cos mx \end{aligned} \quad (\text{III-1})$$

The meaning of the various terms in the above equation are defined in the Nomenclature. The wave number, m , is related to the wavelength by the following equation

$$m = \frac{2\pi}{\lambda} \quad (\text{III-2})$$

The result of the above analysis was an expression for n as a function of the fluid properties, the acceleration, and the wavelength. From Eq. (III-1) it is seen that if n is real, the disturbance is periodic in time, and therefore stable. However, if n is imaginary, the disturbance grows exponentially with time. Taylor's results, applied to the case of a liquid resting above a vapor in a gravitational field, state that the interface is unstable for disturbances of all wavelengths.

The first order approximations used in the analysis presumably limit the applicability of the results to the extent that the amplitude of the wave must be much less than the wavelength. However, Lewis (38) experimentally showed that Taylor's theory satisfactorily predicted the growth of the instability as long as the amplitude was less than 0.4λ . The two dimensional analysis was also found to adequately describe the three dimensional physical situation.

The analytical approach used by Taylor has been utilized to solve the problem including the effects of relative velocity parallel to the interface, and surface tension. The analysis and results are summarized by Lamb (39) and Milne-Thompson (40). Section 14.53 of Milne-Thompson presents the general result, from which the expression for n for any particular case can be derived. In particular, it was found that

surface tension tends to stabilize the interface, making disturbances of short wavelength stable, and decreasing the growth rate for long wavelength disturbances.

It has become conventional to refer to those instabilities of the above type which occur in the absence of relative velocity effects as Taylor Instability. When relative velocity is important, the phenomenon is called a Helmholtz Instability.

Bellman and Pennington (41) analytically included the effect of viscosity on Taylor Instability for the case of infinite fluid depth. They found that viscosity does not remove an instability which would otherwise exist; it merely slows the interface growth rate.

The experiments of Allred and Blount (42) serve to confirm the validity of the above analysis. The two dimensional theory adequately describes three dimensional effects, and may be used provided the amplitude is less than 0.4λ .

C. APPLICATION OF TAYLOR-HELMHOLTZ INSTABILITY TO FILM BOILING FROM A HORIZONTAL SURFACE

1. General Result

The general solution of the irrotational flow kinematic equation yields the following relation between wave speed, gravity, surface tension, fluid velocity parallel to the interface, and fluid depth, for the case of a liquid over a vapor (40).

$$m \rho_v (V_v - c)^2 \coth ma + m \rho_l (V_l - c)^2 \coth ma_2 = g \sigma m^2 - g(\rho_l - \rho_v) \quad (\text{III-3})$$

The wave speed, c , is defined by the following relation.

$$c = \frac{n}{m} \quad (\text{III-4})$$

The simplifying assumptions which are valid for film boiling from a horizontal surface in the absence of forced convection are,

$$\begin{aligned} V_2 &= 0 \\ \coth ma_2 &= 1 \end{aligned} \quad (\text{III-5})$$

Combining Eq. (III-3) and (III-5) yields the result,

$$m \rho_v (V_v - c)^2 \coth ma + m \rho_l c^2 = g_0 \sigma m^2 - g(\rho_l - \rho_v) \quad (\text{III-6})$$

The parameter of interest in predicting the growth of the two phase boundary is the coefficient of t in Eq. (III-1); that is, $-in$. This growth coefficient is abbreviated with the letter b in the following sections.

2. Particular Results

A number of simplifying assumptions can be introduced into Eq. (III-6) which make it possible to obtain explicit expressions for c , and therefore b . The equations for the growth coefficient b , which result from specific assumptions are presented below.

- a. Assume the effect of vapor velocity and depth are negligible, i.e.

$$\begin{aligned} V_v &= 0 \\ \coth ma &= 1 \end{aligned} \quad (\text{III-7})$$

Combining Eq. (III-7), (III-6), and (III-4) results in the following expression for b.

$$b = \left[\frac{g(\rho_e - \rho_v)m}{\rho_e + \rho_v} - \frac{g_0 \sigma m^3}{\rho_e + \rho_v} \right]^{1/2} \quad (\text{III-8})$$

- b. Assume the effect of vapor velocity is negligible, and that the vapor thickness is very small, i.e.

$$\begin{aligned} V_v &= 0 \\ \coth ma &= \frac{1}{ma} \end{aligned} \quad (\text{III-9})$$

Combining Eq. (III-9), (III-6), and (III-4) yields

$$b = \left[\frac{g(\rho_e - \rho_v)m}{\rho_e + \rho_v/ma} - \frac{g_0 \sigma m^3}{\rho_e + \rho_v/ma} \right]^{1/2} \quad (\text{III-10})$$

- c. Assume the effect of vapor thickness is negligible, i.e.

$$\coth ma = 1 \quad (\text{III-11})$$

Combine Eq. (III-11), (III-6), and (III-4) to obtain

$$b = \left[\frac{\rho_l \rho_v V_v^2 m^2}{(\rho_l + \rho_v)^2} + \frac{g(\rho_l - \rho_v) m}{\rho_l + \rho_v} - \frac{g_0 \sigma m^3}{\rho_l + \rho_v} \right]^{1/2} \quad (\text{III-12})$$

d. Assume the vapor film is very thin, i.e.

$$\coth ma = \frac{1}{ma} \quad (\text{III-13})$$

Combining Eq. (III-13), (III-6), and (III-4) yields,

$$b = \left[\frac{\rho_l \rho_v V_v^2 m^2}{(\rho_l + \rho_v/ma)^2 ma} + \frac{g(\rho_l - \rho_v) m}{\rho_l + \rho_v/ma} - \frac{g_0 \sigma m^3}{\rho_l + \rho_v/ma} \right]^{1/2} \quad (\text{III-14})$$

3. Application to Film Boiling

Examining the above expressions for b , it is observed that once the fluid properties are fixed, the value of b only depends on the wave number, i.e., the wavelength, of the disturbance. Due to the form of the equations b is real, imaginary, or zero, depending on the particular value of the wave number. If a disturbance occurs whose wavelength corresponds to a real value of b , the interface is unstable, growing at a rate given by Eq. (III-1). The larger the value of b , the greater the growth rate of the boundary. Therefore, the particular

wavelength which becomes visible is that possible wavelength which yields the maximum value of b .

In general, in any mechanical system small disturbances of all wavelengths are present. Therefore the wavelength which is most likely to become visible is that wavelength which maximizes b in the applicable equation. The growth rate of the boundary is then given by Eq. (III-1), with the maximum value of b inserted for ω in. The boundary continues to grow until it ruptures when a bubble departs from the node. The bubble period is therefore established by Eq. (III-1) and the maximum value of b , and the bubble spacing is given by the dominant wavelength, i.e., that wavelength which maximizes b .

Applying one of the above results for b to a particular case serves to illustrate the use and physical interpretation of the stability analysis. Figure 27 is a plot of b vs. m for n -pentane when the effects of finite depth and velocity are neglected, Eq. (III-8). This shows that disturbances of wave number less than 196, or wavelength greater than 5.1×10^{-3} ft, are unstable for the system considered. The dominant wavelength, that which maximizes b , is equal to 8.85×10^{-3} ft, corresponding to m equal to 113. The maximum value of b equals 49 (1/sec). Since the curve in Figure 27 is relatively flat near the maximum, one would expect to observe a spread of wavelengths lying on each side of the maximizing value. Other things being equal, the average wavelength observed should be approximately equal to the maximizing value.

While Eq. (III-8) serves to qualitatively illustrate the application of the stability analysis results to film boiling, it has not yet been established which expression for b provides the correct

quantitative results; that is, what simplifications are valid.

Utilizing the results of Bellman and Pennington (41) one can show that viscosity has a completely negligible effect on the interface growth for n-pentane in particular, and all fluids of practical interest to film boiling, in general.

The effect of vapor film thickness and velocity were not obviously negligible. Calculations based on the experimental results indicate that the film thickness is of the order of 10^{-4} ft, and the vapor velocity is of the order of 1 ft/sec.

To determine the importance of vapor film thickness and vapor velocity on the interface behavior in film boiling, b was plotted vs. m using Eq. (III-12) and (III-14). The value of the vapor film thickness was assumed constant at the average value computed from the experimental results. The vapor velocity varies considerably within the film as shown by Eq. (A-52) in Appendix F. To evaluate the importance of vapor velocity a characteristic value of the velocity, evaluated at a radius from the bubble equal to $\lambda/3$, was used, which resulted in the following equation for the vapor velocity.

$$V_v = .0717 \frac{k_{vf} \Delta T \lambda}{\rho_{vf} \Delta h a^2} = .45 \frac{k_{vf} \Delta T}{\rho_{vf} \Delta h a^2 m} \quad (\text{III-15})$$

The choice of the radius at which the velocity was evaluated is somewhat arbitrary, therefore the results should not be quantitatively interpreted. However, the resulting effect of vapor velocity on the

instability were accurate enough to indicate qualitative effects and to suggest what assumptions are reasonable.

It is interesting to note that the vapor velocity is directly proportional to the temperature difference. Referring to Eq. (III-14) it is seen that as the vapor velocity increases, b increases. Therefore, the growth rate of the boundary tends to increase as the temperature difference is increased. Combining Eq. (III-15) with Eq. (III-12) and (III-14) yields the following expressions.

Neglecting the effect of vapor film thickness:

$$b = \left[\frac{.203 \rho_l \rho_v}{(\rho_l + \rho_v)^2} \left(\frac{k_{vf} \Delta T}{\rho_{vf} \Delta h a^2} \right)^2 + \frac{g(\rho_l - \rho_v) m}{\rho_l + \rho_v} - \frac{g_0 \nu m^3}{\rho_l + \rho_v} \right]^{1/2} \quad (\text{III-16})$$

Including the effect of vapor film thickness:

$$b = \left[\frac{.203 \rho_l \rho_v}{(\rho_l + \rho_v / ma)^2} \left(\frac{k_{vf} \Delta T}{\rho_{vf} \Delta h a^2} \right)^2 \frac{1}{ma} + \frac{g(\rho_l - \rho_v) m}{\rho_l + \rho_v / ma} - \frac{g_0 \nu m^3}{\rho_l + \rho_v / ma} \right]^{1/2} \quad (\text{III-17})$$

The values of the vapor film properties used were those collected by Bromley (14), which are presented in Figures 28 - 34. The results of plotting b vs. m for various temperature differences characteristic of film boiling are as follows. When neglecting vapor film thickness in Eq. (III-16), velocity has a negligible effect on the value of b for

temperature differences less than 500 °F. However, calculating b from Eq. (III-17), which includes the effect of film thickness, yields values of b which show a significant effect of vapor velocity, and therefore film thickness, at values of temperature difference equal to only a few hundred degrees. The results of the latter calculation, for n-pentane, are presented in Figure 35.

Referring to Figure 35, it is seen that while vapor velocity affects the bubble spacing and growth rate at moderate values of the temperature difference in film boiling, as the minimum temperature is approached the effect of vapor velocity becomes negligible. The effect of vapor film thickness, when velocity is neglected, is also shown in Figure 35. Under these conditions, it is reasonable to neglect the effect of vapor film thickness on the bubble spacing and growth rate. In particular, the value of m , at maximum b , which establishes the bubble spacing is not noticeably changed. Therefore, in the neighborhood of the minimum heat flux it is reasonable to assume that Eq. (III-8) specifies the bubble spacing and growth rate. Zuber (36) first proposed these assumptions in his analysis of the minimum heat flux, which is presented with some modifications in Appendix H.

4. Discussion

The bubble spacing in film boiling from a horizontal surface is fixed by the value of the wavelength which maximizes b in the appropriate equation. Near the minimum heat flux it is reasonable to neglect the effect of vapor velocity and vapor film thickness, therefore Eq. (III-8) describes the behavior of the two phase interface.

Once the two phase boundary begins to grow, the growth continues until a bubble departs from the node. Bubble departure has been observed by the author, and is shown in the photographs of Santangelo (25), to occur when the amplitude is approximately equal to the bubble diameter. After the bubble departs, the interface snaps back toward the solid surface, providing the disturbance necessary to start the growth of the neighboring antinode. For neighboring locations on the interface to alternately grow and collapse, the bubble pattern must be visualized as a square lattice. At any time two bubbles are growing in any λ^2 area.

D. ANALYSIS OF FILM BOILING FROM A HORIZONTAL SURFACE

1. Introduction and Assumptions

As a result of the preceding section and the experimental results, it is apparent that the bubble spacing in film boiling from a horizontal surface is fixed by hydrodynamic considerations. A list of the assumptions utilized in the analysis and a short discussion of their validity follows.

- a. Near the minimum heat flux, the bubble spacing is unaffected by the vapor velocity and the vapor film thickness. Referring to Figure 35, it is seen that there is a negligible change in the value of m which maximizes b at values of the temperature difference near the minimum. This same assumption is utilized in the analysis of the minimum heat flux in Appendix H, and leads to a correct result.

- b. The vapor flows radially into the bubble. In the vicinity of the bubble this is probably an excellent approximation and this is where the vapor velocity and therefore the viscous shear stress is greatest.
- c. The momentum forces are negligible in comparison with the viscous forces. Calculation of the Reynolds Number shows this to be an excellent assumption
- d. The flow is laminar. The Reynolds Number calculation also verifies this statement.
- e. The change in height of the vapor-liquid boundary between the bubbles is negligible compared to the average height of the bubble above interface. Since the bubble dimensions are two orders of magnitude greater than the film thickness, this must be valid.
- f. The viscous drag of the liquid vapor interface on the vapor flow lies between zero and the value corresponding to a stationary boundary. These are the two extremes possible without forced convection.
- g. The kinetic energy of the vapor is negligible in comparison with the enthalpy change. This assumption can be shown to be accurate to much better than 1%.
- h. The average value of the vapor properties are equal to those at the average temperature of the hot surface and

the saturated liquid. This is not quite correct, but will not introduce a great enough error to invalidate the results. Also, evaluating the experimental constant on this basis eliminates most of the error.

- i. Heat is transferred through the vapor film by conduction. Radiation is negligible at temperature differences less than 1000 °F. The flow is laminar.
- j. The vapor flowing to any one bubble is generated in an area equal to $\lambda^2/2$. The results of the stability analysis applied to three dimensions requires this condition.
- k. The two dimensional stability analysis may be applied to the three dimensional problem. The experimental investigations of Taylor Instability (38 and 42) have verified this assumption. The only change which might have been required is the value of the constant, and this change was less than the experimental accuracy.

2. Analysis

The actual shape of the liquid-vapor interface, and the physical model used in the analysis are shown in Figure 37. For one dimensional viscous flow in cylindrical coordinates, the momentum equation reduces to the following.

$$\frac{dp}{dr} = \frac{\beta \mu_f V_v}{g_0 a^2} \quad (\text{III-18})$$

The constant, β , is equal to 12 if the vapor-liquid boundary has the same effect as a stationary wall, and 3 if there is no shear stress at the boundary (14).

The vapor velocity varies with radius according to the following equation, derived in Appendix F.

$$V_v = \frac{k_{vf} \Delta T}{\rho_{vf} \Delta h a^2} \frac{\lambda^2/2 - \pi r^2}{2 \pi r} \quad (\text{III-19})$$

Combining Eq. (III-19) with (III-18) yields:

$$dp = \frac{\beta \mu_f k_{vf} \Delta T}{g_0 a^3 \rho_{vf} \Delta h} \frac{\lambda^2/2 - \pi r^2}{2 \pi r} dr \quad (\text{III-20})$$

The pressure difference required to sustain the flow is obtained by integrating Eq. (III-20) from r_1 , where $p = p_1$, to r_2 , where $p = p_2$. Referring to Figure 37, it is seen that r_1 equals the bubble radius which is obtained from the experimental measurements, Eq. (II-3)

$$r_1 = \frac{D_b}{2} = 2.35 \sqrt{\frac{g_0 \sigma}{g(\rho_l - \rho_v)}} \quad (\text{III-21})$$

The radius r_2 , as a result of assumption j is obtained from the following expression.

$$\pi r_2^2 = \frac{\lambda^2}{2} \quad (\text{III-22})$$

The appropriate wavelength is obtained from Eq. (III-8), as a result of assumption a. The wavelength which grows the fastest, and therefore dominates, is that which maximizes b , where for this case b is given by

$$b = -in = \left[\frac{g(\rho_e - \rho_v)m}{\rho_e + \rho_v} - \frac{g_0 \sigma m^3}{\rho_e + \rho_v} \right]^{1/2} \quad (\text{III-23})$$

Differentiating Eq. (III-23) with respect to m and solving for the value which maximizes b , yields the following result.

$$m^* = \left[\frac{g(\rho_e - \rho_v)}{3g_0\sigma} \right]^{1/2} = \frac{2\pi}{\lambda^*} \quad (\text{III-24})$$

Eq. (III-20) is now integrated and combined with Eq. (III-21), (III-22), and (III-24) to yield the required pressure difference.

$$P_2 - P_1 = \frac{8\beta}{\pi} \frac{\mu_f k_{vf} \Delta T}{g_0 a^4 \rho_{vf} \Delta h} \frac{g_0 \sigma}{g(\rho_e - \rho_v)} \quad (\text{III-25})$$

This pressure difference is supplied by the difference in gravity head. Referring to Figure 37, at a height δ above the film, the pressure is independent of radius and equal to p_0 . The following relations exist between p_0 , p_1 and p_2

$$P_2 - P_0 = \rho_2 \frac{g}{g_0} \delta \quad (\text{III-26})$$

$$P_1 - P_0 = \rho_v \frac{g}{g_0} \delta + \frac{2\sigma}{R} \quad (\text{III-27})$$

Where the second term on the right in the latter equation takes into account the pressure difference due to the curvature of the bubble and the surface tension. Solving the above two equations for the pressure difference gives,

$$P_2 - P_1 = \delta (\rho_2 - \rho_v) \frac{g}{g_0} - \frac{2\sigma}{R} \quad (\text{III-28})$$

The radius of curvature R is equal to the bubble radius given by E. (III-21). It is reasonable to assume that δ , the average height of the bubble above the vapor film, is proportional to the bubble diameter, where the proportionality constant must be less than one. Borishansky (34) has measured the proportionality constant, with the following result.

$$\delta = .68 D_b = 3.2 \sqrt{\frac{g_0 \sigma}{g(\rho_2 - \rho_v)}} \quad (\text{III-29})$$

Combining Eq. (III-28), (III-29), and (III-21) gives for the available pressure difference

$$p_2 - p_1 = 2.34 \frac{g}{g_0} (p_2 - p_v) \sqrt{\frac{g_0 \sigma}{g(p_2 - p_v)}} \quad (\text{III-30})$$

Equating Eq. (III-35) to Eq. (III-30), and solving for the vapor film thickness between the bubbles yields,

$$a = \left[\frac{1.09 \beta \mu_f k_{vf} \Delta T}{\Delta h \rho_{vf} g(p_2 - p_v)} \sqrt{\frac{g_0 \sigma}{g(p_2 - p_v)}} \right]^{1/4} \quad (\text{III-31})$$

The average vapor film thickness for the entire surface which gives the same heat transfer rate as the above, is equal to Eq. (III-31) multiplied by the ratio of the total surface area to the area between the bubbles, yielding the result below.

$$a = 1.4 \left[\frac{1.09 \beta \mu_f k_{vf} \Delta T}{\Delta h \rho_{vf} g(p_2 - p_v)} \sqrt{\frac{g_0 \sigma}{g(p_2 - p_v)}} \right]^{1/4} \quad (\text{III-32})$$

Incorporating the two extreme values of β in the result and solving for the vapor film thickness yields

$$a = \begin{matrix} 2.6 \\ \text{or} \\ 1.9 \end{matrix} \left[\frac{\mu_f k_{vf} \Delta T}{\Delta h \rho_{vf} g(p_2 - p_v)} \sqrt{\frac{g_0 \sigma}{g(p_2 - p_v)}} \right]^{1/4} \quad (\text{III-33})$$

Evaluating the constant from the experimental results gives the final correlation equation

$$a = 2.35 \left[\frac{\mu_f k_{vf} \Delta T}{\Delta h \rho_{vf} g (\rho_2 - \rho_v)} \sqrt{\frac{g_0 \sigma}{g (\rho_2 - \rho_v)}} \right]^{1/4} \quad (\text{III-34})$$

A heat transfer coefficient may be defined by use of the following equations.

$$q = \frac{k_{vf}}{a} A \Delta T \equiv h A \Delta T \quad (\text{III-35})$$

Combining Eq. (III-35) with (III-34) and solving for h yields

$$h = 425 \left[\frac{k_{vf}^3 \Delta h \rho_{vf} g (\rho_2 - \rho_v)}{\mu_f \Delta T \sqrt{\frac{g_0 \sigma}{g (\rho_2 - \rho_v)}}} \right]^{1/4} \quad (\text{III-36})$$

3. Discussion

It is interesting to compare the above result with that of Bromley (14) for horizontal tubes which is given below

$$h = .62 \left[\frac{k_{vf}^3 \Delta h \rho_{vf} g (\rho_L - \rho_v)}{\mu_f \Delta T D} \right]^{1/4} \quad (\text{III-37})$$

The major difference is the substitution of $\sqrt{\frac{\rho_L \sigma}{g(\rho_L - \rho_v)}}$ for the tube diameter D . These are the geometrical scale factors for horizontal plates and tubes, respectively. From dimensional analysis this change might have been predicted. In both equations the experimental value of the constant was the average of the values obtained utilizing the extreme values of β . The similarity between Eq. (III-36) and (III-37) provides added confidence in the validity of Eq. (III-36), since Bromley's equation has been thoroughly verified.

Presumably Eq. (III-36) is only valid in the neighborhood of the minimum since the assumed bubble spacing only applies there. It is suspected that the range of practical application is larger than implied due to the small influence of the characteristic length on the heat transfer coefficient. Eq. (III-36) probably applies to temperature differences as high as 1000°. This remains to be verified.

E. ANALYSIS OF THE TEMPERATURE DIFFERENCE AT THE MINIMUM HEAT FLUX

The results of the preceding section, combined with the results of Appendix H, make it possible to predict the temperature difference at the minimum for fluid-surface combinations with finite values of contact angle.

The equation for the minimum temperature difference may be

written as follows from the heat conduction equation

$$(\Delta T)_{\min} = \frac{(q/A)_{\min}}{(h)_{\min}} \quad (\text{III-38})$$

The heat flux at the minimum is given by Eq. (A-83) in Appendix H.

$$(q/A)_{\min} = .09 \rho_{vf} \Delta h \left[\frac{q(\rho_2 - \rho_v)}{\rho_2 + \rho_v} \right]^{1/2} \left[\frac{q_0 \sigma}{q(\rho_2 - \rho_v)} \right]^{1/4} \quad (\text{III-39})$$

Combining Eq. (III-39), (III-38), and (III-36) yields the following expression for the minimum temperature difference.

$$(\Delta T)_{\min} = .127 \frac{\rho_{vf} \Delta h}{k_{vf}} \left[\frac{q(\rho_2 - \rho_v)}{\rho_2 + \rho_v} \right]^{2/3} \left[\frac{q_0 \sigma}{q(\rho_2 - \rho_v)} \right]^{1/2} \left[\frac{\mu_F}{q_0(\rho_2 - \rho_v)} \right]^{1/3} \quad (\text{III-40})$$

The agreement between the experimental results and the temperature difference predicted by Eq. (III-40) is given below. The pressure is one atmosphere.

Fluid	ΔT_{\min} measured (°F)	ΔT_{\min} predicted (Eq. III-40) (°F)
n-Pentane	105 ± 10%	98
Carbon Tetrachloride	145 ± 10%	153

CHAPTER IV

CONCLUSION

A. DISCUSSION

It is concluded that there are only two distinct regimes of boiling heat transfer. In nucleate boiling the heat is transferred directly from the solid heating surface to the liquid. In film boiling the heat is conducted through a vapor film to the liquid. Transition boiling is a combination of nucleate boiling and film boiling over that range of temperature difference where neither is stable. Therefore, the term transition boiling is appropriate since this portion of the boiling curve is a gradual transition from stable steady nucleate boiling to stable steady film boiling.

The maximum heat flux of transition boiling, which is also the maximum heat flux of nucleate boiling, is a result of a Helmholtz Instability. That is, the vapor generated by the maximum heat flux corresponds to the maximum counterflow of vapor and liquid normal to the heating surface which can occur in steady flow and remain stable.

The minimum heat flux of transition boiling, which is also the minimum heat flux of film boiling, is a result of Taylor Instability. That is, the vapor generated by heat transfer through the vapor film, below a certain temperature difference, is not great enough to supply the vapor demanded by the growth and bubble departure rates of the liquid-vapor boundary, which are determined by Taylor Hydrodynamic Instability.

At temperature differences within the transition region the amount of vapor generated by film boiling is too small to support

the vapor film, and the amount of vapor generated by nucleate boiling is too great to allow sufficient liquid to reach the heating surface in steady flow. Therefore, each of these boiling heat transfer mechanisms probably alternately occur at a given location on the heating surface. Heat is transferred through a vapor film at a rate which is not great enough to generate the vapor mass flow necessary to support the film, therefore the film collapses. Heat is next transferred directly to the liquid, which contacts the surface when the vapor film collapses, generating vapor at such a high rate that the liquid necessary to sustain the heat transfer-vapor generation rate is unable to reach the surface. Therefore, a vapor blanket once again forms. This combination of unstable fluid mechanics, and the resulting heat transfer, continues indefinitely at any given value of the temperature difference within the transition region.

As the temperature difference approaches the value at the minimum heat flux, film boiling becomes more stable and nucleate boiling becomes more unstable, where the relative stability is determined by the amount of time it takes for the given mode of heat transfer to collapse. That is, the amount of vapor generated by heat conduction through the vapor film becomes almost great enough to support the film. And the amount of vapor generated by nucleate boiling is much greater than the maximum steady state value allowed by Helmholtz Hydrodynamic Instability, resulting in a rapid collapse of the nucleate mode of boiling. Therefore, as the temperature difference approaches the value at the minimum, the fraction of time during which film boiling exists increases until, at the minimum, film boiling is stable and exists steadily. The reverse reasoning applies

when approaching the temperature difference at the maximum. That is, nucleate boiling becomes more stable and film boiling less stable.

In summary, it is concluded that transition boiling is a combination of unstable film boiling and unstable nucleate boiling, each of which alternately exists at a given location on the heating surface. The variation of average heat transfer rate with temperature difference is probably primarily a result of the change in the fraction of time with which each boiling regime exists at a given location.

B. SUMMARY OF RESULTS AND CONCLUSIONS

1. Experimental

- a. Since contact angle is an important variable in transition boiling, liquid-solid contact occurs, as well as vapor-solid contact.
- b. For contact angles of commercial importance, and probably provided spreading of the liquid on the heating surface does not occur, the location of the minimum point is independent of surface material and roughness. The minimum heat flux attained in these circumstances is the minimum-minimum heat flux, higher values occurring if spreading takes place.
- c. All of the variables which affect nucleate boiling affect transition boiling in the same qualitative way. The result is a change in the slope of the transition boiling curve.

- d. The maximum (burnout) heat flux is, to all practical significance, independent of surface material, roughness, and cleanliness.
- e. The nucleate boiling heat transfer coefficient can be changed by a factor of five due to surface roughness variations.
- f. The nucleate boiling heat transfer coefficient can be changed by a factor of two due to surface material variations.
- g. The film boiling portion of the boiling curve is independent of surface material, cleanliness, and roughness provided that the roughness height is less than the film thickness.
- h. The relation between heat flux and temperature difference in the transition region is correlated by a straight line on log-log graph paper which connects the burnout point with the minimum point.
- i. The measured quantitative parameters which are independent of surface characteristics for the two fluids tested are:

	$(q/A)_{\max}$ (BTU/hr ft ²)	$(q/A)_{\min}$ (BTU/hr ft ²)	$(\Delta T)_{\min}$ (°F)
n-pentane	90,000 ± 10%	3,500 ± 10%	105 ± 10%
carbon tetrachloride	100,000 ± 10%	3,500 ± 10%	145 ± 5%

2. Theoretical

- a. It is quantitatively reasonable to neglect the effect of vapor velocity and film thickness on the liquid-vapor boundary behavior in film boiling near the minimum temperature difference.
- b. An analytical expression, Equation (II-6), is derived which predicts the heat transfer coefficient for film pool boiling from a horizontal surface within $\pm 10\%$.
- c. Combining the analytical expression for the minimum heat flux with the above expression for the heat transfer coefficient, yields an expression for the temperature difference at the minimum-minimum which agrees with the experimental results within $\pm 10\%$.

NOMENCLATURE

Capital Letters

A	Area (ft ²)
C	Constant
D	Diameter (ft)
E	Internal energy (BTU)
F	Force (lb.)
I	Electrical current (amp.)
R	Radius of curvature (ft)
S	Entropy (BTU)
T	Temperature (°F)
v	Velocity (ft/sec)
W	Power (watts)

Lower Case Letters

a	vapor film thickness (ft)
b	-in growth coefficient (1/sec)
c	Wave speed (ft/sec)
c _p	specific heat at constant pressure (BTU/lb _m °F)
g	Acceleration of gravity (ft/sec ²)
g _o	Conversion factor 32.2 (lb _m ft/lb sec ²)
h	Heat transfer coefficient (BTU/hr ft ² °F)
Δ h	Average enthalpy difference between vapor and liquid (BTU/lb _m)
k	Thermal conductivity (BTU/hr ft °F)
l	Length (ft)
m	Wave number (ft)

n	Wave frequency (1/sec)
p	Pressure (lb/ft ²)
q	Heat transfer rate (BTU/hr ft ²)
r	Radius (ft)
t	Time (sec)
w	Flow rate (lb _m /sec)
x	Length coordinate (ft)
z	Height in gravitational field (ft)

Greek Letters

α	Thermal diffusivity (ft ² /hr)
β	Constant, Eq. (III-18)
δ	Average bubble height (ft)
Δ	Change or difference
η	Distance perpendicular to liquid-vapor interface (ft)
λ	Wavelength (ft)
μ	Vapor viscosity (lb/hr ft)
ρ	Density (lb _m /ft ³)
σ	Surface tension (lb/ft)
τ	Bubble period (sec)
θ	Contact angle (degree)

Subscripts

atm Atmosphere
b Bubble
f Film
j Jet
l Liquid
m Mass
max Maximum
min Minimum
net Net
o Initial or reference value
s Surface, solid
v Vapor
w Wire

Superscript

* Maximum or maximizing

BIBLIOGRAPHY

1. Nukiyama, S., Soc. Mech. Eng. Japan, Vol. 37, No. 206, 1934, p. 367.
2. Farber, E. A. and R. L. Scorah, "Heat Transfer to Water Boiling Under Pressure," A.S.M.E. Trans., Vol. 70, No. 64, May 1948, p. 369-384.
3. Jakob, M., Heat Transfer, Vol. I, John Wiley and Sons, Inc., New York, 1955.
4. Corty, C. and A. S. Foust, "Surface Variables in Nucleate Boiling," A.I.Ch.E. Heat Transfer Symposium, Preprint No. 1, St. Louis, Mo., December 1953.
5. Clark, H. H., P. S. Streng, and J. W. Westwater, "Active Sites for Nucleate Boiling," A.I.Ch.E. - A.S.M.E. 2nd National Heat Transfer Congress, Preprint No. 13, Chicago, Ill., August 1958.
6. Griffith, P. and J. D. Wallis, "The Role of Surface Conditions in Nucleate Boiling," A.S.M.E. - A.I.Ch.E. Third National Heat Transfer Conference, Preprint No. 106, Storrs, Connecticut, August 1959.
7. Forster, H. K. and N. Zuber, "Growth of a Vapor Bubble in a Superheated Liquid," J. of Applied Physics, Vol. 24, 1953, p. 474-478.
8. Griffith, P., "Bubble Growth Rates in Boiling," A.S.M.E. Trans., Vol. 80, 1958, p. 721-722.
9. Bankoff, S. A. and R. D. Mikesell, "Growth of Bubbles in a Liquid of Initially Non-Uniform Temperature," A.S.M.E. Paper 58-A-105.
10. Rohsenow, W. M., "A Method of Correlating Heat Transfer Data for Surface Boiling of Liquids," A.S.M.E. Trans., August 1952, p. 969-976.
11. Kutateladze, S. S., "A Hydrodynamic Theory of Changes in the Boiling Process Under Free Convection Conditions," Izv. Akad. Nauk. SSSR, Otd. Tekh. Nauk, No. 4, 1951, p. 529-536.
12. Zuber, N. and M. Tribus, "Further Remarks on the Stability of Boiling Heat Transfer," Report No. 58-5, U.C.L.A., Dept. of Eng., January 1958.
13. Borishansky, V. M., "Influence of Pressure and Properties of the Liquid on the Cessation of Film Boiling with Free Convection in a Large Space," in Problems of Heat Transfer During a Change of State by S. S. Kutateladze, 1953, p. 101, AEC-tr-3405.

14. Bromley, L. A., "Heat Transfer in Stable Film Boiling," Chem. Eng. Prog., Vol. 46, No. 5, May 1950, p. 221-227.
15. Westwater, J. W., "Boiling of Liquids," Advances in Chemical Engineering, Academic Press, Inc., New York, 1956.
16. Rohsenow, W. M., Heat Transfer - A Symposium, U. of Michigan, 1952, p. 101.
17. Drew, T. B. and A. C. Mueller, A.I.Ch.E. Trans., Vol. 33, 1937, p. 449.
18. Braunlich, R. H., "Heat Transfer to Boiling Liquids Under Vacuum," M.S. Thesis, Chem. Eng. Dept., Mass. Inst. of Tech., 1941.
19. Kaulakis, A. F. and L. M. Sherman, S.B. Thesis, Chem. Eng. Dept., Mass. Inst. of Tech., 1938.
20. McAdams, W. H., Heat Transmission, Ch. 14, McGraw Hill Book Co., Inc., New York, 1954.
21. Miller, L. B., "The Transition Region of Boiling," M.S. Thesis, Dept. of Chem. and Chem. Eng., U. of Illinois, 1955.
22. Pramuk, F. S., "Effect of Agitation on Metastable Boiling," M.S. Thesis, Dept. of Chem. and Chem. Eng., U. of Illinois, 1955.
23. Perkins, A. S., "The Critical Region of Boiling," M.S. Thesis, Dept. of Chem. and Chem. Eng., U. of Illinois, 1957.
24. Dunskus, T., "Effect of Trace Additives on Boiling Heat Transfer," M.S. Thesis, Dept. of Chem. and Chem. Eng., U. of Illinois, 1957.
25. Westwater, J. W. and J. G. Santangelo, "Photographic Study of Boiling," Ind. Eng. Chem., Vol. 47, August 1955, p. 1605.
26. Ellison, M. E., "A Study of the Mechanism of Boiling Heat Transfer," Memorandum No. 20-88, Jet Prop. Lab., Cal. Inst. of Tech., March 1954.
27. Rohsenow, W. M. and P. Griffith, "Correlation of Maximum Heat Flux Data for Boiling of Saturated Liquids," A.I.Ch.E. - A.S.M.E. Heat Transfer Symposium, Louisville, Ky., Preprint No. 9, March 1955.
28. Keenan, J. H., Thermodynamics, John Wiley and Sons, New York, 1953, p. 479-484.
29. Harkins, W. D., The Physical Chemistry of Surface Films, Reinhold Publishing Co., New York, 1954, p. 6, 41, 80, 175.
30. Gibbs, J. W., Collected Works Vol. I, Longmans, 1931, p. 326.
31. Harkins, W. D., Ibid., p. 64.

32. Cichelli, M. T. and C. F. Bonilla, "Heat Transfer to Liquids Boiling Under Pressure," A.I.Ch. E. Trans., Vol. 41, December 1945, p. 755.
33. Harkins, W. D., Ibid., p. 284.
34. Borishansky, V. M., "Heat Transfer to a Liquid Freely Flowing Over a Surface Heated to a Temperature Above the Boiling Point," in Problems of Heat Transfer During a Change of State by S. S. Kutateladze, 1953, AEC-tr-3405.
35. Bashforth, F. and J. Adams, Capillary Action, Cambridge, England, 1883.
36. Zuber, N., "Hydrodynamic Aspects of Boiling Heat Transfer," Ph.D. Thesis, Dept. of Eng., U.C.L.A., June 1959.
37. Taylor, G. I., "The Instability of Liquid Surfaces When Accelerated in a Direction Perpendicular to Their Plane," I, Proc. Royal Soc. London, A-201, 1950, p. 192.
38. Lewis, D. J., "The Instability of Liquid Surfaces When Accelerated in a Direction Perpendicular to Their Plane," II, Proc. Royal Soc. London, A-202, 1950, p. 81.
39. Lamb, H., Hydrodynamics, Dover Publications, New York, 1945, p. 455.
40. Milne-Thompson, L. M., Theoretical Hydrodynamics, The Macmillan Company, New York, 1950, p. 371.
41. Bellman, R., and R. H. Pennington, "Effects of Surface Tension and Viscosity on Taylor Instability," Quar. Appl. Math., Vol. 12, 1954, p. 151.
42. Allred, J. C. and G. H. Blount, "Experimental Studies of Taylor Instability," U. of Calif. Los Alamos Laboratory, Report LA-1600, February 1, 1954.
43. Bromley, L. A., "Heat Transfer in Stable Film Boiling," Ph.D. Thesis, Dept. of Chem., U. of California, Berkeley, Calif., June 1948.
44. Staniszewski, B. E., Personal Communication, Mass. Inst. of Tech., 1959.
45. Sommerfeld, A., Mechanics of Deformable Bodies, Academic Press, 1950, p. 9.
46. Lord Rayleigh, Theory of Sound, Dover Publications, New York, 1945, p. 343-365.
47. Jacob, M., Heat Transfer, Vol. I, John Wiley and Sons, New York, 1955, p. 630.

APPENDIX A
HEATER DESIGN

1. Nomenclature

A	wire surface area (ft ²)
D _w	wire diameter (ft)
I	electrical current (amp.)
J	conversion factor 0.293 (watt hr/BTU)
L	wire length (ft)
W	electrical power (watt)
R	wire total electrical resistance (ohms)
V	voltage (volts)
q/A	heat flux (BTU/hr ft ²)
$\rho = \frac{R}{L}$	electrical resistance per unit length ($\frac{\text{ohms}}{\text{ft}}$)
Ω	ohms

2. Specifications

- a. The maximum current allowed by the variac is 9 amp.

$$I_{\max} = \frac{V_{\max}}{R} \leq 9 \quad (\text{A-1})$$

- b. The power should be as high as possible, while utilizing the available voltage supply, where the power output is given by

$$P = \frac{V^2}{R} \quad (\text{A-2})$$

Therefore the resistance should be as low as possible.

- c. The power generated within the wire must correspond to a heat flux less than 300,000 BTU/hr ft², therefore

$$(I^2R)_{\max} \leq 300,000 \pi D_w L J \quad (A-3)$$

- d. The coiled wire must be structurally stiff enough to support itself and must fit within a volume approximately equivalent to a cube 2" on a side.

3. Analysis

Combining Eq. (A-1) and (A-2) yields the required value for the wire resistance.

$$R = \frac{V_{\max}}{9} = \frac{115}{9} = 12.8 \Omega \quad (A-4)$$

Eq. (A-3) may be written in the following way.

$$\frac{J}{D} \leq \frac{300,000 \pi J}{I_{\max}^2}$$

which, when the values for J and I_{max} are inserted, yield the requirement for an acceptable heating wire; i.e.

$$\frac{J}{D} \leq 3410 \frac{\text{ohms}}{\text{ft}^2} \quad (A-5)$$

The nominal resistance and diameter of Chromel-A heating wire is given in the following table.

TABLE A-1

CHROMEL-A HEATING WIRE SPECIFICATIONS

Wire Gauge	D_w in	D_w 10^{-3} ft	ρ ohms/ft	ρ/D_w ohms/ft ²	$L = \frac{12.8}{\rho}$ ft
20	0.032	2.67	0.632	236	20.3
22	0.025	2.08	1.02	490	12.55
24	0.020	1.67	1.60	960	8.0
26	0.0159	1.325	2.59	1950	4.95
28	0.0126	1.05	4.01	3820	3.20
30	0.010	0.833	6.52	7820	1.95

The shortest wire which satisfies Eq. (A-5) is 26 gauge, which is therefore chosen.

4. Heater Assembly

The heater is assembled in the following steps.

- a. Tightly wind two 30" lengths of #26 Chromel-A wire on 0.2" diameter tubing.
- b. Stretch each coil to a free length of 4 1/2" to 5", where the spacing between the windings is approximately 0.1".
- c. Solder the ends of the wires to short sections of copper lead wire and attach to a teflon base in series.

The resulting heater, 2 1/2" high and fitting within a 2" D circular base, is shown in Figure 8. When tested in water at atmospheric pressure with a current of 10 amps, operation was successful.

APPENDIX B
THERMOCOUPLE CALIBRATION

Thermocouples of iron and constantan were used for temperature measurements. These particular metals were selected for their high thermal emf output per degree of temperature difference and stability over the temperature range anticipated.

The thermocouples were calibrated in the Heat Transfer Laboratory, utilizing the standard calibration devices available. Data was taken with the same potentiometer and external galvanometer subsequently used to take the test data, at the following reference points.

- a. Melting ice
- b. Boiling water
- c. Freezing tin

The temperature values are based on the International Scale of 1948 which is presented in Table 1. The E.M.F. values are expressed in Absolute Electrical Volts. The calibration measurements are tabulated below. Each thermocouple used was individually calibrated as an added precaution.

Boiling Water

Temperature = 211.65 °F

Standard mv = 5.259

Millivolts Observed (mv)	Deviation (mv)
5.193	0.066
5.194	0.065
5.190	0.069
5.187	0.072
5.194	0.065
5.195	0.064
5.196	0.063
5.195	0.064
5.199	0.060
5.194	0.065

average deviation = 0.065 ± 5%

Freezing Tin

Temperature = 449.4 °F

Standard Millivolt = 12.5526

Millivolts Observed (mv)	Deviation (mv)
12.41	0.1426
12.40	0.1526
12.41	0.1426
12.41	0.1426
12.41	0.1426

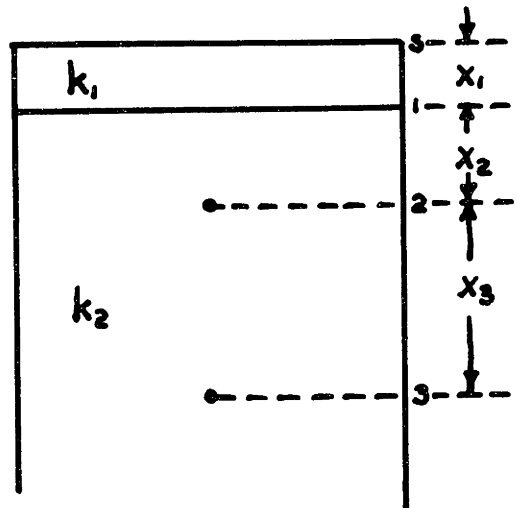
average deviation = 0.145 ± 5%

It is estimated that the measurements are accurate to ± 0.002 mv.

APPENDIX C

SURFACE TEMPERATURE CALCULATION EQUATION

The surface temperature, T_s , is determined by extrapolation of the temperature measured at axial locations 2 and 3. It is assumed that the temperature only varies in the axial direction, therefore linear extrapolation may be used. Since the temperature difference



is proportional to the thermocouple millivolt difference, the value of the millivolts will be determined at the surface, which can then be converted into a surface temperature. The case shown in the figure is the general case, where a disk of a different thermal conductivity from that of copper is soldered to the copper block. The temperature drop in the solder is neglected.

For steady state heat conduction in the axial direction only, the following equation is satisfied, assuming the cross section area is constant

$$k \frac{\Delta T}{\Delta x} = \text{const.} \quad (\text{A-6})$$

Since the temperature difference is proportional to the induced millivolt difference, this is equivalent to

$$k \frac{\Delta mv}{\Delta x} = \text{const.} \quad (\text{A-7})$$

Expressing Eq. (A-7) for the three axial positions yields:

$$k_1 \frac{(mv_1 - mv_s)}{x_1} = k_2 \frac{(mv_3 - mv_2)}{x_3} \quad (A-8)$$

and

$$k_2 \frac{(mv_2 - mv_1)}{x_2} = k_2 \frac{(mv_3 - mv_2)}{x_3} \quad (A-9)$$

Eliminating mv_1 from the preceding two equations and solving for mv_s gives the following result.

$$mv_s = mv_2 - (mv_3 - mv_2) \left[\frac{x_2}{x_3} + \frac{k_2}{k_1} \frac{x_1}{x_3} \right] \quad (A-10)$$

The values of the quantities on the right side of Eq. (A-10) are fixed by geometry, material, and experimental data.

APPENDIX D

SURFACE TENSION, CONTACT ANGLE, AND SPREADING

1. Surface Tension

The term surface tension is somewhat misleading and often misused. There are a number of definitions of σ , the surface tension, all of which result in the same interpretation. Keenan (28) defines the surface tension in the following way.

$$\sigma = \left(\frac{\partial E}{\partial A} \right)_{s,m} \quad (\text{A-11})$$

The subscripts, s and m , specify a process at constant entropy and mass, respectively.

The First Law of Thermodynamics states,

$$dE = dQ - dW \quad (\text{A-12})$$

For reversible change, the second law may be stated as

$$dQ = T ds \quad (\text{A-13})$$

Combining the above equations yields the result,

$$\sigma = \left(\frac{\partial E}{\partial A} \right)_{s,m} = \left(\frac{\partial W}{\partial A} \right)_{s,m} \quad (\text{A-14})$$

Therefore, the surface tension represents the work necessary to increase the interface area a unit amount in a reversible adiabatic process. The above interpretation was also arrived at by Harkins (29).

It can further be shown that the surface tension is equivalent to the free energy per unit area, neglecting the mass contained in the film; i.e.

$$\sigma = E - TS \quad (\text{A-15})$$

It is therefore, more general to refer to σ as the surface energy, rather than the surface tension. In particular cases the concept of a surface tension is applicable and useful. In particular consider a saturated surface film of length, l , and imagine stretching it an amount ds reversibly and adiabatically at constant temperature. Analyzing this process from the thermodynamic point of view, one proceeds in the following manner.

$$dQ - dW = dE \quad (\text{A-16})$$

For a reversible adiabatic process $dQ = 0$.

$$E = f(T, z, V, p, A) \quad (\text{A-17})$$

Neglecting the effects of z and V in the above process yields the following result.

$$E = f(A) \quad (\text{A-18})$$

But $\left(\frac{\partial E}{\partial A}\right)_{s,m} = \sigma$, therefore

$$dE = \sigma dA \quad (\text{A-19})$$

Combining Eq. (A-16) and (A-19) yields

$$-dW = \sigma dA \quad (A-20)$$

Analyzing the problem from the mechanical point of view, one starts with the concept that work is force times distance, i.e.

$$dW = F ds \quad (A-21)$$

Identifying σ as the tension per unit length of surface (lb/ft) yields the following expression for the total force

$$F = \sigma l \quad (A-22)$$

Combining (A-21) and (A-22) yields

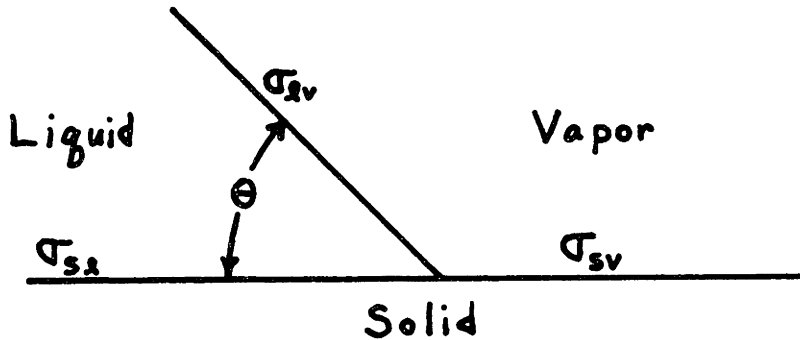
$$dW = \sigma l ds = \sigma dA \quad (A-23)$$

which is identical to Eq. (A-20). The sign difference arises due to the fact that Eq. (A-20) is an expression for the work done by the surface, and Eq. (A-23) for the work done on the surface. It can therefore be seen that analyzing the process considering σ as a surface tension is equivalent to analyzing the problem considering σ a surface energy. In some cases it is conceptually simpler to think of σ as a surface tension, eg. when thinking of contact angle.

2. Contact Angle

Contact angles only exist when at least three surfaces coexist at a point. The three surfaces which exist in boiling are the liquid-

vapor surface, and vapor-solid surface. Each of these interfaces have associated with it a value of the surface energy, σ . The notation adopted is shown in the figure. The contact angle θ is defined as the angle through the liquid phase.



A value of the contact angle exists only if the three phases are in equilibrium at the triple interface. If this is not possible, spreading, discussed in the next section, occurs.

Treating σ as a surface tension, and equating the horizontal components of the force associated with each interface yields the following equation, which was derived by Gibbs (30) in a more thorough way.

$$\sigma_{sl} + \sigma_{lv} \cos \theta = \sigma_{sv} \quad (\text{A-24})$$

Solving Eq. (A-24) for the contact angle results in

$$\theta = \cos^{-1} \left(\frac{\sigma_{sv} - \sigma_{sl}}{\sigma_{lv}} \right) \quad (\text{A-25})$$

This equation only applies when equilibrium exists, that is, as will be shown below when

$$\sigma_{lv} > C_1 | \sigma_{sv} - \sigma_{sl} | \quad (\text{A-26})$$

where C_1 is a function of the surface roughness.

3. Spreading

The phenomenon of spreading is discussed in detail by Harkins (29). It occurs when it is impossible for the three surface tensions to statically balance one another for any value of the angle θ . When spreading occurs the liquid-vapor interface will be parallel to the solid plane. The criteria for spreading may be derived in a number of ways; the approach utilized here is the application of Gibbs' equilibrium criteria (30). That is, a system is in a state of equilibrium if the change of energy at constant entropy is greater than zero, for all possible variations.

$$(\delta E)_S \geq 0 \quad (\text{A-27})$$

Applying Gibbs' criteria to the three phases yields the following result

$$\delta E = \left(\frac{\partial E}{\partial A_{lv}} \right)_{S,m} \delta A_{lv} + \left(\frac{\partial E}{\partial A_{ls}} \right)_{S,m} \delta A_{ls} + \left(\frac{\partial E}{\partial A_{sv}} \right)_{S,m} \delta A_{sv} \quad (\text{A-28})$$

Combining Eq. (A-11) and (A-28) gives

$$\delta E = \sigma_{lv} \delta A_{lv} + \sigma_{ls} \delta A_{ls} + \sigma_{sv} \delta A_{sv} \geq 0 \quad (\text{A-29})$$

The solid surface area is not equal to the projected area for a rough surface, while the liquid vapor interface area is flat and therefore equivalent to the projected area. Displacing the triple interface a projected area δA , therefore increases the solid areas by

an amount $C_1 \delta A$, where C_1 is the ratio of the total solid area to the projected area.

A variation where the triple interface moves δA into the solid vapor region maintains the following geometrical relation

$$\delta A_{lv} = \frac{\delta A_{ls}}{C_1} = - \frac{\delta A_{sv}}{C_1} = \delta A \quad (\text{A-30})$$

Combining Eq. (A-29) and (A-30) yields

$$\sigma_{lv} + C_1 (\sigma_{ls} - \sigma_{sv}) \geq 0 \quad (\text{A-31})$$

If this equation is not satisfied, the system is unstable and the variation will take place. Therefore, for the liquid to spread on the solid, the following relation must be satisfied

$$\sigma_{lv} < C_1 (\sigma_{sv} - \sigma_{ls}) \quad (\text{A-32})$$

Examining a possible variation where the triple interface moves an amount δA into the liquid-solid region yields the following relation

$$\delta A_{lv} = - \frac{\delta A_{ls}}{C_1} = \frac{\delta A_{sv}}{C_1} = \delta A \quad (\text{A-33})$$

Combining Eq. (A-29) and (A-33) results in the following equilibrium criteria

$$\sigma_{lv} + C_1 (\sigma_{sv} - \sigma_{ls}) \geq 0 \quad (\text{A-34})$$

Therefore, for the vapor to spread on the solid the following equation applies.

$$\sigma_{lv} < C_1 (\sigma_{ls} - \sigma_{sv}) \quad (\text{A-35})$$

Comparing Eq. (A-32) and (A-35), a general criteria for spreading may be stated as follows

$$\sigma_{lv} < C_1 |\sigma_{sv} - \sigma_{ls}| \quad (\text{A-36})$$

Harkins defines a spreading coefficient S as the surface energy difference.

$$S \equiv |\sigma_{sv} - \sigma_{ls}| - \sigma_{lv} \quad (\text{A-37})$$

While S has been measured for a number of triple interface combinations, no information on the rate of spreading is available.

APPENDIX E
SAMPLE CALCULATION

Run 17, Point #3

1. Preliminary Calculations

- a. Equation for converting net power input to boiling heat flux.

$$q/A = C \frac{W_{\text{net}}}{A} \left(\frac{\text{BTU}}{\text{hr ft}^2} \right) \quad (\text{A-38})$$

where $C = 3.41 \text{ Btu/hr watt}$

$$A = \frac{\pi D^2}{4} (\text{ft}^2) \quad (\text{A-39})$$

Combine Eq. (A-38) and (A-39) to obtain

$$q/A = \frac{4.34}{D^2} W_{\text{net}} \quad (\text{A-40})$$

$$D = 1 \frac{31}{32}'' \pm 1/64'' = 0.1642 \text{ ft.}$$

finally

$$q/A = 161 W_{\text{net}} \left(\frac{\text{Btu}}{\text{hr ft}^2} \right) \quad (\text{A-41})$$

- b. Equation for converting axial millivolt difference to boiling heat flux.

$$q/A = k \frac{\Delta T}{\Delta x} \quad (\text{A-42})$$

For iron-constantan thermocouples,

$$\Delta T = \frac{\Delta \text{MV}}{0.03} (^\circ\text{F}) \quad (\text{A-43})$$

$$\Delta x = x_3 = 1 \frac{1}{8}'' \pm 1/32''$$

$$k = 223 \pm 1\% (\text{BTU/hr ft } ^\circ\text{F})$$

Combining the above, yields

$$q/A = 79,000 \Delta mv \left(\frac{\text{BTU}}{\text{hr ft}^2} \right) \quad (\text{A-44})$$

c. Equation for converting axial millivolt readings to boiling surface millivolts.

From Eq. (A-10) in Appendix C,

$$mv_s = mv_2 - (mv_3 - mv_2) \left(\frac{x_2}{x_3} + \frac{k_2}{k_1} \frac{x_1}{x_3} \right) \quad (\text{A-45})$$

The following geometry was used in Run #7

$$\begin{aligned} x_1 &= 0 \\ x_2 &= 3/16" \\ x_3 &= 1.125" \end{aligned}$$

Inserting the above values in Eq. (A-45) gives,

$$mv_s = mv_2 - 0.165 \Delta mv \quad (\text{A-46})$$

2. Calculation of Point #3, Run #17

a. Measured Data

$$T_{\text{room}} = 77 \text{ } ^\circ\text{F}$$

Pressure (psia)	Power (watts)	mv_3 center	mv_3 side	mv_2 center	mv_2 side
5	80 ± 2	3.720	3.720	3.600	3.585

The thermocouple readings are accurate to within ± 0.005 mv.

b. Derived Data

The saturation temperature of water corresponding to 5 psia is 162 $^\circ\text{F}$. Subtracting the room temperature of

77 °F, yields a temperature difference of 85 °F.

Referring to Figure 15, one determines that this is equivalent to a heat loss of 15 watts. The net power input is therefore,

$$W_{\text{net}} = 80 - 15 = 65 \text{ watts} \pm 2 \quad (\text{A-47})$$

Converting the thermocouple readings to the standard by the use of Figure 14, yields the following results

$$\begin{aligned} \Delta mv &= 0.129 \pm 0.005 \\ mv_2 &= 3.635 \end{aligned} \quad (\text{A-48})$$

Combining Eq. (A-41) and (A-47) yields,

$$q/A = 10,500 \pm 300 \left(\frac{\text{BTU}}{\text{hr ft}^2} \right)$$

Combining Eq. (A-44) and (A-48) results in

$$q/A = 10,200 \pm 500 \left(\frac{\text{BTU}}{\text{hr ft}^2} \right)$$

Combining Eq. (A-46) and (A-48) gives the surface millivolts,

$$mv_s = 3.615$$

which from Table 1 is equivalent to a surface temperature of 157 °F. Combining this with the saturation temperature of normal pentane results in a boiling temperature difference of 60 °F.

Due to the fact that calculating the heat flux utilizing Eq. (A-44) is the more accurate, the result of this calculation is the value tabulated.

APPENDIX F

VAPOR VELOCITY PARALLEL TO SURFACE IN FILM BOILING

1. Assumptions

- a. Vapor film thickness, a , is constant between bubbles.
- b. The vapor flows radially inward.
- c. The vapor generated in an area equal to $\lambda^2/2$ flows to one bubble.
- d. The geometry is given by Figure 36.

2. Analysis

Continuity

$$\begin{aligned} w &= \rho_{vf} V_v A \\ &= \rho_{vf} V_v 2\pi r a \end{aligned} \quad (\text{A-49})$$

First Law

$$q = w \Delta h \quad (\text{A-50})$$

Heat Transfer

$$q = \frac{k_{vf}}{a} (\pi r_2^2 - \pi r^2) \Delta T \quad (\text{A-51})$$

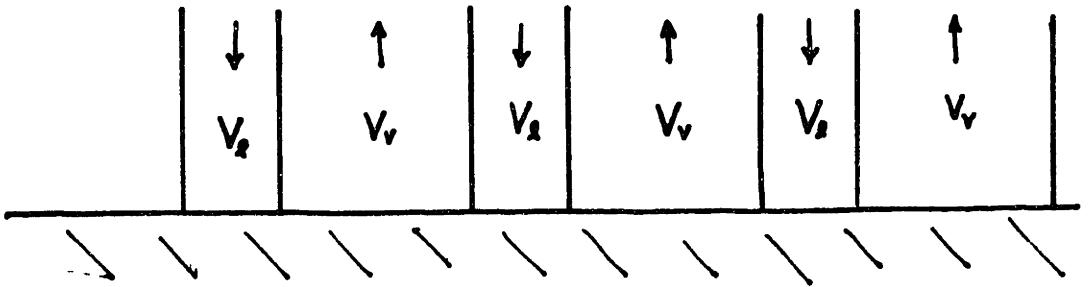
From assumption C, $(\lambda^2/2) = \pi r_2^2$. Eliminating q , and w from Eq. (A-49), Eq. (A-50), and Eq. (A-51), and solving for the vapor velocity, V_v , yields the following relation,

$$V_v = \frac{k_{vf} \Delta T}{\rho_{vf} \Delta h a^2} \frac{\lambda^2/2 - \pi r^2}{2\pi r} \quad (\text{A-52})$$

APPENDIX G

APPLICATION OF HELMHOLTZ INSTABILITY
TO THE ANALYSIS OF THE BURNOUT HEAT FLUX

Zuber (36) discusses the phenomenon of the burnout heat flux in great detail, concluding that the maximum heat flux is due to the Helmholtz Hydrodynamic Instability of the boundary between the liquid and vapor phases counterflowing normal to the heating surface. The physical picture used in the analysis visualizes jets of vapor and liquid flowing opposite to one another. A two dimensional model of the flow pattern is shown below.



Neglecting the effect of fluid depth on the instability in Eq. (III-3), combined with the fact that there is no gravity effect in this geometry, yields the following result.

$$C^2 = \frac{g_0 \sigma m}{\rho_l + \rho_v} - \frac{\rho_l \rho_v}{(\rho_l + \rho_v)^2} (V_v - V_l)^2 \quad (\text{A-53})$$

For the boundary to remain stable, C must be real, therefore for stability the relative velocity must satisfy the following equation.

$$V_{rel} = |V_v| + |V_l| \leq \left[\frac{g_0 \sigma m (\rho_l + \rho_v)^2}{(\rho_l + \rho_v) \rho_l \rho_v} \right]^{1/2} \quad (\text{A-54})$$

The following derivation of an expression for the burnout heat flux considers the burnout point to be the limit of nucleate boiling. Staniszewski (44) observed that in the nucleate boiling regime at heat fluxes within 25% of the burnout heat flux, the nucleate boiling bubbles tended to join together in columns. This tendency becomes more pronounced as the burnout point is approached, the bubbles coalescing to form jets of vapor. Thus experimental observations support the analytical picture in the nucleate region.

The vapor mass flow away from the surface must equal the liquid flow towards the surface, therefore from continuity,

$$\omega = \rho_{vf} V_v A_v = \rho_l V_l A_l \quad (\text{A-55})$$

Defining a constant, C_1 , where

$$C_1 \equiv \frac{A_v}{A} \quad (\text{A-56})$$

transforms Eq. (A-55) to,

$$\omega = \rho_{vf} V_v A C_1 = \rho_l V_l A (1 - C_1) \quad (\text{A-57})$$

The relative velocity, which is the sum of the vapor and the liquid velocity, is therefore given by

$$V_{rel} = \frac{\omega}{A} \left[\frac{1}{\rho_{vf} C_1} + \frac{1}{(1 - C_1) \rho_l} \right] \quad (\text{A-58})$$

The flow distribution is fixed by the classical potential flow result that the volume integral of the kinetic energy must be a minimum (45). This is equivalent to minimizing the kinetic energy at

any plane for the assumed model.

$$K.E. = \frac{\omega}{g} [V_e^2 + V_v^2] \quad (A-59)$$

Combining Eq. (A-59) and (A-55) yields

$$K.E. = \frac{\omega^3}{2gA^2} \left[\frac{1}{(\rho_{vf}/\rho_e)^2 C_1^2} + \frac{1}{\rho_e^2 (1-C_1)^2} \right] \quad (A-60)$$

Minimizing Eq. (A-60) with respect to the area ratio, C_1 , yields the following criteria,

$$C_1 = \frac{1}{1 + (\rho_{vf}/\rho_e)^{2/3}} \quad (A-61)$$

Combining Eq. (A-61) with Eq. (A-58) gives the result,

$$V_{rel} = \frac{\omega}{A \rho_{vf}} \left[1 + (\rho_{vf}/\rho_e)^{1/3} + (\rho_{vf}/\rho_e)^{2/3} + \rho_{vf}/\rho_e \right] \quad (A-62)$$

Applying the First Law provides a relation between the flow rate and heat transfer rate

$$q = \omega \Delta h \quad (A-63)$$

Combining Eq. (A-62) and (A-63) yields,

$$V_{rel} = \frac{q/A}{\rho_{vf} \Delta h} \left[1 + (\rho_{vf}/\rho_e)^{1/3} + (\rho_{vf}/\rho_e)^{2/3} + \rho_{vf}/\rho_e \right] \quad (A-64)$$

Classical analysis of the instability of jets (46) show that the most unstable wavelength is proportional to the jet diameter as follows.

$$\lambda^* = \frac{2\pi}{m^*} = 4.51 D_j \quad (\text{A-65})$$

The observations of Staniszewski (44) reveal that the jet diameter is proportional to the nucleate boiling bubble diameter, therefore,

$$D_j = C_2 D_b \quad (\text{A-66})$$

The nucleate boiling bubble diameter at departure is given by the following equation (47) for contact angles characteristic of commercial surfaces.

$$D_b = .75 \sqrt{\frac{g_0 \sigma}{g(\rho_e - \rho_v)}} \quad (\text{A-67})$$

Combining Eq. (A-67), (A-66) and (A-65) yields the following equation for the dominant wave number.

$$m^* = \frac{1.85}{C_2} \sqrt{\frac{g(\rho_e - \rho_v)}{g_0 \sigma}} \quad (\text{A-68})$$

Combining Eq. (A-54) and (A-68) yields,

$$V_{rel} \leq \left[\frac{1.85}{C_2} \left(\frac{\rho_e + \rho_v}{\rho_e \rho_v} \right) \sqrt{g_0 \sigma (\rho_e - \rho_v)} \right]^{1/2} \quad (\text{A-69})$$

Finally, combining Eq. (A-69) and (A-64), and solving for the heat flux yields the expression for the burnout heat flux.

$$(q/A)_{\max} = \left(\frac{1.85}{C_2} \right) \frac{\rho_{vf} \Delta h \left(\frac{\rho_l + \rho_v}{\rho_l \rho_v} \right)^{1/2} \left[g g_0 (\rho_l - \rho_v) \right]^{1/4}}{1 + (\rho_{vf}/\rho_l)^{1/3} + (\rho_{vf}/\rho_l)^{2/3} + \rho_{vf}/\rho_l} \quad (\text{A-70})$$

The experimental value of the constant determined by Zuber (36) yields the final pool boiling burnout correlation equation.

$$(q/A)_{\max} = 0.16 \frac{\rho_{vf} \Delta h \left(\frac{\rho_l + \rho_v}{\rho_l \rho_v} \right)^{1/2} \left[g g_0 (\rho_l - \rho_v) \right]^{1/4}}{1 + (\rho_{vf}/\rho_l)^{1/3} + (\rho_{vf}/\rho_l)^{2/3} + \rho_{vf}/\rho_l} \quad (\text{A-71})$$

APPENDIX H

APPLICATION OF TAYLOR INSTABILITY TO THE
ANALYSIS OF THE MINIMUM HEAT FLUX

Due to the hydrodynamic instability of the liquid-vapor boundary in film boiling, bubbles grow and depart, demanding a certain vapor flow rate. The vapor is generated by evaporation due to heat transfer across the vapor film. It can be shown that the minimum vapor flow rate is required when the effect of vapor velocity and thickness on the interface dynamics is neglected. Zuber (36) first analyzed the minimum point utilizing this simplification. In Chapter III it was quantitatively shown to be reasonable to assume the effect of vapor velocity and film thickness is negligible near the minimum point.

The following analysis of the minimum point assumes that the minimum heat flux is established by the minimum allowable vapor flow required by the liquid-vapor boundary behavior. The appropriate stability equations are (III-1) and (III-8), which are given below with b substituted for $-in$.

$$\eta = \eta_0 e^{bt} \cos mx \quad (\text{A-72})$$

$$b = \left[\frac{g(\rho_l - \rho_v)m}{\rho_l + \rho_v} - \frac{g_0 \sigma m^3}{\rho_l + \rho_v} \right]^{1/2} \quad (\text{A-73})$$

Equating the heat flux to the enthalpy flux required to generate the vapor carried away by the bubbles yields the following equation

$$g/A = \rho_{vf} \frac{\pi}{6} D_b^3 \Delta h n' \quad (\text{A-74})$$

where n' represents the number of bubbles departing per unit time and area. In a surface area equal to λ^2 , four bubbles depart in one period, therefore

$$n' = \frac{4}{\lambda^2 \tau} \quad (\text{A-75})$$

The wavelength, λ , is that value which maximizes b , since that grows the fastest and therefore dominates. Differentiating Eq. (A-73) with respect to m , and solving for the maximizing value, yields the following result

$$m^* = \left[\frac{g(\rho_l - \rho_v)}{3g_0\sigma} \right]^{1/2} = \frac{2\pi}{\lambda^*} \quad (\text{A-76})$$

Assuming that the bubble period equals four times the time it takes the boundary to grow to a height equal to the bubble diameter gives, from Eq. (A-72),

$$\tau = 4 t_{D_b} = \frac{4}{b} \ln\left(\frac{D_b}{\eta_0}\right) \quad (\text{A-77})$$

Assuming the magnitude of the initial disturbance is proportional to the bubble size results in

$$\tau = \frac{4C_3}{b} \quad (\text{A-78})$$

where $C_3 = \ln\left(\frac{D_b}{\eta_0}\right)$

Combining Eq. (A-78), (A-76) and (A-75) yields an expression for the number of bubbles departing per unit area, per unit time

$$n' = \frac{3 g_0 \sigma b}{4 \pi^2 C_3 g(\rho_2 - \rho_v)} \quad (\text{A-79})$$

In Eq. (A-79) b is the maximum value which is obtained from Eq. (A-73) with m from Eq. (A-76)

$$b^* = \left[\frac{2 g(\rho_2 - \rho_v)}{3\sqrt{3}(\rho_2 + \rho_v)} \sqrt{\frac{g(\rho_2 - \rho_v)}{g_0 \sigma}} \right]^{1/2} \quad (\text{A-80})$$

The bubble diameter was experimentally shown to be given by

$$D_b = 4.7 \sqrt{\frac{g_0 \sigma}{g(\rho_2 - \rho_v)}} \quad (\text{A-81})$$

Combining Eq. (A-74), (A-79), (A-80), and (A-81) yields the following expression for the minimum heat flux which will generate enough vapor to support the two phase boundary.

$$(q/A)_{\min} = \frac{.278}{C_2} \rho_{vf} \Delta h \left[\frac{g(\rho_2 - \rho_v)}{\rho_2 + \rho_v} \right]^{1/2} \left[\frac{g_0 \sigma}{g(\rho_2 - \rho_v)} \right]^{1/4} \quad (\text{A-82})$$

Comparing the predicted results from Eq. (A-82) with the experimental results reported in Chapter II, determines the value of

the empirical constant as 0.09. The final expression for the minimum heat flux in pool boiling from a horizontal surface is therefore,

$$(q/A)_{\min} = .09 \rho_{vf} \Delta h \left[\frac{g(\rho_s - \rho_v)}{\rho_s + \rho_v} \right]^{1/2} \left[\frac{g_0 \sigma}{g(\rho_s - \rho_v)} \right]^{1/4} \quad (\text{A-83})$$

Comparison between theory and experiment:

Fluid	Predicted $(q/A)_{\min}$ (Eq. A-83) (BTU/hr ft ²)	Measured $(q/A)_{\min}$ (BTU/hr ft ²)
n-Pentane	3,550	3,500 ± 10%
Carbon Tetrachloride	3,450	3,500 ± 10%

TABLE 1

IRON CONSTANTAN THERMOCOUPLE STANDARD 1948

Reference: 32 °F ice point

Degrees F	emf (mv)	Degrees F	emf (mv)	Degrees F	emf (mv)
100	1.94	200	4.91	300	7.94
105	2.09	205	5.06	305	8.10
110	2.23	210	5.21	310	8.25
115	2.38	215	5.36	315	8.40
120	2.52	220	5.51	320	8.56
125	2.67	225	5.66	325	8.71
130	2.82	230	5.81	330	8.87
135	2.97	235	5.96	335	9.02
140	3.11	240	6.11	340	9.17
145	3.26	245	6.27	345	9.33
150	3.41	250	6.42	350	9.48
155	3.56	255	6.57	355	9.64
160	3.71	260	6.72	360	9.79
165	3.86	265	6.87	365	9.95
170	4.01	270	7.03	370	10.10
175	4.16	275	7.18	375	10.25
180	4.31	280	7.33	380	10.41
185	4.46	285	7.48	385	10.56
190	4.61	290	7.64	390	10.72
195	4.76	295	7.79	395	10.87

TABLE 2
TEST DATA

Test Fluid: n-pentane; Surface Material: copper
Surface Finish: mirror finish
Surface Cleanliness: cleaned with CCl_4 immediately before test

Run: 2

Date: 11/1/58

Point #	q/A $\frac{\text{BTU}}{\text{hr ft}^2}$	Uncertainty $\pm \frac{\text{BTU}}{\text{hr ft}^2}$	ΔT °F	Point #	q/A $\frac{\text{BTU}}{\text{hr ft}^2}$	Uncertainty $\pm \frac{\text{BTU}}{\text{hr ft}^2}$	ΔT °F
1	26,000	500	43	8	3,400	200	110
2	40,500	500	52	9	56,500	300	67
3	55,000	500	66	10	79,500	400	80
4	70,000	500	76.5	11	82,000	500	85
5	4,200	500	137	12	4,200	200	105
6	3,850	500	130	13	5,950	200	160
7	3,550	300	120	14	7,250	300	181
				15	7,730	300	206

Run: 3

Date: 11/4/58

Point #	q/A $\frac{\text{BTU}}{\text{hr ft}^2}$	Uncertainty $\pm \frac{\text{BTU}}{\text{hr ft}^2}$	ΔT °F	Point #	q/A $\frac{\text{BTU}}{\text{hr ft}^2}$	Uncertainty $\pm \frac{\text{BTU}}{\text{hr ft}^2}$	ΔT °F
1	7,250	200	25	7	4,850	200	142
2	14,500	300	36	8	4,200	200	124
3	24,000	500	44	9	4,000	200	110
4	47,000	500	56	10	7,100	300	191
5	74,200	500	69	11	11,000	400	258
6	78,500	500	73				

TABLE 3
TEST DATA

Test Fluid: n-pentane; Surface Material: copper
Surface Finish: lapped in one direction with grit A (#280)
Surface Cleanliness: cleaned with CCl_4

Run: 4 Date: 11/8/58

Point #	q/A $\frac{\text{BTU}}{\text{hr ft}^2}$	Uncertainty		ΔT °F
		±	$\frac{\text{BTU}}{\text{hr ft}^2}$	
1	4,500	300		113
2	4,200	300		104
3	4,000	300		94
4	4,200	300		87
5	4,500	300		79
6	4,800	300		71
7	8,000	400		62
8	11,000	400		53
9	16,500	500		46
10	49,500	600		19
11	11,300	300		15
12	3,400	300		13
13	24,000	300		17
14	75,000	600		21
15	88,000	600		24
16	3,550	300		91
17	4,650	300		141
18	6,250	400		181
19	8,700	500		230

TABLE 4
TEST DATA

Test Fluid: n-pentane; Surface Material: copper
Surface Finish: lapped in one direction with grit A (#280)
Surface Cleanliness: oxidized, not cleaned before test

Run: 5

Date: 11/11/58

Point #	q/A $\frac{\text{BTU}}{\text{hr ft}^2}$	Uncertainty $\pm \frac{\text{BTU}}{\text{hr ft}^2}$	ΔT °F	Point #	q/A $\frac{\text{BTU}}{\text{hr ft}^2}$	Uncertainty $\pm \frac{\text{BTU}}{\text{hr ft}^2}$	ΔT °F
1	75,500	800	62	10	85,500	800	28
2	44,500	500	101	11	59,300	600	52
3	12,500	400	142	12	32,700	500	84
4	97,000	800	39	13	12,000	500	122
5	35,500	300	19	14	8,500	500	150
6	6,600	300	16	15	25,000	500	164
7	19,500	300	18	16	8,200	500	177
8	63,500	600	23	17	8,700	500	197
9	87,500	600	28	18	9,500	600	241

Run: 6

Date: 11/13/58

Point #	q/A $\frac{\text{BTU}}{\text{hr ft}^2}$	Uncertainty $\pm \frac{\text{BTU}}{\text{hr ft}^2}$	ΔT °F	Point #	q/A $\frac{\text{BTU}}{\text{hr ft}^2}$	Uncertainty $\pm \frac{\text{BTU}}{\text{hr ft}^2}$	ΔT °F
1	87,000	1000	54	7	57,500	1000	87
2	39,500	800	110	8	17,000	500	143
3	16,000	300	18	9	8,200	500	168
4	41,500	300	21	10	9,100	500	223
5	88,000	800	28	11	12,000	600	269
6	98,500	1000	38				

TABLE 5
TEST DATA

Test Fluid: n-pentane; Surface Material: copper
 Surface Finish: lapped in one direction with grit E (#120)
 Surface Cleanliness: slightly oxidized, not cleaned before test

Run: 7

Date: 11/15/58

Point #	q/A $\frac{\text{BTU}}{\text{hr ft}^2}$	Uncertainty $\pm \frac{\text{BTU}}{\text{hr ft}^2}$	ΔT °F
1	93,500	1000	45
2	6,600	300	13
3	25,300	300	15
4	44,000	600	17
5	74,000	800	21
6	92,500	1000	25
7	99,000	1000	30
8	75,000	1000	72
9	40,000	800	121
10	18,000	600	157
11	9,800	500	187
12	9,000	500	209
13	15,000	500	171
14	27,200	600	142
15	9,650	500	234
16	12,000	600	267

TABLE 6

TEST DATA

Test Fluid: n-pentane; Surface Material: copper
 Surface Finish: lapped in one direction with grit E (#120)
 Surface Cleanliness: oxidized, not cleaned before test

Run: 8

Date: 11/20/58

Point #	q/A $\frac{\text{BTU}}{\text{hr ft}^2}$	Uncertainty $\pm \frac{\text{BTU}}{\text{hr ft}^2}$	ΔT °F	Point #	q/A $\frac{\text{BTU}}{\text{hr ft}^2}$	Uncertainty $\pm \frac{\text{BTU}}{\text{hr ft}^2}$	ΔT °F
1	90,000	1000	52	8	75,000	1000	84
2	13,800	300	14	9	10,300	500	167
3	33,000	800	16	10	28,000	600	141
4	59,000	800	19	11	21,500	600	153
5	85,000	800	23	12	9,800	500	187
6	100,000	1000	28	13	9,700	500	221
7	97,000	1000	41	14	12,000	600	266

Run: 9

Date: 11/22/58

Point #	q/A $\frac{\text{BTU}}{\text{hr ft}^2}$	Uncertainty $\pm \frac{\text{BTU}}{\text{hr ft}^2}$	ΔT °F	Point #	q/A $\frac{\text{BTU}}{\text{hr ft}^2}$	Uncertainty $\pm \frac{\text{BTU}}{\text{hr ft}^2}$	ΔT °F
1	95,000	1000	46	9	43,500	1000	123
2	64,500	1000	102	10	23,500	800	143
3	9,500	300	14	11	9,500	800	177
4	19,000	300	15	12	16,500	800	157
5	47,000	600	18	13	9,200	500	194
6	76,500	800	22	14	9,500	500	230
7	103,000	1000	34	15	10,800	600	260
8	83,000	1000	72				

TABLE 7

TEST DATA

Test Fluid: n-pentane; Surface Material: copper
 Surface Finish: lapped in one direction with grit E (#120)
 Surface Cleanliness: cleaned with CCl_4 immediately before test

Run: 10

Date: 11/28/58

Point #	q/A $\frac{\text{BTU}}{\text{hr ft}^2}$	Uncertainty		ΔT °F
		+	-	
1	4,300	300		110
2	4,200	300		91
3	4,500	300		75
4	9,300	500		60
5	13,000	500		50
6	20,500	800		41
7	60,000	800		17
8	6,600	300		11
9	21,000	300		13
10	44,000	800		15
11	7,900	500		65
12	89,500	1000		19
13	6,600	300		70
14	3,850	300		81
15	4,000	400		104
16	4,650	500		138
17	6,600	500		178
18	8,500	500		221
19	11,000	600		263

TABLE 8

TEST DATA

Test Fluid: n-pentane; Surface Material: copper
 Surface Finish: lapped circularly with grit E (#120)
 Surface Cleanliness: cleaned with CCl_4 immediately before test

Run: 16

Date: 12/27/58

Point #	q/A $\frac{\text{BTU}}{\text{hr ft}^2}$	Uncertainty + - $\frac{\text{BTU}}{\text{hr ft}^2}$	ΔT °F	Point #	q/A $\frac{\text{BTU}}{\text{hr ft}^2}$	Uncertainty + - $\frac{\text{BTU}}{\text{hr ft}^2}$	ΔT °F
1	55,000	800	13	4	82,000	800	14
2	7,400	200	9	5	92,000	1000	16
3	28,500	300	11				

Run: 17

Date: 12/30/58

Point #	q/A $\frac{\text{BTU}}{\text{hr ft}^2}$	Uncertainty + - $\frac{\text{BTU}}{\text{hr ft}^2}$	ΔT °F	Point #	q/A $\frac{\text{BTU}}{\text{hr ft}^2}$	Uncertainty + - $\frac{\text{BTU}}{\text{hr ft}^2}$	ΔT °F
1	6,700	300	109	8	5,800	300	91
2	6,400	300	81	9	7,700	300	70
3	10,500	300	60	10	5,500	400	104
4	16,700	800	43	11	6,450	400	138
5	62,000	800	13	12	7,250	500	180
6	20,600	400	10	13	9,350	500	226
7	90,000	800	14				

TABLE 9
TEST DATA

Test Fluid: carbon tetrachloride; Surface Material: copper
 Surface Finish: lapped circularly with grit E (#120)
 Surface Cleanliness: cleaned with CCl_4 immediately before test

Run: 19

Date: 1/31/59

Point #	q/A $\frac{\text{BTU}}{\text{hr ft}^2}$	Uncertainty + - $\frac{\text{BTU}}{\text{hr ft}^2}$	ΔT °F	Point #	q/A $\frac{\text{BTU}}{\text{hr ft}^2}$	Uncertainty + - $\frac{\text{BTU}}{\text{hr ft}^2}$	ΔT °F
1	37,000	800	17	8	23,000	800	53
2	72,000	800	20	9	7,300	300	15
3	91,000	800	22	10	94,500	800	23
4	6,500	400	96	11	98,500	800	25
5	3,500	400	138	12	4,800	500	168
6	9,700	400	84	13	6,300	600	197
7	14,500	300	68				

Run: 20

Date: 2/2/59

Point #	q/A $\frac{\text{BTU}}{\text{hr ft}^2}$	Uncertainty + - $\frac{\text{BTU}}{\text{hr ft}^2}$	ΔT °F	Point #	q/A $\frac{\text{BTU}}{\text{hr ft}^2}$	Uncertainty + - $\frac{\text{BTU}}{\text{hr ft}^2}$	ΔT °F
1	13,000	500	15	6	5,000	500	121
2	45,000	600	18	7	4,500	500	143
3	90,000	800	23	8	5,500	600	170
4	99,000	800	24	9	6,750	700	193
5	7,700	500	99				

12

TABLE 10

TEST DATA

Test Fluid: n-pentane; Surface Material: copper
 Surface Finish: lapped circularly with grit E (#120)
 Surface Cleanliness: cleaned with CCl_4 immediately before test

Run: 22

Date: 2/7/59

surface oxidized

Point #	q/A $\frac{\text{BTU}}{\text{hr ft}^2}$	Uncertainty $\pm \frac{\text{BTU}}{\text{hr ft}^2}$	ΔT °F	Point #	q/A $\frac{\text{BTU}}{\text{hr ft}^2}$	Uncertainty $\pm \frac{\text{BTU}}{\text{hr ft}^2}$	ΔT °F
1	5,500	300	110	6	88,500	800	14
2	5,800	300	76	7	96,000	800	16
3	15,000	600	46	8	6,000	300	93
4	10,500	300	9	9	6,600	400	147
5	33,500	300	11	10	8,000	500	193

Run: 23

Date: 2/10/59

photographs taken for bubble diameter measurements

Point #	q/A $\frac{\text{BTU}}{\text{hr ft}^2}$	Uncertainty $\pm \frac{\text{BTU}}{\text{hr ft}^2}$	ΔT °F	Point #	q/A $\frac{\text{BTU}}{\text{hr ft}^2}$	Uncertainty $\pm \frac{\text{BTU}}{\text{hr ft}^2}$	ΔT °F
1	11,500	300	55	4	6,600	400	93
2	19,000	800	40	5	11,500	600	261
3	94,500	800	16				

TABLE 11

TEST DATA

Test Fluid: n-pentane; Surface Material: copper
 Surface Finish: lapped circularly with grit E (#120)
 Surface Cleanliness: cleaned with CCl_4 immediately before test

Run: 25

Date: 2/17/59

Point #	q/A $\frac{\text{BTU}}{\text{hr ft}^2}$	Uncertainty + $\frac{\text{BTU}}{\text{hr ft}^2}$ - $\frac{\text{BTU}}{\text{hr ft}^2}$	ΔT °F
1	6,100	400	109
2	6,800	400	75

three drops of oleic acid added

3	54,000	1000	72
4	34,000	800	41
5	22,000	300	10
6	86,000	800	15
7	93,000	800	16
8	42,000	800	54

three drops of oleic acid added

9	78,000	1000	52
---	--------	------	----

TABLE 12

TEST DATA

Test Fluid: n-pentane; Surface Material: copper
 Surface Cleanliness: cleaned with CCl_4 immediately before test

Run: 31

Date: 3/17/59

Surface Finish: #320 emery rubbed in one direction

Point #	q/A $\frac{\text{BTU}}{\text{hr ft}^2}$	Uncertainty + - $\frac{\text{BTU}}{\text{hr ft}^2}$	ΔT °F	Point #	q/A $\frac{\text{BTU}}{\text{hr ft}^2}$	Uncertainty + - $\frac{\text{BTU}}{\text{hr ft}^2}$	ΔT °F
1	71,000	800	35	8	13,500	800	23
2	86,000	800	38	9	26,500	300	27
3	90,000	800	42	10	49,000	800	31
4	4,000	300	121	11	3,000	300	110
5	3,700	300	99	12	5,100	400	154
6	4,600	500	88	13	6,700	400	193
7	7,700	600	82	14	9,600	500	245

Run: 32

Date: 3/19/59

Surface Finish: #60 emery rubbed in one direction

Point #	q/A $\frac{\text{BTU}}{\text{hr ft}^2}$	Uncertainty + - $\frac{\text{BTU}}{\text{hr ft}^2}$	ΔT °F	Point #	q/A $\frac{\text{BTU}}{\text{hr ft}^2}$	Uncertainty + - $\frac{\text{BTU}}{\text{hr ft}^2}$	ΔT °F
1	79,000	800	23	8	6,900	500	79
2	91,000	1000	26	9	16,000	300	14
3	96,000	1000	27	10	29,000	300	16
4	100,000	1000	29	11	52,000	800	19
5	4,000	400	121	12	4,500	400	149
6	3,400	300	102	13	7,700	500	213
7	3,800	300	87				

TABLE 13

TEST DATA

Test Fluid: n-pentane; Surface Material: inconel

Surface Finish: mirror finish

Surface Cleanliness: cleaned with CCl_4 immediately before test

Run: 33

Date: 3/31/59

Point #	q/A $\frac{\text{BTU}}{\text{hr ft}^2}$	Uncertainty $\pm \frac{\text{BTU}}{\text{hr ft}^2}$	ΔT $^{\circ}\text{F}$	Point #	q/A $\frac{\text{BTU}}{\text{hr ft}^2}$	Uncertainty $\pm \frac{\text{BTU}}{\text{hr ft}^2}$	ΔT $^{\circ}\text{F}$
1	48,000	800	58	8	5,000	400	123
2	64,000	800	67	9	53,000	800	61
3	71,000	800	76	10	10,500	300	37
4	73,000	800	82	11	15,500	500	45
5	5,600	500	155	12	23,000	800	49
6	4,600	400	129	13	33,000	800	52
7	4,600	400	125				

Run: 36

Date: 4/16/59

Point #	q/A $\frac{\text{BTU}}{\text{hr ft}^2}$	Uncertainty $\pm \frac{\text{BTU}}{\text{hr ft}^2}$	ΔT $^{\circ}\text{F}$	Point #	q/A $\frac{\text{BTU}}{\text{hr ft}^2}$	Uncertainty $\pm \frac{\text{BTU}}{\text{hr ft}^2}$	ΔT $^{\circ}\text{F}$
1	41,000	600	54	8	4,300	400	121
2	67,000	800	71	9	31,000	500	53
3	71,000	800	78	10	10,000	300	39
4	5,700	500	158	11	15,000	500	45
5	4,900	500	142	12	22,000	500	50
6	4,600	400	132	13	51,000	600	63
7	4,450	400	128	14	7,200	500	190

see 12

TABLE 14
TEST DATA

Test Fluid: n-pentane; Surface Material: inconel
Surface Finish: lapped circularly with grit D (#160)
Surface Cleanliness: cleaned with CCl_4 immediately before test

Run: 34

Date: 4/2/59

Point #	q/A $\frac{\text{BTU}}{\text{hr ft}^2}$	Uncertainty $\pm \frac{\text{BTU}}{\text{hr ft}^2}$	ΔT °F	Point #	q/A $\frac{\text{BTU}}{\text{hr ft}^2}$	Uncertainty $\pm \frac{\text{BTU}}{\text{hr ft}^2}$	ΔT °F
1	71,000	800	28	6	9,500	600	86
2	79,000	800	30	7	54,000	600	25
3	4,700	300	111	8	11,000	300	17
4	5,800	300	98	9	20,000	500	19
5	7,500	500	92	10	35,000	500	22

Run: 35

Date: 4/4/59

Point #	q/A $\frac{\text{BTU}}{\text{hr ft}^2}$	Uncertainty $\pm \frac{\text{BTU}}{\text{hr ft}^2}$	ΔT °F	Point #	q/A $\frac{\text{BTU}}{\text{hr ft}^2}$	Uncertainty $\pm \frac{\text{BTU}}{\text{hr ft}^2}$	ΔT °F
1	71,000	800	27	7	45,000	600	23
2	79,500	800	30	8	14,500	300	18
3	5,000	500	122	9	27,000	500	20
4	5,000	400	108	10	6,700	500	165
5	6,400	500	95	11	9,100	600	220
6	10,000	600	82				

TABLE 15

TEST DATA

Test Fluid: n-pentane; Surface Material: inconel
 Surface Finish: lapped circularly with grit D (#160)
 Surface Cleanliness: cleaned with CCl_4 immediately before test

Run: 37

Date: 4/23/59

Point #	q/A $\frac{\text{BTU}}{\text{hr ft}^2}$	Uncertainty		ΔT °F
		+	-	
1	59,000	800		27
2	76,000	800		29
3	80,000	800		31
4	4,450	400		125
5	4,300	400		111
6	4,300	300		101
7	4,450	300		91
8	5,200	300		81
9	45,000	500		25
10	14,000	300		21
11	21,000	500		21.5
12	31,000	500		23
13	6,400	500		164
14	7,900	600		200

si9

TABLE 16

TEST DATA

Test Fluid: n-pentant; Surface Material: nickel
 Surface Cleanliness: cleaned with CCl_4 immediately before test

Run: 38

Date: 5/5/59

Surface Finish: mirror finish

Point #	q/A $\frac{\text{BTU}}{\text{hr ft}^2}$	Uncertainty + - $\frac{\text{BTU}}{\text{hr ft}^2}$	ΔT °F	Point #	q/A $\frac{\text{BTU}}{\text{hr ft}^2}$	Uncertainty + - $\frac{\text{BTU}}{\text{hr ft}^2}$	ΔT °F
1	49,000	500	49	8	4,200	400	118
2	68,000	800	64	9	3,800	300	108
3	75,000	800	71	10	10,000	300	28
4	77,000	800	75	11	17,500	300	35
5	5,800	500	155	12	29,000	300	41
6	4,800	500	138	13	7,900	500	199
7	4,500	400	128				

Run: 39

Date: 5/7/59

Surface Finish: lapped circularly with grit D (#160)

Point #	q/A $\frac{\text{BTU}}{\text{hr ft}^2}$	Uncertainty + - $\frac{\text{BTU}}{\text{hr ft}^2}$	ΔT °F	Point #	q/A $\frac{\text{BTU}}{\text{hr ft}^2}$	Uncertainty + - $\frac{\text{BTU}}{\text{hr ft}^2}$	ΔT °F
1	73,000	800	16	9	4,700	300	98
2	82,000	800	16.5	10	5,100	300	90
3	86,000	800	17	11	6,300	300	68
4	90,000	800	17	12	9,500	300	11
5	93,000	800	17.5	13	17,500	300	12
6	4,800	300	120	14	29,000	500	13
7	4,700	300	111	15	45,000	500	14
8	4,500	300	104	16	6,800	500	177

TABLE 17

RESULTS OF BUBBLE DIAMETER MEASUREMENTS

n-Pentane

$\frac{q/A}{\text{hr ft}^2}$	D_b in. ±10%	$\frac{q/A}{\text{hr ft}^2}$	D_b in. ±10%
6,800	0.29	10,500	0.28
6,800	0.29	10,500	0.26
6,800	0.26	11,500	0.28
6,800	0.25	11,500	0.24
6,800	0.29	11,500	0.26
10,500	0.28	6,600	0.29
10,500	0.23	6,600	0.28
10,500	0.28	11,500	0.33
10,500	0.30		

$$D_b \text{ av} = 0.28''$$

Carbon Tetrachloride

$\frac{q/A}{\text{hr ft}^2}$	D_b in. ±10%	$\frac{q/A}{\text{hr ft}^2}$	D_b in. ±10%
8,000	0.26	8,000	0.26
8,000	0.28	8,000	0.24
8,000	0.26	8,000	0.25
8,000	0.26		

$$D_b \text{ av} = 0.26''$$

TABLE 18
FLUID SATURATION PROPERTIES

$$p = p_{atm} = 14.7 \text{ psia}$$

Property	n-Pentane	Carbon Tetrachloride
Saturation temperature ($^{\circ}\text{F}$)	97	170
Liquid density (lb/ft^3)	37.8	95.5
Vapor density (lb/ft^3)	0.187	0.34
Surface tension (lb/ft)	0.000979	0.0019
Heat of vaporization (BTU/lb)	146	83.5
Molecular weight ($\text{lb}/\text{lb mole}$)	72	154

Property	Benzene	Ethyl Alcohol
Saturation temperature ($^{\circ}\text{F}$)	177	173
Liquid density (lb/ft^3)	51	46
Vapor density (lb/ft^3)	0.172	0.1030
Surface tension (lb/ft)	0.001452	0.00115
Heat of vaporization (BTU/lb)	170	368
Molecular weight ($\text{lb}/\text{lb mole}$)	78	46

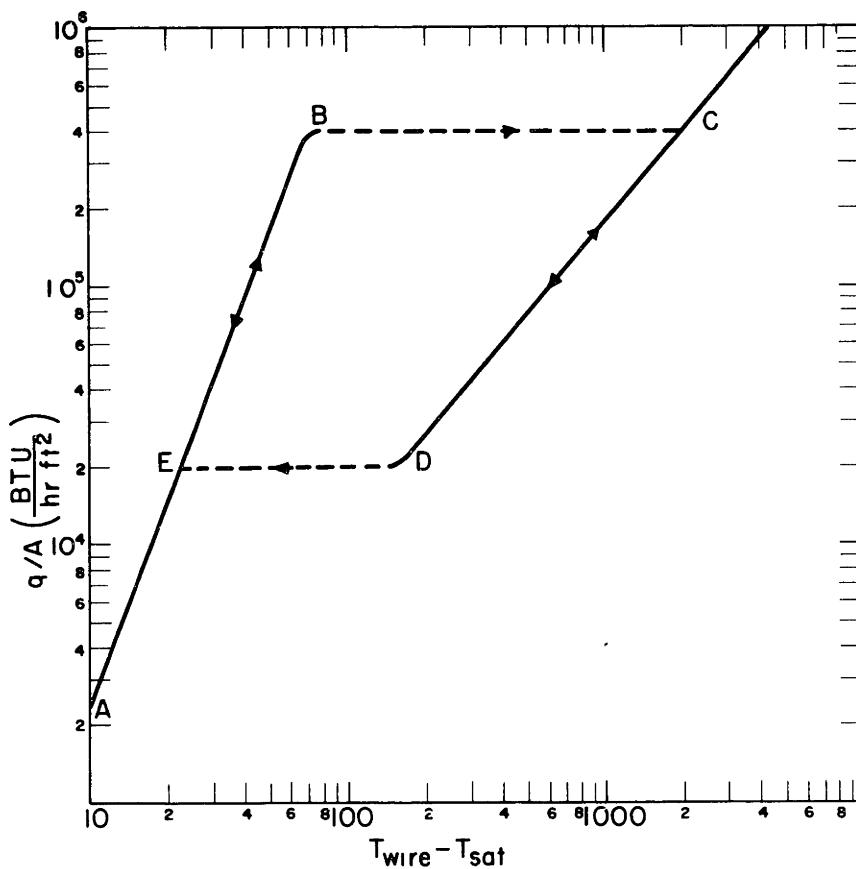


FIG 1 NUKIYAMA'S EXPERIMENTAL RESULTS

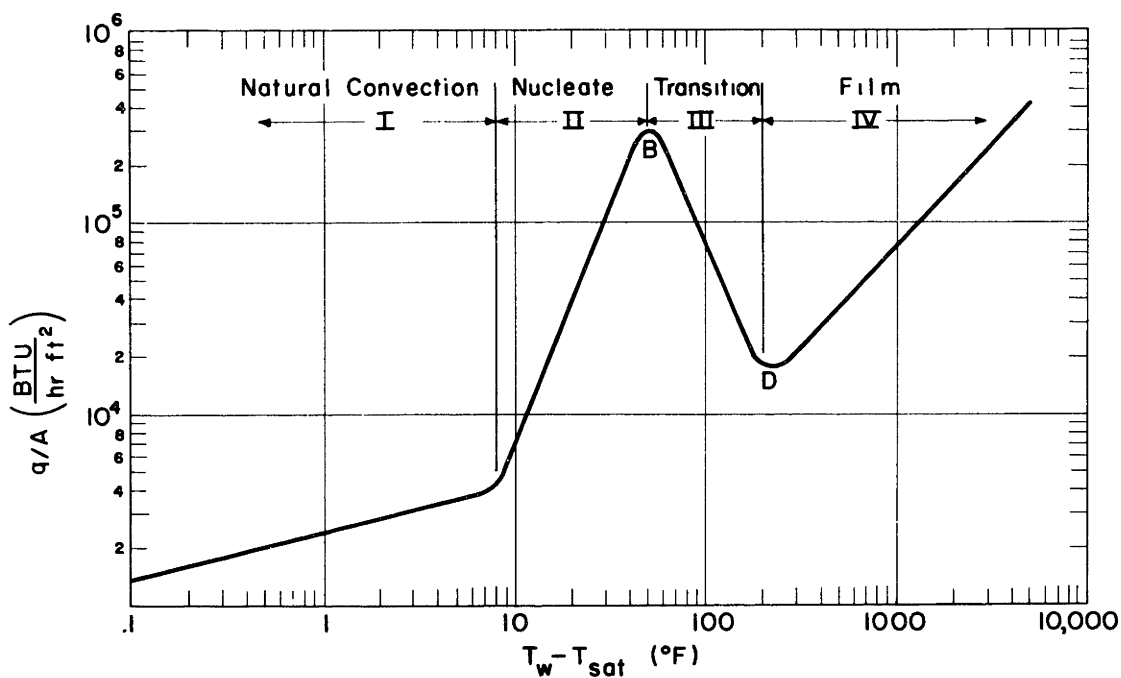


FIG. 2 CHARACTERISTIC BOILING CURVE

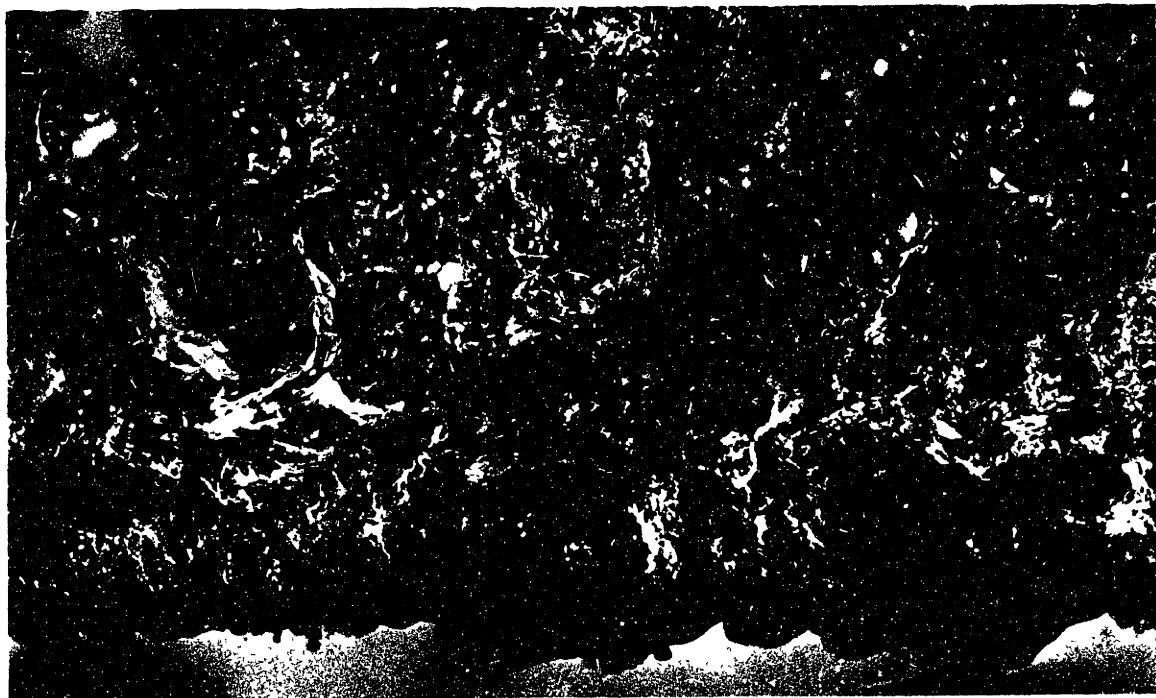


FIG 3 TRANSITION BOILING: $(q/A)_{\max} = 170,000 \frac{\text{BTU}}{\text{hr. ft.}^2} (25)$

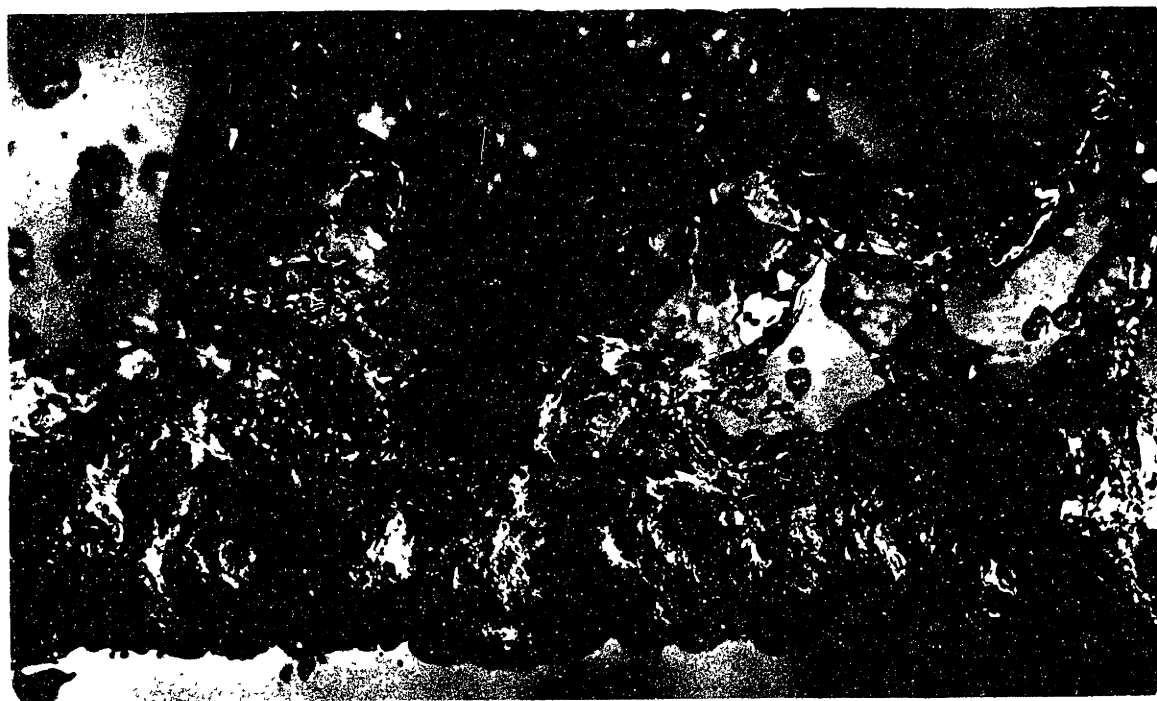


FIG 4 TRANSITION BOILING: $q/A = 69,000 \frac{\text{BTU}}{\text{hr. ft.}^2} (25)$



FIG 5 TRANSITION BOILING: $q/A = 27,000 \frac{\text{BTU}}{\text{hr. ft.}^2} (25)$



FIG 6 TRANSITION BOILING: $q/A = 13,000 \frac{\text{BTU}}{\text{hr. ft.}^2} (25)$



FIG 7 TRANSITION BOILING: $(q/A)_{\min} = 5,500 \frac{\text{BTU}}{\text{hr.ft.}^2} (25)$

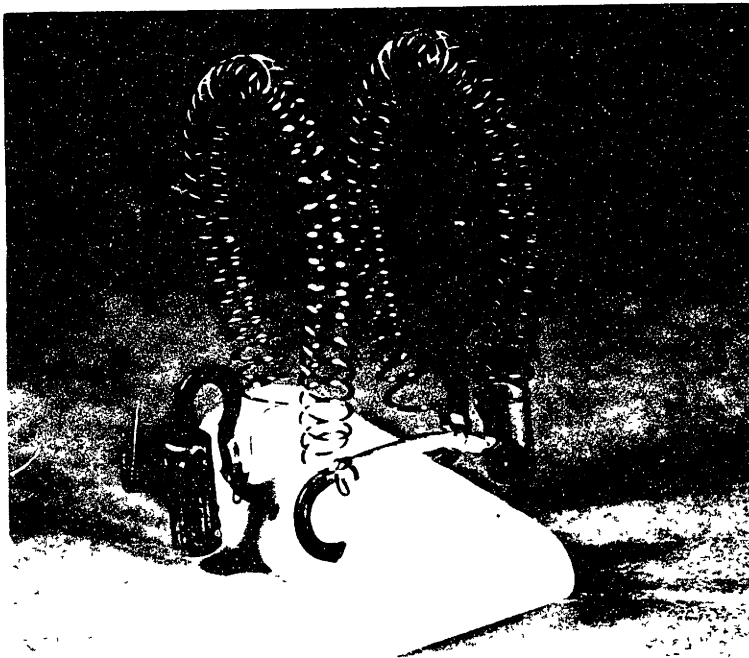


FIG 8 HEATER ASSEMBLY

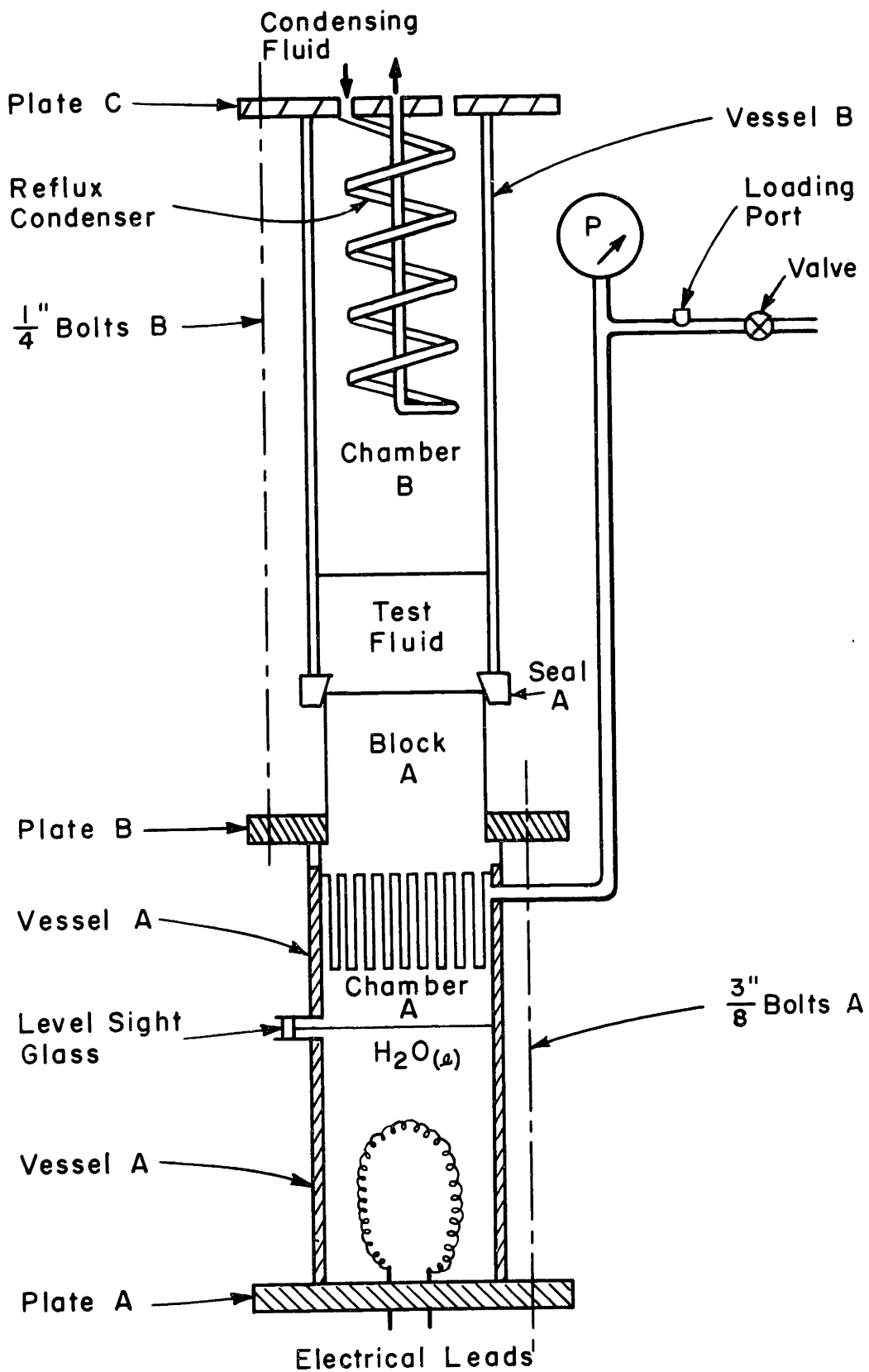


FIG. 9 TEST SET UP ASSEMBLY

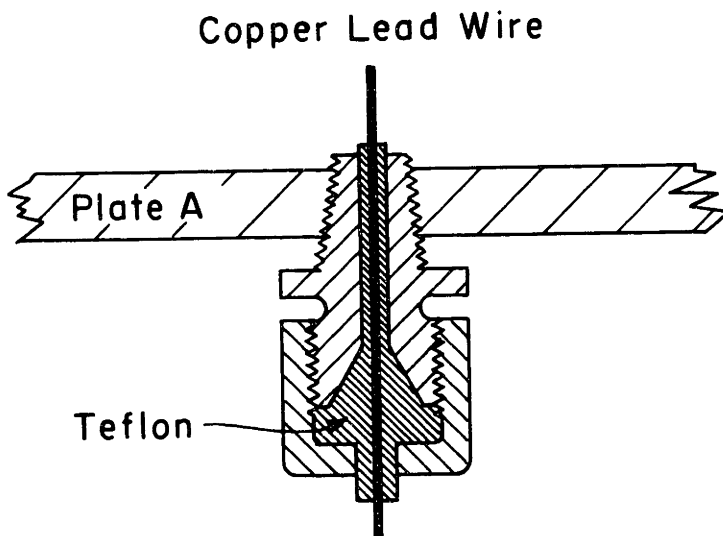


FIG. 10 ELECTRICAL POWER LEAD ASSEMBLY

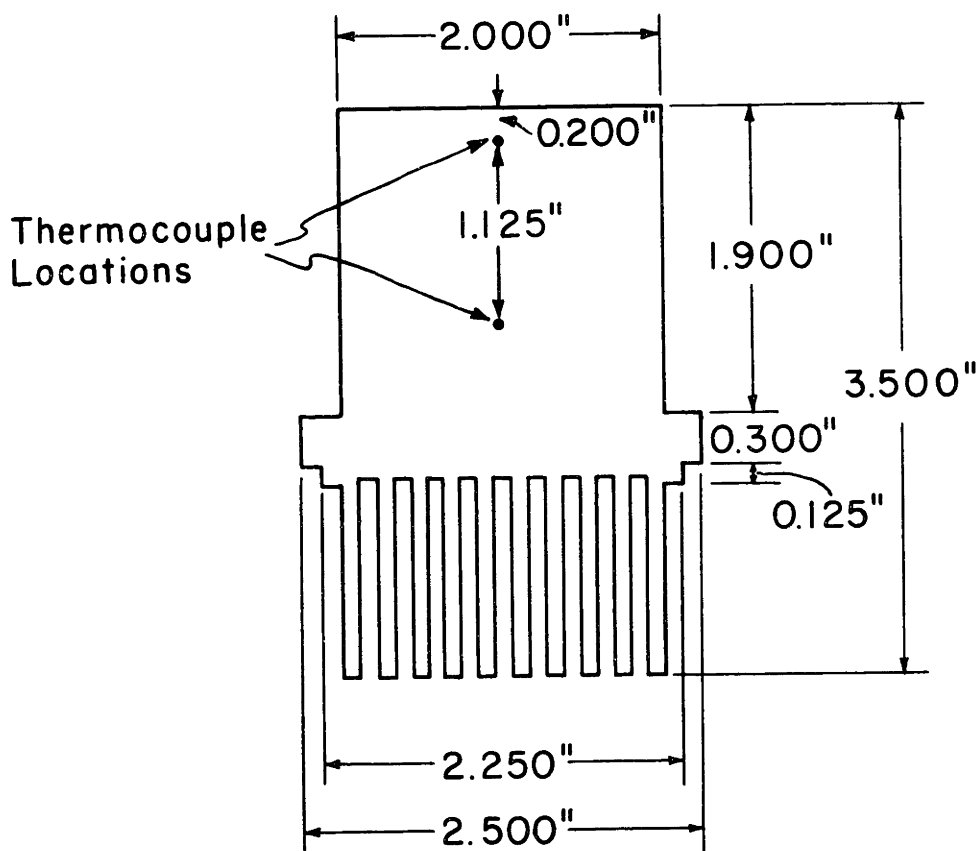


FIG. II TYPICAL COPPER HEATING BLOCK DESIGN

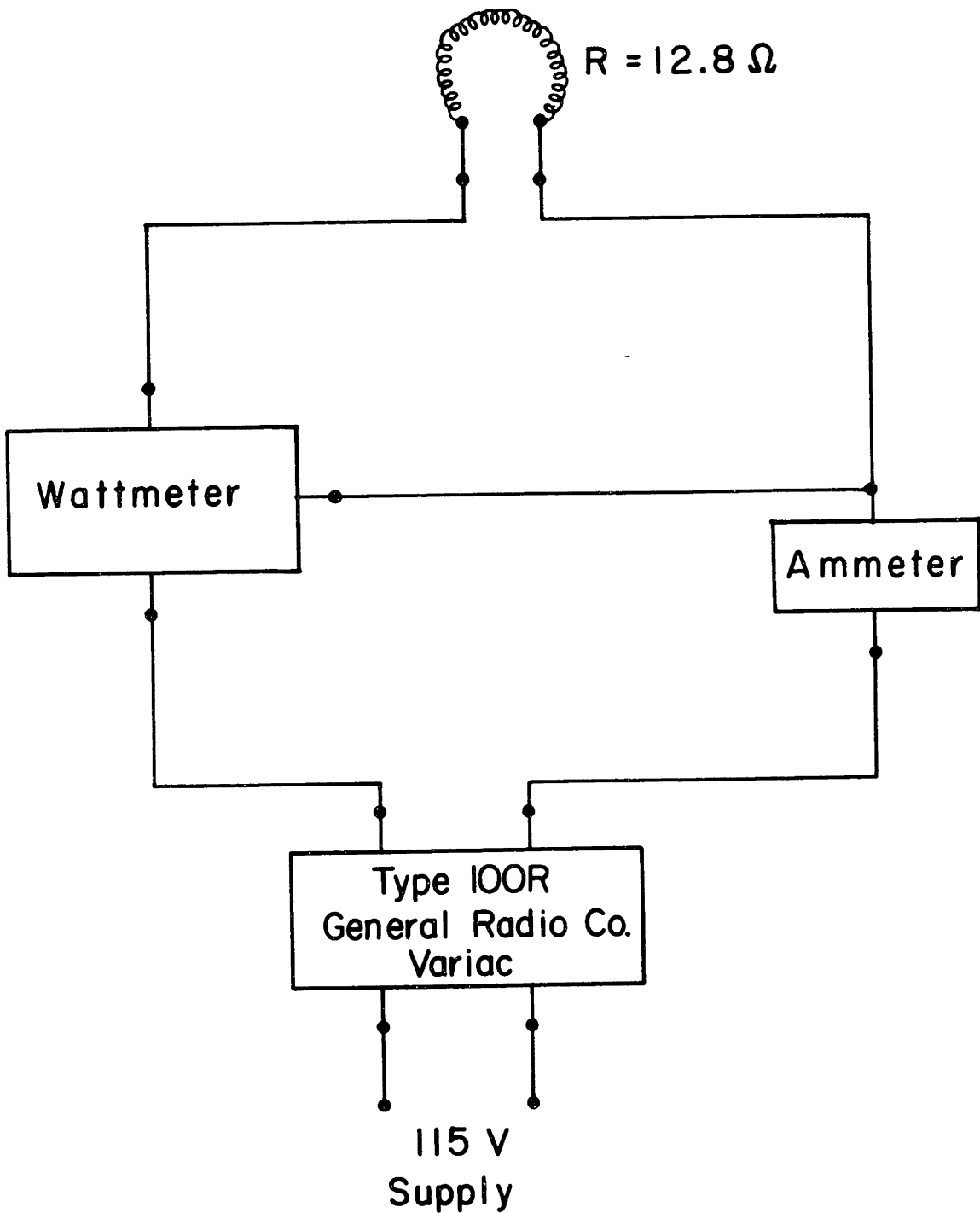


FIG. 12 WIRING DIAGRAM FOR POWER SUPPLY

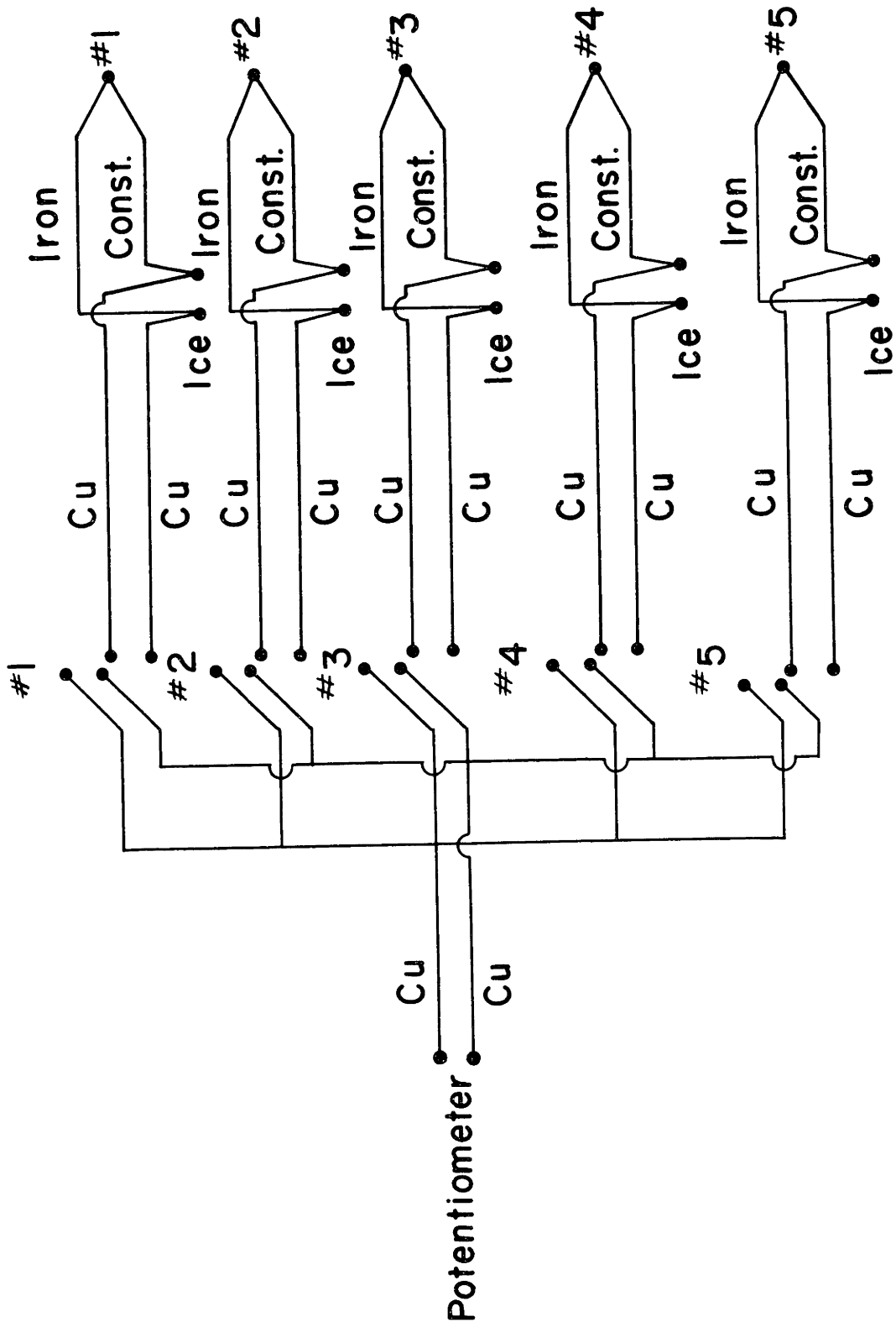


FIG. 13 THERMOCOUPLE WIRING DIAGRAM

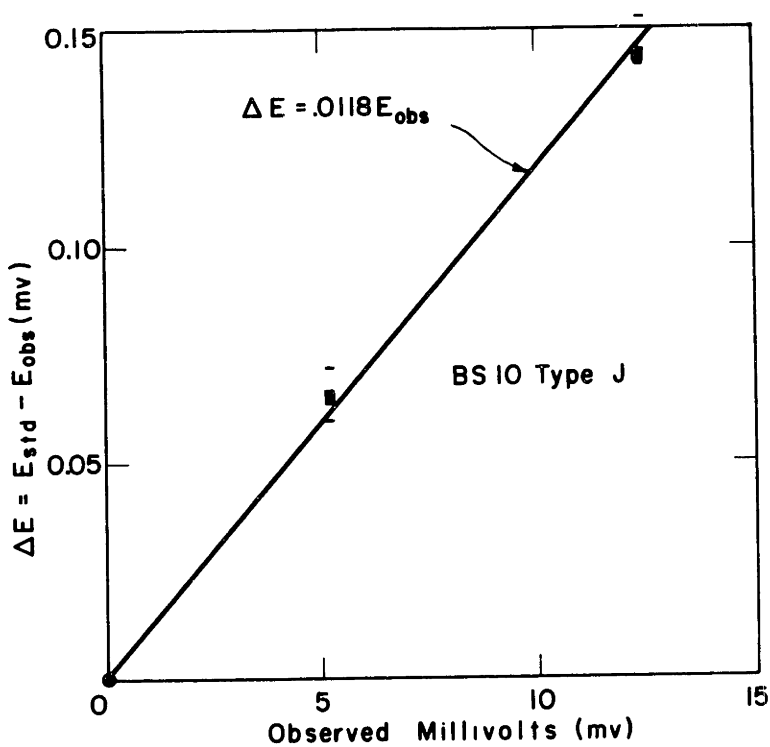


FIG. 14 DEVIATION CURVE FOR IRON CONSTANTAN THERMOCOUPLES

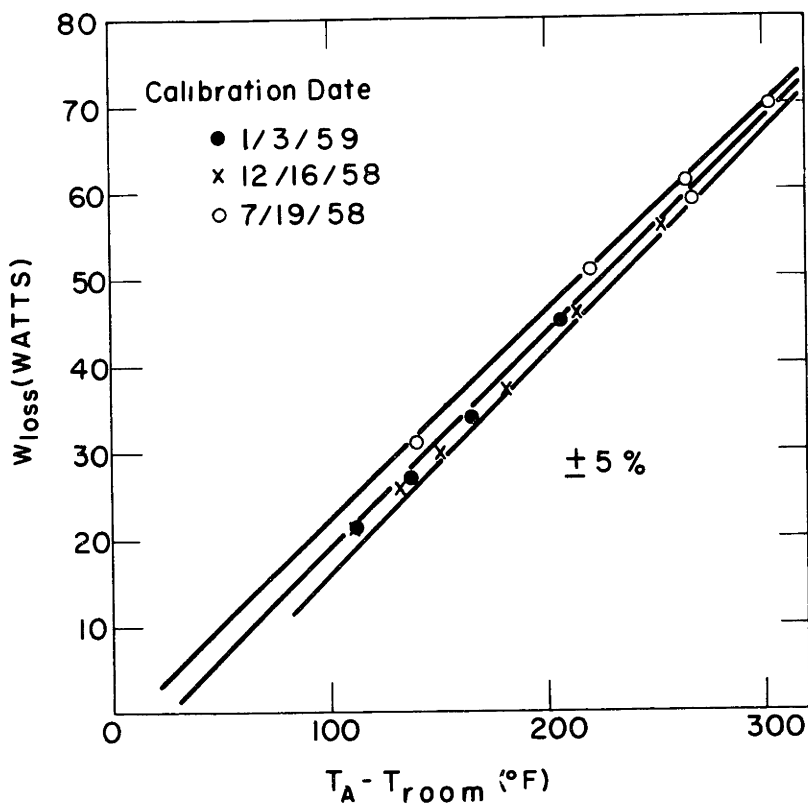
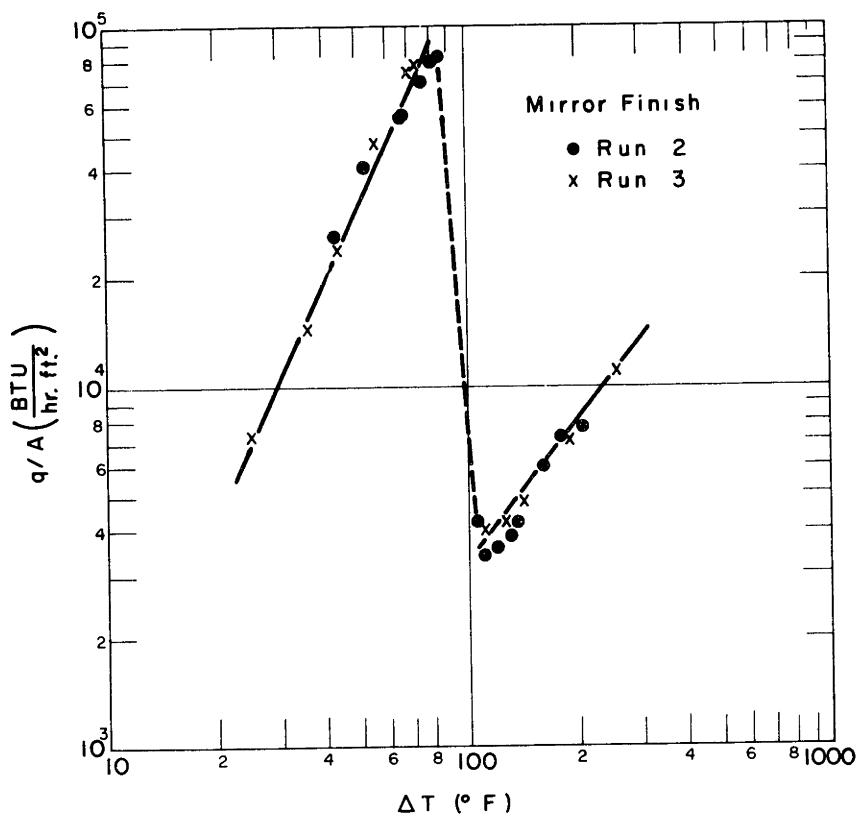


FIG. 15 HEAT LOSS CALIBRATION



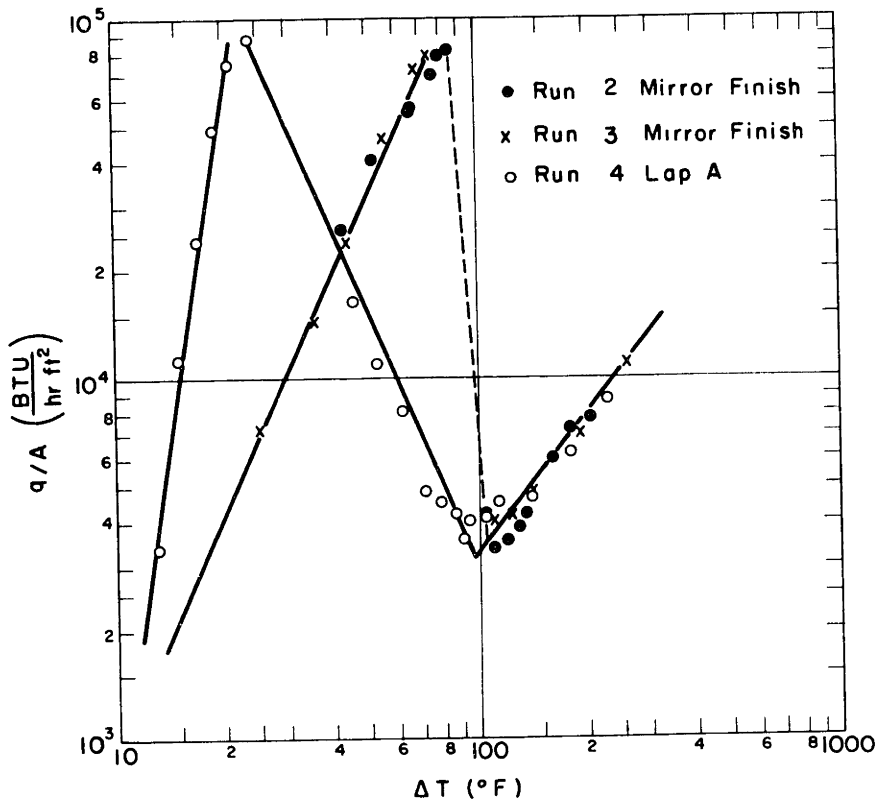


FIG 18 COPPER PENTANE TEST RESULTS EFFECT OF ROUGHNESS

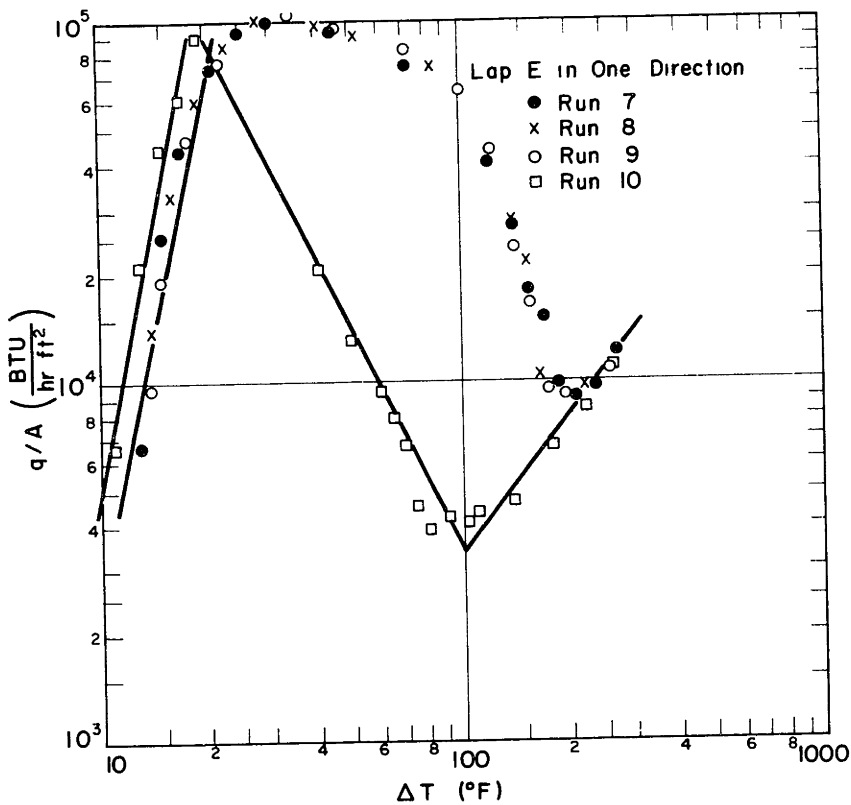


FIG. 19 COPPER PENTANE TEST RESULTS EFFECT OF SURFACE CLEANLINESS

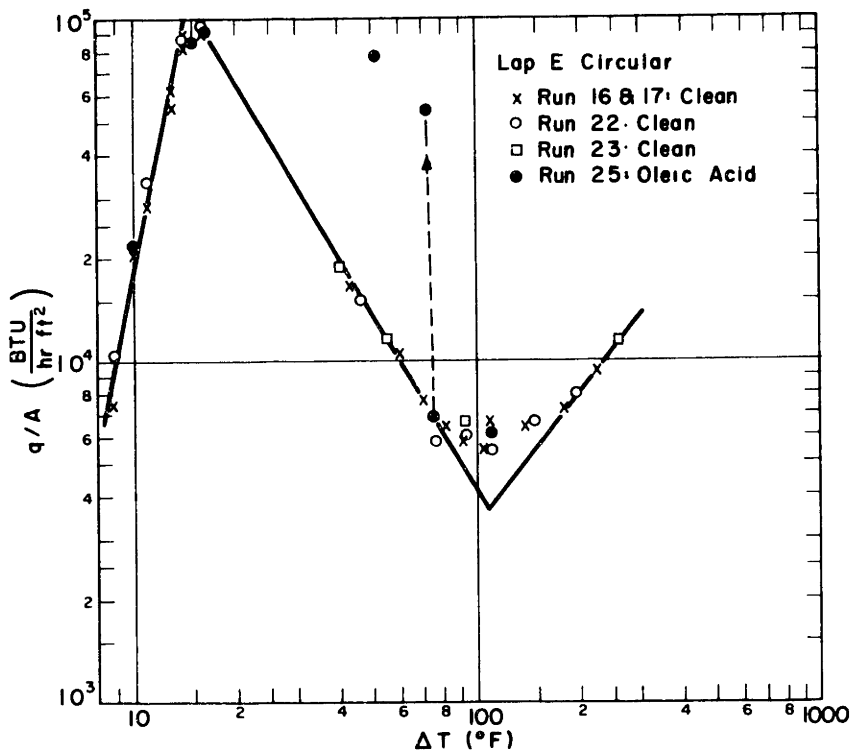


FIG. 20 COPPER PENTANE TEST RESULTS: EFFECT OF WETTING AGENT

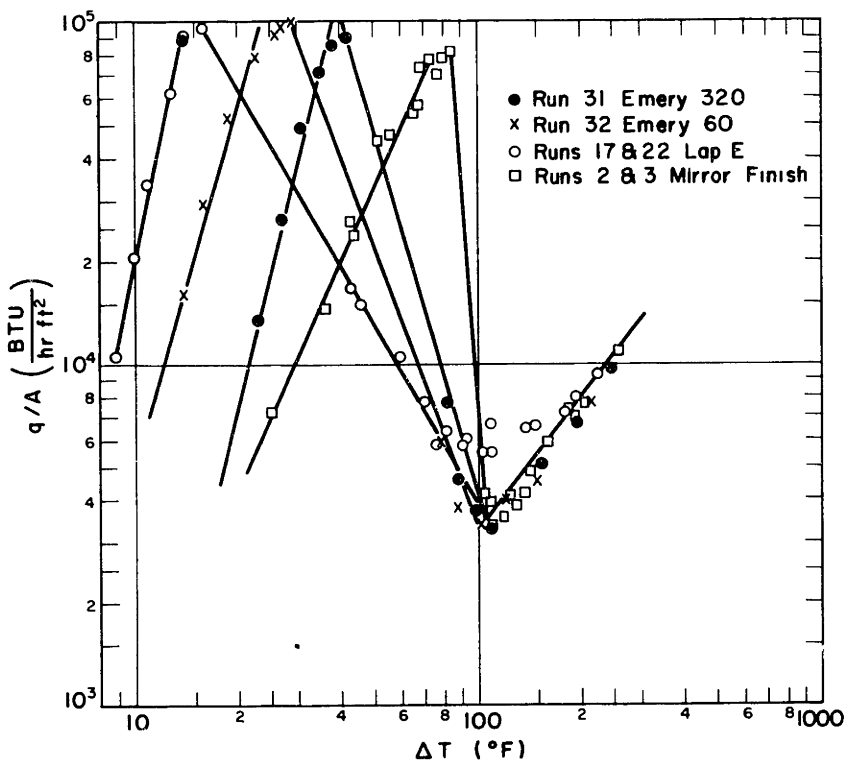


FIG. 21 COPPER PENTANE TEST RESULTS: EFFECT OF ROUGHNESS

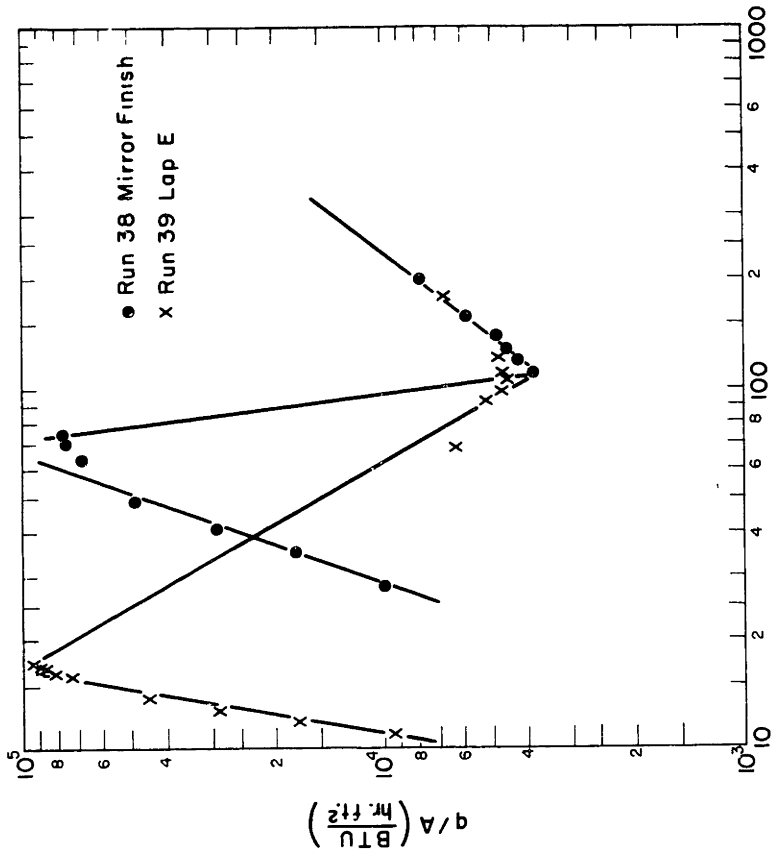


FIG 23 NICKEL-PENTANE TEST RESULTS · EFFECT OF ROUGHNESS

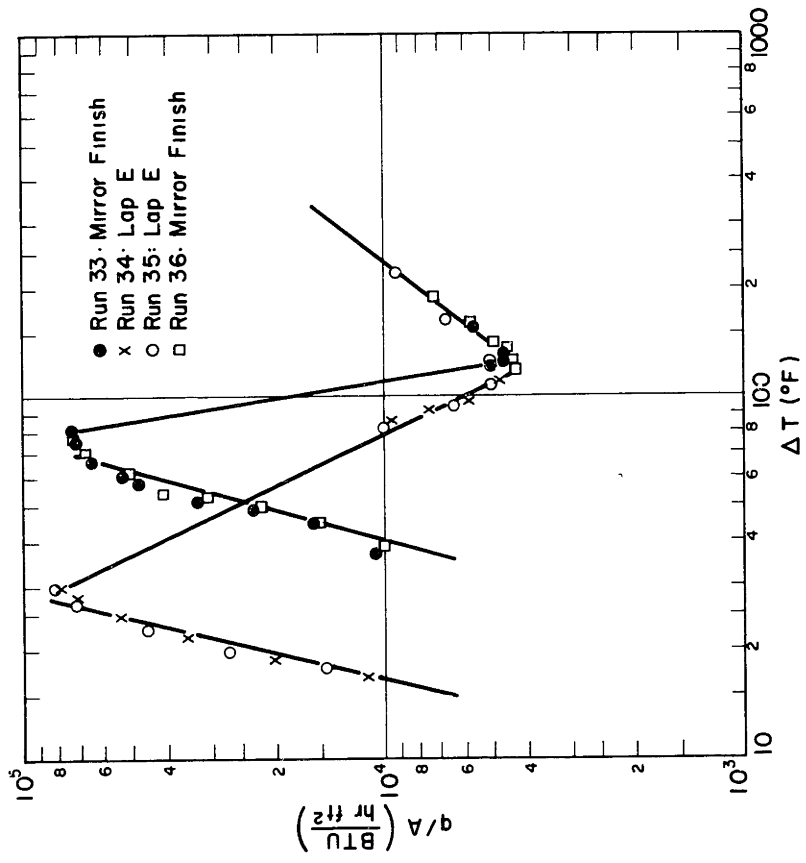


FIG. 22 INCONEL - PENTANE TEST RESULTS · EFFECT OF ROUGHNESS

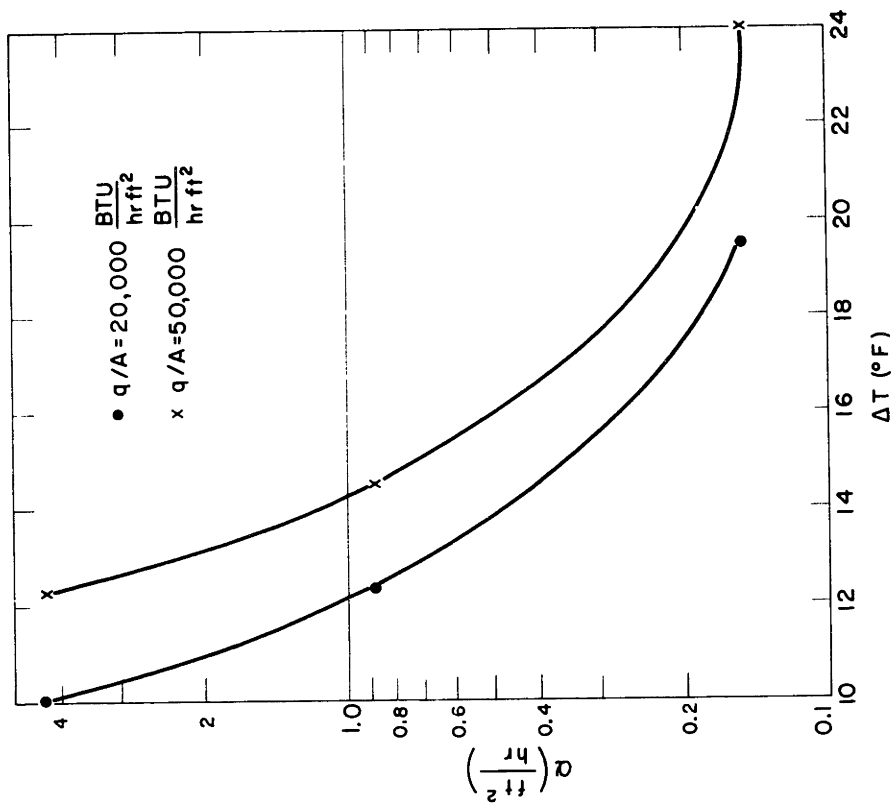


FIG 25 EFFECT OF MATERIAL THERMAL DIFFUSIVITY ON NUCLEATE BOILING TEMPERATURE DIFFERENCE.

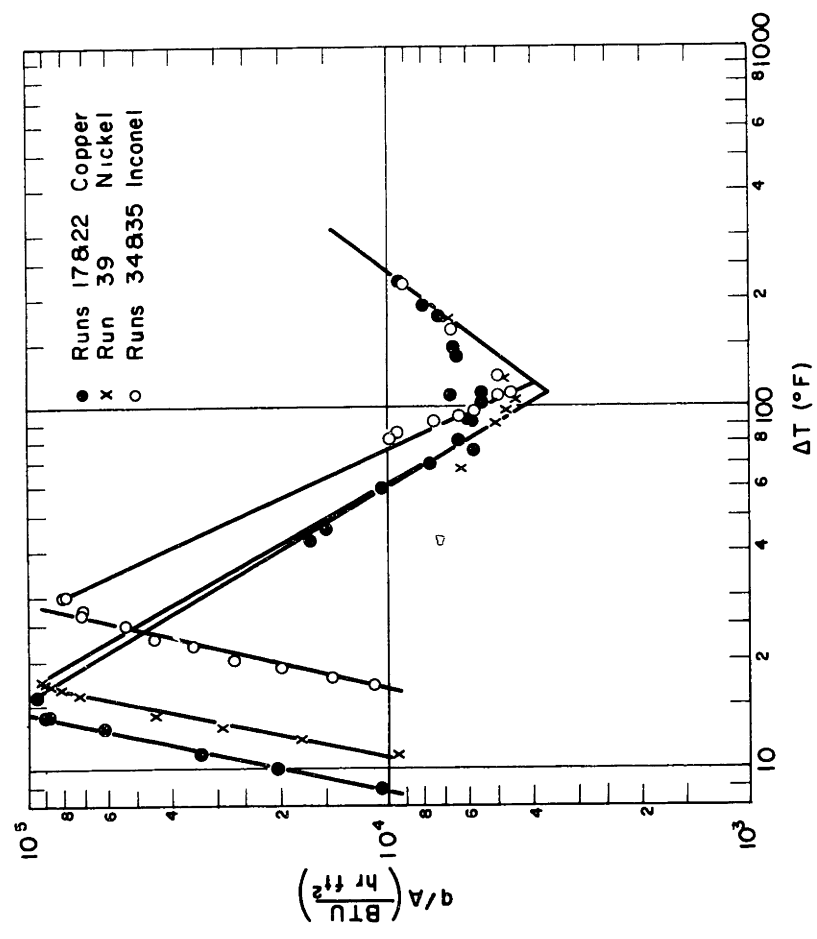


FIG 24 COPPER-LAP E CIRCULAR TEST RESULTS EFFECT OF MATERIAL

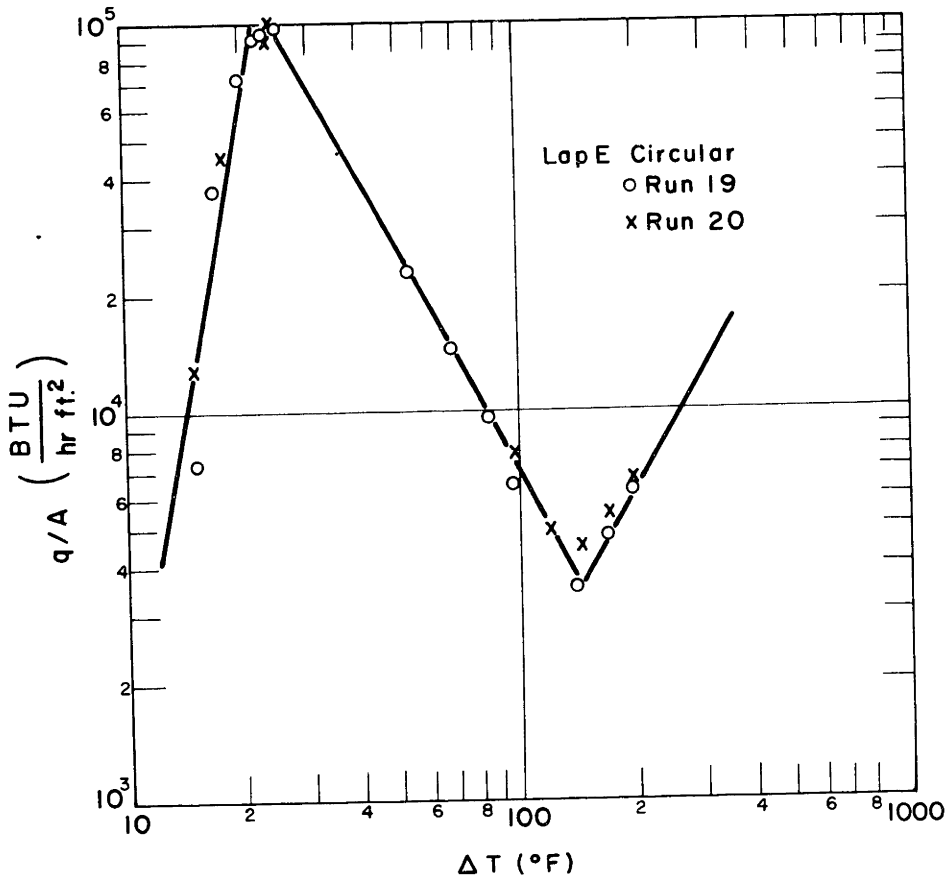


FIG. 26 COPPER CARBON TETRACHLORIDE TEST RESULTS

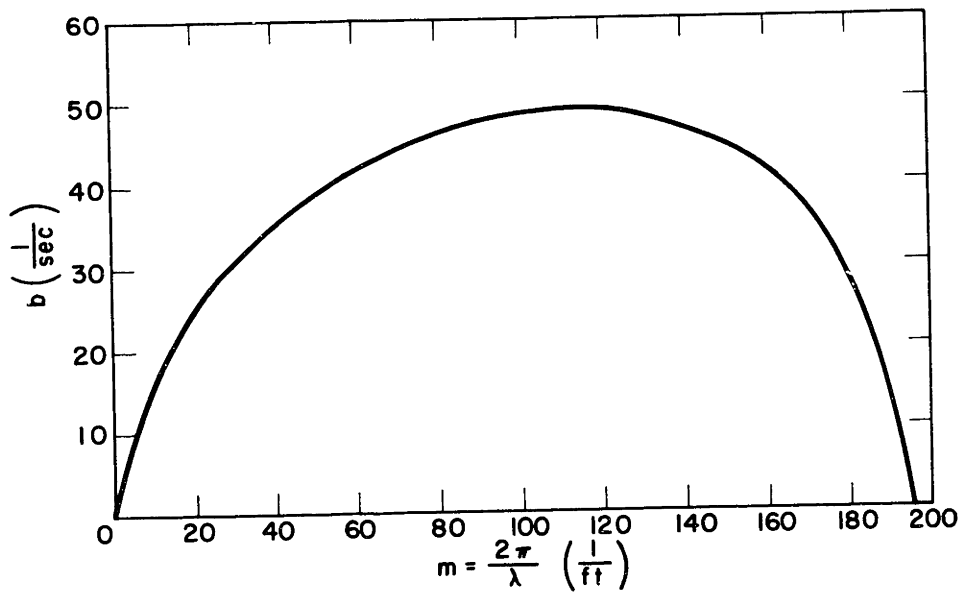


FIG. 27 PLOT OF b AS A FUNCTION OF m FOR n -PENTANE
 NEGLECTING THE EFFECT OF VELOCITY AND
 FLUID DEPTH

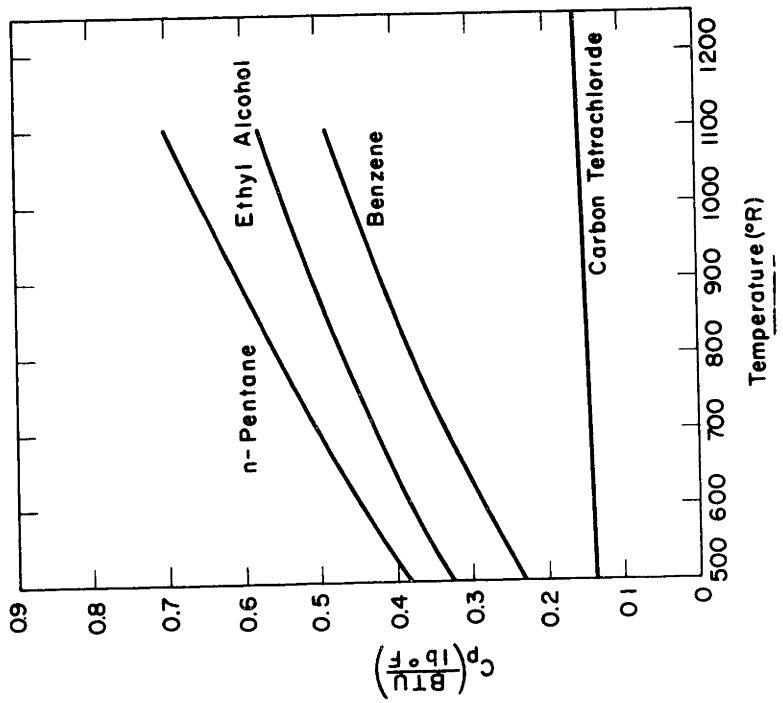


FIG. 29 VAPOR SPECIFIC HEAT AS A FUNCTION OF TEMPERATURE.

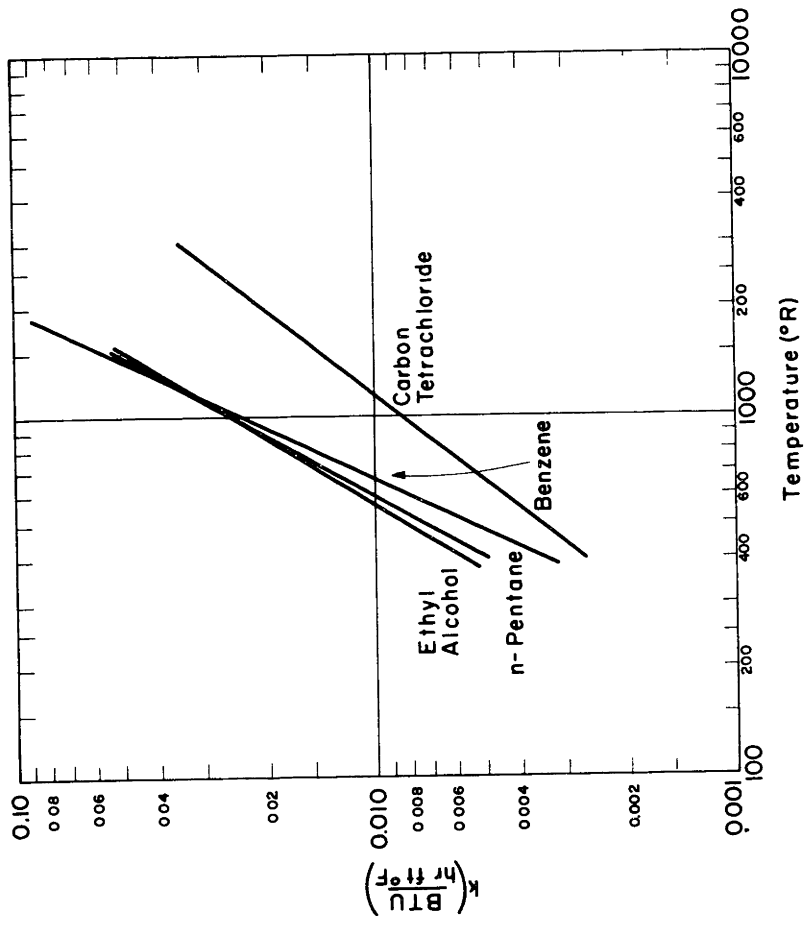


FIG 28 VAPOR THERMAL CONDUCTIVITY AS A FUNCTION OF TEMPERATURE

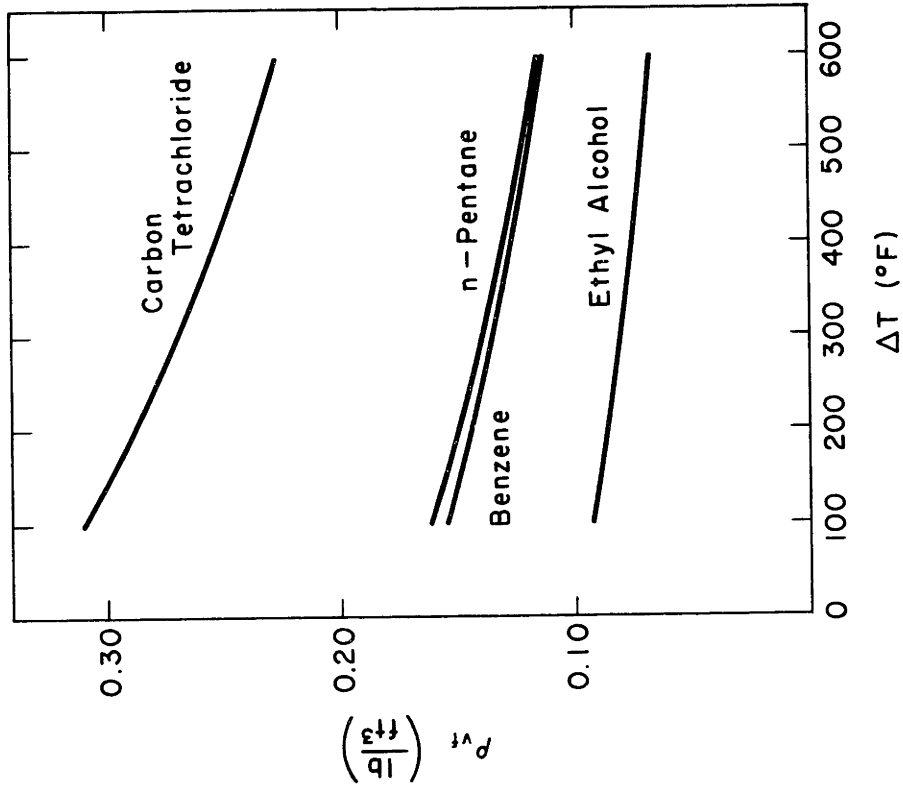


FIG. 31 VAPOR FILM DENSITY AS A FUNCTION OF TEMPERATURE DIFFERENCE

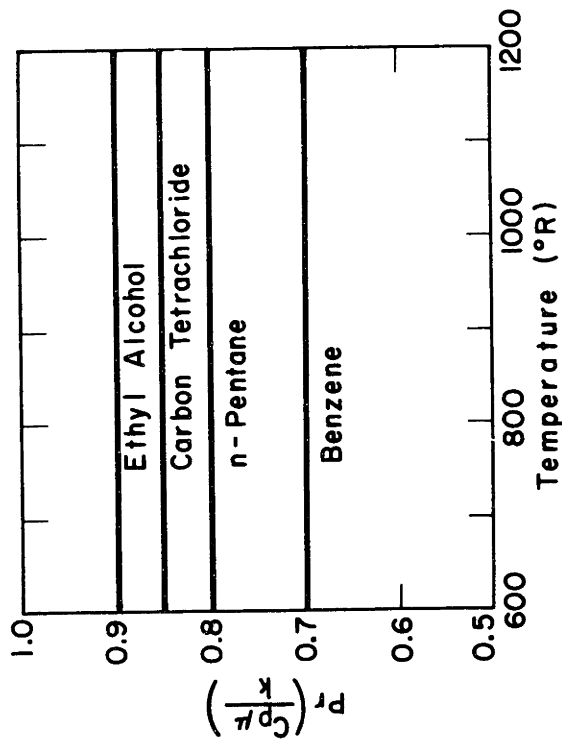


FIG. 30 VAPOR PRANDTL NUMBER AS A FUNCTION OF TEMPERATURE

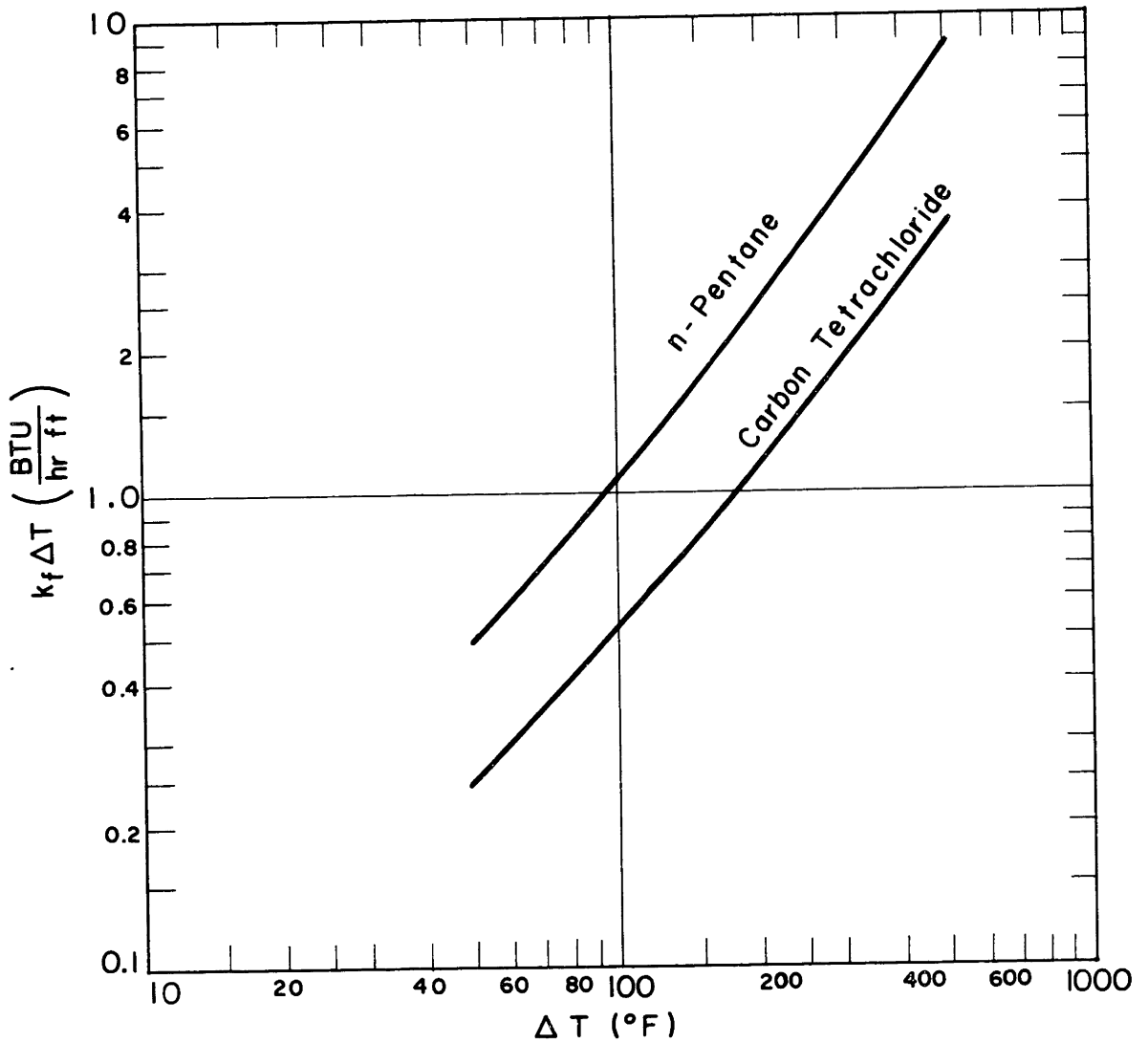


FIG. 32 PLOT OF $k_f \Delta T$ AS A FUNCTION OF TEMPERATURE DIFFERENCE

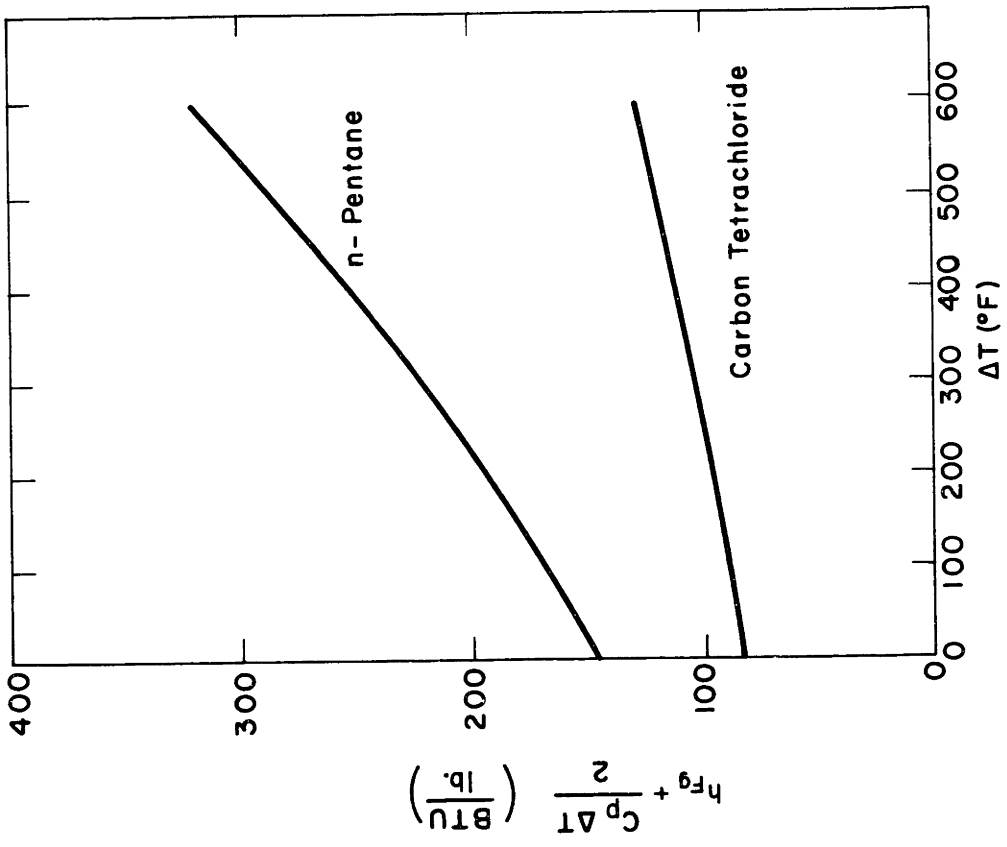


FIG.33 SATURATED VAPOR ENTHALPY CHANGE AS A FUNCTION OF TEMPERATURE DIFFERENCE

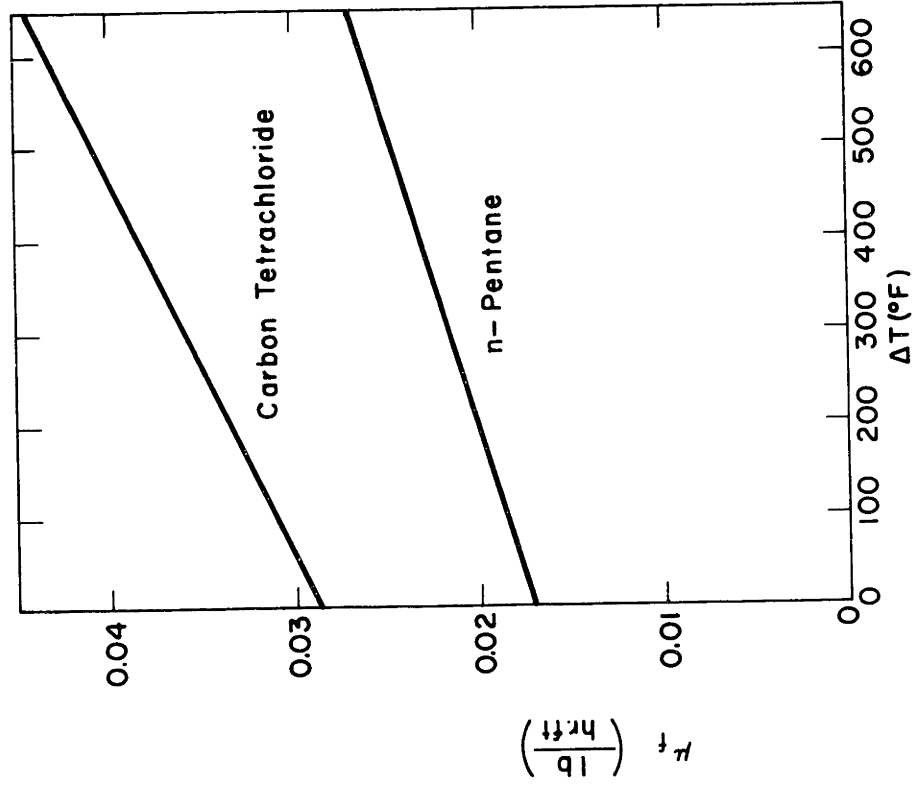


FIG.34 VAPOR FILM VISCOSITY AS A FUNCTION OF TEMPERATURE DIFFERENCE

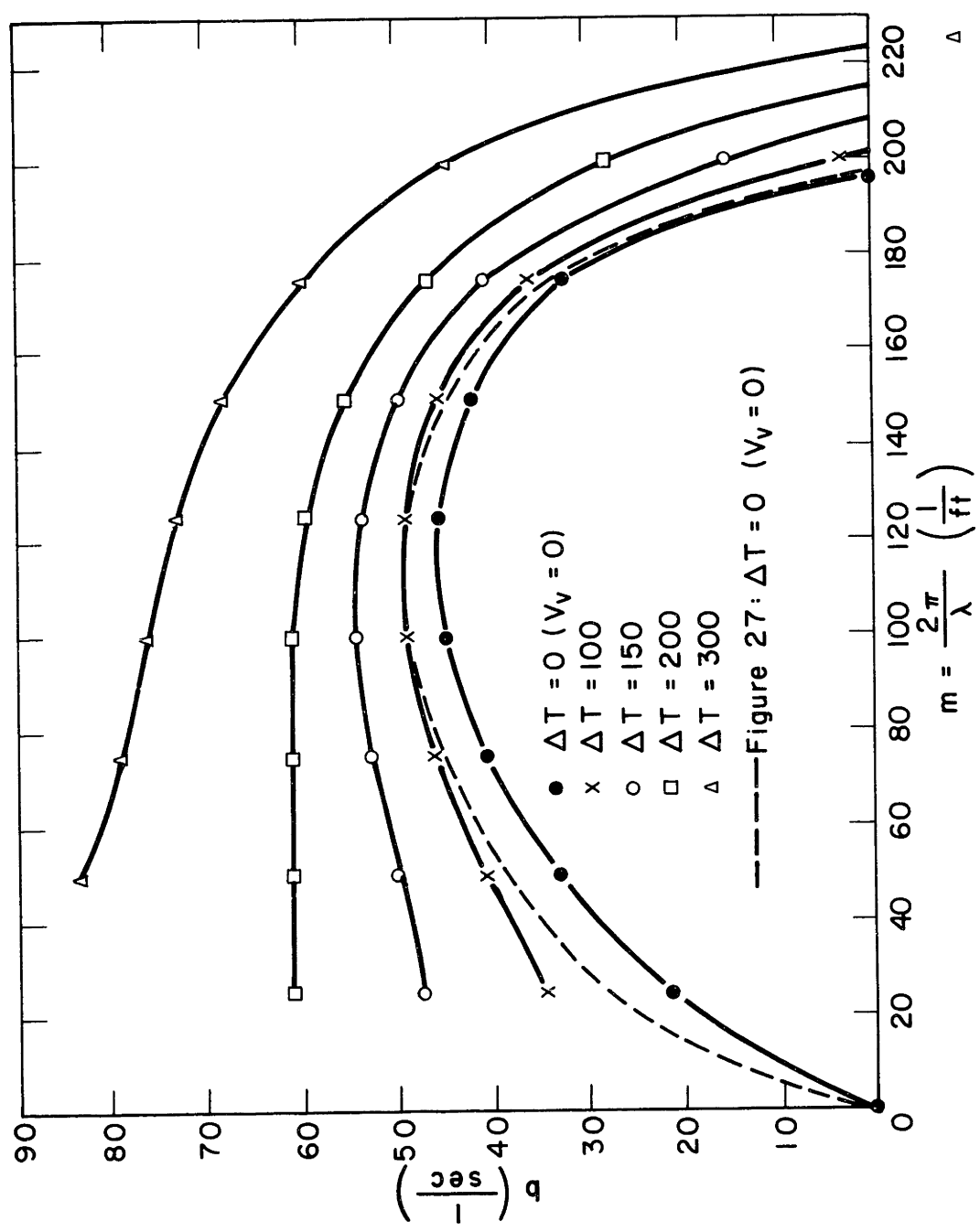


FIG. 35 PLOT OF b AS A FUNCTION OF m FROM EQ. III - 17 FOR n - PENTANE

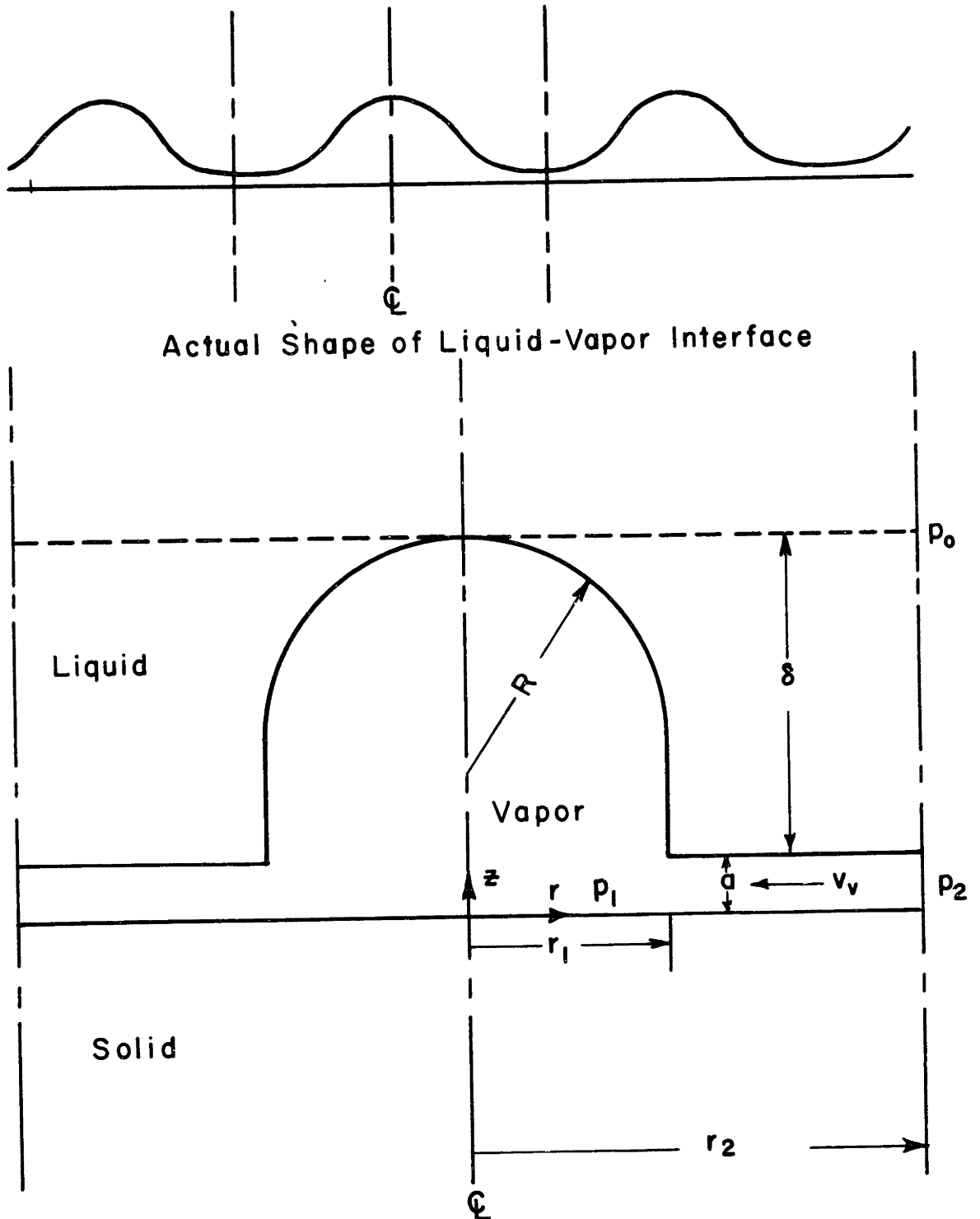


FIG 36 PHYSICAL MODEL OF FILM BOILING FROM A HORIZONTAL SURFACE

BIOGRAPHICAL NOTES

NAME: Paul Jerome Berenson

BORN: Portland, Oregon, July 12, 1934

MARRIED: August 25, 1957; one child

EDUCATION: S.B. in Mechanical Engineering, Massachusetts Institute of Technology, 1952-1956
S.M. in Nuclear Engineering, Massachusetts Institute of Technology, 1956-1957
Mech. E. in Mechanical Engineering, Massachusetts Institute of Technology, 1957-1958

FELLOWSHIP: National Science Foundation Predoctoral Fellowship, 1956-1957

MEMBERSHIP: Tau Beta Pi
Society of the Sigma Xi
Pi Tau Sigma

PROFESSIONAL EXPERIENCE:

1957-1959 Instructor of Mechanical Engineering,
Massachusetts Institute of Technology

1957-1959 Principal Engineer and Head of Heat Transfer
Research, Microtech Research Company,
Cambridge, Massachusetts

1957 Research Engineer, Atomics International
Canoga Park, California

1956 Engineer, Douglas Aircraft Missiles Division,
Santa Monica, California